



**HAL**  
open science

## Biomécanique verrouillage distal du clou centro-médullaire.

Vytautas Gasiunas

► **To cite this version:**

Vytautas Gasiunas. Biomécanique verrouillage distal du clou centro-médullaire.. Biomécanique [physics.med-ph]. École Nationale Supérieure des Arts et Métiers, 2024. Français. NNT : 2024ENAME041 . tel-04951010

**HAL Id: tel-04951010**

**<https://pastel.hal.science/tel-04951010v1>**

Submitted on 17 Feb 2025

**HAL** is a multi-disciplinary open access archive for the deposit and dissemination of scientific research documents, whether they are published or not. The documents may come from teaching and research institutions in France or abroad, or from public or private research centers.

L'archive ouverte pluridisciplinaire **HAL**, est destinée au dépôt et à la diffusion de documents scientifiques de niveau recherche, publiés ou non, émanant des établissements d'enseignement et de recherche français ou étrangers, des laboratoires publics ou privés.

**ÉCOLE DOCTORALE SCIENCES DES MÉTIERS DE L'INGÉNIEUR**  
Institut de Biomécanique Humaine Georges Charpak (IBHGC)  
Campus de Paris

# THÈSE

présentée par : **Vytautas GASIUNAS**  
soutenue le : 4 octobre 2024

pour obtenir le grade de : **Docteur d'HESAM Université**

préparée à : **École Nationale Supérieure d'Arts et Métiers**  
Spécialité : **Biomécanique**

## **Biomécanique du verrouillage distal du clou centromédullaire**

**THÈSE dirigée par :**  
**Pr Sébastien Laporte**

**et co-encadrée par :**  
**Mme Marianne Prot**

### **Jury**

**M. Louis DAGNEAUX** Professeur des universités - Praticien  
hospitalier Lapeyronie University Hospital of Montpellier  
**M. Yoann LAFON** Directeur de recherche Université Gustave  
Eiffel, Champs-sur-Marne,  
**M. Sébastien LAPORTE** Professeur École nationale  
supérieure d'Arts et Métiers, Paris  
**Mme Marianne PROT** Professeur agrégé Stanislas Cannes  
**Mme Sophie PUTMAN** Praticien hospitalier CHRU de Lille  
**M. Philippe ROUCH** Professeur des universités École  
nationale supérieure d'Arts et Métiers, Paris

Rapporteur  
Président, rapporteur  
Examineur  
Examineur  
Examineur



## **Acknowledgements**

Completing this dissertation has been a journey of both personal and academic growth, and it would not have been possible without the support and guidance of numerous people. I am deeply grateful to everyone who contributed to this work.

I would like to thank the Arts et Métiers Institute of Technology, Université Sorbonne Paris Nord, IBHGC - Institut de Biomécanique Humaine Georges Charpak for the opportunity to perform this scientific work.

I extend my sincerest thanks to my thesis director, Pr. Sébastien Laporte and supervisor Ms. Marianne Prot, for their support, insightful feedback and continuous encouragement. Their expertise and dedication have been invaluable, providing me with the guidance necessary to navigate the complexities of my research. Their belief in my abilities and their commitment to excellence have inspired me to go forward with my research.

I am also grateful to the members of my dissertation committee, Mr Pierre Yves Rohan and Mr Baptiste Sandoz for their constructive critiques and suggestions. Their diverse perspectives have greatly enriched my work and pushed me to refine my ideas and methodologies.

Special thanks are due to the administrative and technical staff at Institut de Biomécanique Humaine Georges Charpak, whose assistance and efficiency have facilitated my research process. Their behind-the-scenes work often goes unnoticed, but it is crucial for the successful completion of any project.

On a personal note, I would like to thank my family for their patience, love, and encouragement. My spouse, Indré Gasiuné, deserves special recognition for their support and understanding during the many late nights, long weekends and shortened vacations dedicated to this dissertation. Their belief in me has been a constant source of motivation.

My parents have always been my pillars of strength, instilling in me the value of perseverance and hard work.

This dissertation is the culmination of a long and challenging journey, and it would not have been possible without the contributions and support of the many people mentioned above.



## **Table of contents**



1. Introduction	27
2. Literature review	31
2.1 Introduction.	33
2.2. General context.	33
2.2.1. Intramedullary nailing.	34
2.2.2. Bone-compatible material.	35
2.2.3. Long bone cases.	35
2.2.4. Conclusion.	38
2.3. The bone development and healing at the bone/implant interface.	38
2.3.1. Bone formation.	38
2.3.2. Bone healing.	39
2.3.3. Bone remodelling.	40
2.3.4. Osteo-integration.	41
2.3.5. Conclusion.	42
2.4. Surgery related problematics.	43
2.4.1. Fracture treatment	43
2.4.2. Fracture treatment options.	44
2.5. Surgical technique of intramedullary nailing and nail related problematics.	55
2.5.1. Nail related problematics.	57
2.5.2. Distal locking. Existing aiming techniques.	61
2.6. Cortical bone density, strength, mechanical parameters and fracture propagation.	68
2.7. Experimentation and mechanical loading.	78
2.8. Hertz Theory of Cylindrical Contact.	80
2.9. Synthesis, aims and objectives of this thesis.	88
3. Mechanical behaviour of the cortical bone under local loading	90

3.1. Introduction.	92
3.2. Material and Methods.	93
3.2.1. Specimens.	93
3.2.2. Pre-experimental Imaging.	93
3.2.3. Mechanical testing.	97
3.2.4. Mechanical Data Analysis.	98
3.2.5. Post-experimental imaging.	103
3.2.6. Relationship between the data obtained in microCT and curve analysis.	105
3.3. Results.	106
3.3.1. Qualitative and quantitative curve analysis.	106
3.3.2. Imaging.	107
3.3.3. Correlation between the imaging and the mechanical parameters.	109
3.4. Discussion.	111
3.4.1. Experimental method.	111
3.4.2. Discussion of the results.	113
3.4.3 Conclusion.	140
3.4.4. Mathematical analysis of the contact area.	140
3.5. Relationship between the curves and the imaging.	149
3.6. Conclusion.	150
4. Experimental model of local strain at the bone and locking screw contact area	151
4.1. Introduction.	153
4.2. Material and Methods.	153
4.2.1. Specimens.	153
4.2.2. Mechanical testing.	154
4.2.3. Mathematical analysis.	156
4.2.4. Data analysis.	158

4.3. Results.	159
4.3.1. Qualitative and quantitative curve analysis.	159
4.3.2. Mathematical analysis of the bone and the screw interface during the local loading.	161
4.4. Discussion and Conclusion.	163
4.4.1. Experimental method.	163
4.4.2. Discussion of the results.	164
5. General Conclusion and Perspectives	168
References	174
Annexes	194
Annex I. X-rays' related problematics and risks.	196
Annex II. Force-displacement curves and their types, scale adjusted.	209
Annex III. Mechanical parameters and imaging data.	210
Annex IV. Fracture propagation cartography with segmental BV/TV.	211
Group1	211
Group 2	212
Group 3	213
Annex V. Matlab/Octave Code	214
Annex VI: Summary of Results of curve fitting.	217



## **Index of Figures**

Figure 1: Beginning of intramedullary nailing [Bart10].	34
Figure 2: Incidence of tibial fractures [Lars15].	37
Figure 3: Endochondral and intramembranous ossification [Hill20].	39
Figure 4: Distal locking screw failure. A) screw loosening and backing out. B) screw rupture [Wild20].	42
Figure 5: Orthopaedic treatment.	44
Figure 6: Functional treatment.	45
Figure 7: External fixation device.	46
Figure 8: Dynamic compression plate. <a href="http://www.aofoundation.org">www.aofoundation.org</a>	46
Figure 9: Examples of locking plates. <a href="http://www.aofoundation.org">www.aofoundation.org</a>	47
Figure 10: Importance of the fracture haematoma: cartilage cells that will later undergo ossification can be seen after 4 days following the subperiosteal injection of a TGF- $\beta$ (usually present in fracture haematoma) at a non fractured rat femur [Bola92].	48
Figure 11: "Internal fixator". <a href="http://www.aofoundation.org">www.aofoundation.org</a>	48
Figure 12: Example of a neutralisation plate. <a href="http://www.aofoundation.org">www.aofoundation.org</a>	49
Figure 13: Full and cannulated intramedullary nails. <a href="http://periodictable.com/Items/022.4/index.html">periodictable.com/Items/022.4/index.html</a>	50
Figure 14: Parts of the intramedullary nail. (Adapted from [Hedg17]).	52
Figure 15: Retrograde nail. <a href="http://www.aofoundation.org">www.aofoundation.org</a>	53
Figure 16: Choosing the entry point that would allow good nail alignment inside the bone. <a href="http://www.aofoundation.org">www.aofoundation.org</a>	55
Figure 17: A guidewire put an the medullary canal with the reamer and the nail.	56
Figure 18: Nail and guide handle.	57
Figure 19: Distal locking holes.	57
Figure 20: Fractured anterior cortical bone the distal femur [Egolo4].	59

Figure 21: Freehand technique.	61
Figure 22: “H”-shape guide.	62
Figure 23: Shifted guide.	62
Figure 24: Stable guide, fixed to the operating table.	63
Figure 25: Mechanically stabilised guide.	65
Figure 26: Navigation. Experimental setting.	65
Figure 27: Computer assisted freehand technique.	66
Figure 28: Device using electromagnetic waves.	67
Figure 29: Time gain using the electromagnetic wave assisted in comparison to the freehand technique.	67
Figure 30: Trabecular bone resistance to fracture (BMC: bone mineral content; vBMD: volumetric bone mineral density) [Aers98].	72
Figure 31: Crack extension parallel and perpendicular to the collagen fibres [Pete05].	74
Figure 32: Bridging [Nallo3].	75
Figure 33: Collagen bridging [Nallo3].	75
Figure 34: Bone hierarchy and dilatational bands [Atha12].	76
Figure 35: Usual experimentation setting [Zhao18].	79
Figure 36: Two elliptical bodies in contact [John85].	81
Figure 37: Cylinder in contact with a flat surface.	82
Figure 38: a) Diagram of regular stress strain diagram identifying critical points, and b) Diagram of von Mises and Tresca criterion. Adapted from Wang and Zhu. [Wang13].	84
Figure 39: Fracture initiation.	86
Figure 40: Measurements of the femoral shaft radius and cortical thickness	95
Figure 41: Position of the rod on the specimen and definition of zones of analysis.	96
Figure 42: Defining the region of interest for BT/TV calculations.	96
Figure 43: Segmentation adjusted for bone substance.	97

Figure 44: Experimentation setting.	98
Figure 45: Discarded part of the curve.	100
Figure 46: Yielding.	101
Figure 47: Yielding strength (arrow) using 0.2% offset.	101
Figure 48: Bone damage before the complete rupture seen in this curve.	102
Figure 49: Force to rupture (F <sub>rup</sub> ) and distance to rupture (D <sub>rup</sub> ).	102
Figure 50: Apparent stiffness calculation.	103
Figure 51: Measurement of fragment displacement and fracture propagation length.	104
Figure 52: Example of pattern of rupture obtained from MicroCT analysis. Colours relate to the size of crack for the pattern of damage.	105
Figure 53: Bone damage as yielding phenomenon seen in the curve. There is more comminution and fragment displacement in the upper part of the specimen and less bone damage in the area where the metallic rod stopped. Yielding in this case is related to a local bone damage. Note the absence of major fracture.	108
Figure 54: Bone damage reflecting a fragile rupture in the curve.	109
Figure 55: Examples of fracture propagation and mechanical behaviour (typical curves).	110
Figure 56: Micro-fractures seen in this curve.	116
Figure 57: A slight local bone damage could be seen in pre-experimental MicroCT scan.	117
Figure 58: Post-experimental MicroCT scan. Comminution at the contact area and fracture lines joining distally (the same specimen).	118
Figure 59: L+Y type of the curve, specimen Nr.8, 1st group.	120
Figure 60: Proximal bone damage (specimen 8, 1st group).	120
Figure 61: A nearly 5 mm bony defect.	121
Figure 62: a) Parallel cuts. b) Satisfactory alignment (specimen 8, 1st group).	122
Figure 63: a) Force/displacement curve, specimen Nr.9, 1st group. b) Mapping of fracture lines.	123

Figure 64: Proximal and distal end damage, note damage on both proximal cortical bones.	123
Figure 65: Slight misalignment of proximal and distal cuts.	124
Figure 66: a) 2L + Y type of the curve, but showing several small ruptures, specimen Nr.3, 2nd group. b) Mapping of fracture lines.	124
Figure 67: Slight cortical bone damage, specimen Nr.3, 2nd group.	125
Figure 68: a) 4° Misalignment (note a blood vessel entering the bone). b) alignment with the longitudinal axis, specimen Nr.3, 2nd group.	126
Figure 69: Comminution of the post-experimental micro CT scan, specimen Nr3, 2nd group.	126
Figure 70: The bone chip detached leaving some of the cortical bone intact, specimen Nr3, 2nd group.	127
Figure 71: Small incomplete fracture seen in the curve (a) and fracture mapping (b), specimen Nr.5, 2nd group.	127
Figure 72: Fracture lines up to 3mm, specimen Nr.5, 2nd group.	128
Figure 73: Fracture extension in post-experimental micro CT scan at the distal part of the specimen Nr.5, 2nd group.	128
Figure 74: a) Proximal and distal cuts almost parallel. b) The cuts were perpendicular to the longitudinal axis, specimen Nr5, 2nd group.	129
Figure 75: 2L + Crack type of the curve but showing several small incomplete fractures.	129
Figure 76: The fractures seen in the pre-experimental micro CT scan, specimen Nr. 13, 2nd group.	130
Figure 77: Proximal and distal fracture lines seen in the post-experimental micro CT scan, specimen Nr.13 in the 2nd group, the distal line was seen in pre-experimental micro CT scan.	130
Figure 78: a) 2L+Crack+FR fracture type of the curve. b) Fracture mapping, specimen 14,	

2nd group.	131
Figure 79: Brittle fracture. Note little signs of local bone damaging at the contact area.	131
Figure 80: a) Several drops in the force/displacement curve showing incomplete fractures. b) fracture mapping, specimen number 9, 3rd group.	132
Figure 81: Fracture lines in pre-experimental micro CT scan (a). The same fracture with greater displacement (b), specimen Nr.9, 3rd group.	132
Figure 82: Satisfactory alignment, specimen 9, 3rd group.	133
Figure 83: Comminution (black arrow) and a cortical fracture with communication (white arrow), specimen Nr.9, 3rd group.	133
Figure 84: Incomplete fractures seen in the force/displacement curve, specimen Nr.12, 3rd group.	134
Figure 85: Bony defect extending for about 3 mm at the proximal part of the specimen Nr.12, 3rd group.	134
Figure 86: A tiny fracture line seen on the opposite side, distal part, specimen Nr.12, 3rd group.	135
Figure 87: a) 5° Misalignment of the proximal and distal cut. b) Misalignment of the cut and the longitudinal axis, specimen Nr.12, 3rd group.	136
Figure 88: A small fragment seen at the distal part of the specimen Nr12, 3rd group.	136
Figure 89: Fracture line seen in post-experimental micro CT, specimen Nr.12, 3rd group.	137
Figure 90: a) Force/displacement curve and mapping (b) specimen Nr.14, 3rd group.	137
Figure 91: Proximal and distal cuts are parallel and aligned with the longitudinal axis, specimen Nr.14, 3rd group.	138
Figure 92: Pre-experimental bone damage, specimen Nr.14, 3rd group.	138
Figure 93: Extension of the fracture lines at the distal part of the specimen Nr. 14, 3rd group.	139

Figure 94: Fracture line propagating down from the metallic rod, specimen Nr14, 3rd group. It is interesting to note that this fracture line disperses laterally within the cortical bone at the very distal part of it.	140
Figure 95: A non-linear beginning of the curve (arrow).	141
Figure 96: Loading configurations: a) elastic behaviour, b) elastic behaviour with rupture, c) elastic-plastic behaviour with rupture. The curve d) represents a very initial part of an obtained curve (grey), theoretical calculated curve related to Hertz's theory (red dotted curve) and theoretical curve of linear behaviour (blue dotted curve).	142
Figure 97: Elastic non-linear behaviour. Adapted from [Wang16].	142
Figure 98: Example of Curve-fitted Graph of Experimental Data. a) Particular data set before reaching error <sup>2</sup> , b) Extended graph of experimental data with curve-fitted graph.	147
Figure 99: a) Custom made nail. b) Diagram of specimen orientation before embedding. c) The specimens were fixed and embedded in polymethyl methacrylate.	154
Figure 100: Drilling direction guide.	155
Figure 101: a) Group 1: locking screw was inserted perpendicularly to the axis of the nail and in the frontal plane. b) Group 2: locking screw inserted perpendicular to the axis but with 15° angulation the transversal plane. c) Group 3: locking screw was inserted in the frontal plane with 15° angulation to the axis of the nail.	156
Figure 102: Simplified diagram of local loading.	157
Figure 103: Diagram showing the way different parameters were assessed.	158
Figure 104: The shape of force-displacement curves have multiple fracture patterns. Scale adjusted.	160
Figure 105: Schematic representation on the nail and screw compression.	162
Figure 106: Lever arm diagram as the shear forces occur between the nail and the cortical bone.	163
Figure 107: Angles of interlocking screws.[Kuhno8]	164

Figure 108: Annual X-ray dose while performing femoral and tibial nailing depending on distance [Kesa12].	197
Figure 109: Annual cumulative X-rays dose depending on surgeon's experience [Kesa12].	203
Figure 110: Annual cumulative X-rays dose depending on surgeon's experience [Kesa12].	203
Figure 111: Annual cumulative X-rays dose depending on surgeon's experience [Kesa12].	203
Figure 112: Annual cumulative X-rays dose depending on surgeon's experience [Kesa12].	203
Figure 113: Annual cumulative X-rays dose depending on surgeon's experience [Kesa12].	203
Figure 114: Annual cumulative X-rays dose depending on surgeon's experience [Kesa12].	203
Figure 115: Annual cumulative X-rays dose depending on surgeon's experience [Kesa12].	203
Figure 116: Annual cumulative X-rays dose depending on surgeon's experience [Kesa12].	203
Figure 117: Annual cumulative X-rays dose depending on surgeon's experience [Kesa12].	203
Figure 118: Annual cumulative X-rays dose depending on surgeon's experience [Kesa12].	203
Figure 119: Annual cumulative X-rays dose depending on surgeon's experience [Kesa12].	203
Figure 120: Annual cumulative X-rays dose depending on surgeon's experience [Kesa12].	203

Figure 121: Annual cumulative X-rays dose depending on surgeon's experience [Kesa12].	203
Figure 122: Annual cumulative X-rays dose depending on surgeon's experience [Kesa12].	203
Figure 123: Annual cumulative X-rays dose depending on surgeon's experience [Kesa12].	203
Figure 124: Annual cumulative X-rays dose depending on surgeon's experience [Kesa12].	203
Figure 125: Cumulative doses received by orthopaedic surgeons performing minimally invasive or open surgery [Kesa12].	203
Figure 126: Medical exposure to ionising radiation.	205
Figure 127: Annual cumulative dose received by surgeon on his assistant to his eyes or forehead [Kesa12][Van098][Mill83][Harso5][Muza05].	206

## **Index of Tables**



Table 1: Distal locking hole displacement in literature.	60
Table 2: Trabecular bone parameters [Aers98].	72
Table 3: Elastic modulus and the bone tissue	79
Table 4: Yield Strength Values	83
Table 5: Experimental groups	98
Table 6: Curve types.	99
Table 7: Average values of different parameters classified by types of curves.	106
Table 8 : Average BV/TV, cortical bone width and cortical area	107
Table 9: Fracture propagation length and fracture score. The overall fracture propagation score was greater in a greater displacement group.	108
Table 10: BV/TV ratio in segments containing a fracture (seen in the microCT) in relationship with the fracture gap.	111
Table 11: Assumptions on Curve Fit Values.	144
Table 12: Summary of Data Obtained.	148
Table 13. Results of the compression experimentation of a locking screw.	161
Table 14. Calculated and obtained stiffness.	162



# **1. Introduction**

## 1. Introduction

The intramedullary nailing is one of the most common technique to fix broken long bones in the human body [Bart13][Lars15]. There are basically four parts of the human body where the intramedullary nailing can be performed : thigh, leg, arm, forearm. Sometimes, a similar and modified technique can also be applied for hands and feet. The intramedullary nailing technique is increasingly used not only in diaphyseal bone fractures but also around the metaphyseal areas. Indeed, it offers a relatively minimal surgical approach allowing to keep more of the soft tissues intact and thus accelerating recovery and overall functional outcome. Therefore because of technological improvements and evolution of surgical techniques the intramedullary nailing has gained popularity in orthopaedic and trauma surgery [Bart13][Lars15].

Despite the technological evolution and improvements made, some aspects of the intramedullary nailing still remains problematic. The intramedullary nail must be locked proximally and distally to maintain good longitudinal and rotational stability of the bone fixation. The locking is usually done applying locking screws : the screw passes through the bone and through the nail which is already in the intramedullary canal. The proximal locking can be done using an automatic aiming device as there is almost no deformation of the nail in the proximal area. This is not the case distally. The distal screws' locking holes shift as there is some bending when the nail is pushed into the intramedullary canal. The automatic mechanical aiming device cannot be used because there is a shift, therefore the most commonly used technique for distal locking is a freehand technique.

The **general purpose** of this work was to study the phenomena that take place around the distal locking screw and to analyse the interaction between the bone and the distal locking screw of intramedullary nail in order to better understand whether the position of the screw can have influence to the bone resistance and eventually to the fracture propagation if it occurs in the contact area. In order to achieve this goal work was

done in different directions resulting in several parts of this study.

First of all, an extensive literature review was conducted. This has allowed to evaluate the general context and different aspects related to the surgical techniques of a fractured bone fixation, x-rays, implants as well as bone mechanical properties and phenomena occurring during the bone damage and fracture propagation. Then, a broad experimental work was performed and presented in chapter 3 with the purpose to understand the local strain phenomena occurring at the interface between the bone and a metallic rod. It included medical imaging and compression. Medical imaging was used before and after the experimentation to obtain the bone geometry but also the bone density (with the BV/TV ratio), in all the segments under the surface that had undergone a local mechanical compression loadings at different quasi-static strain rates. This in vitro experimentation allowed to evaluate the influence of microscopic parameters to the phenomena occurring locally at the mechanical loading area which has allowed to relate them to the bone damage occurring due the local loading. The bone resistance and the fracture propagation under the metallic rod which is a simplified model of a locking screw was investigated. The data acquired following the medical imaging before and after the experimentation was evaluated in order to understand the influence of the cortical bone configuration but also the influence of the bone density to the bone resistance and fracture propagation. The recorded force and displacement curves were classified into several types and the relationship between them and different bone parameters were discussed. The bone substance density in different bone segments under the metallic rod was evaluated and its relationship with the fracture propagation was analysed.

The chapter 4 referred to another experimental work which approached the real conditions that take place during the mechanical loading of the intramedullary nail locking screw. Introducing some alignment error and comparing it to the reference where the screw is perpendicularly inserted to the nail permitted to evaluate the influence of the

position change to the strain and eventually the fracture propagation.

This has shown that a certain alignment error leads to an earlier system destabilisation. This has a potential clinical impact as the destabilised structure can end up with a secondary bone fragments displacement, deformity, fracture of the bone or fixation failure.

Further studies would be needed to evaluate greater error in distal locking screw direction, define what locking screw angle is acceptable, evaluate the effect of cyclical loading *in vitro* and *in vivo*.

## **2. Literature review**



## **2.1 Introduction.**

The aim was to better understand the problematics related to the intramedullary locking nails and the distal locking aiming techniques. Therefore, the following literature review addressed general aspects of bone fracture treatment, its economical and social implications, surgical techniques and intramedullary locking nails. The literature review also focused on mechanical properties of the cortical bone further synthesized for compression loading, fracture propagation patterns in cortical bone but also issues related to the bone healing and phenomena occurring at the bone/implant interface.

## **2.2. General context.**

Osteosynthesis is from the the Greek words “osteo” meaning “bone” and “synthesis” which means “combining separate materials or elements into a united entity” [Bart10]. The rapid industrialization in the 1900s has led to more trauma cases and thus faster and better options to treat bone fractures became a real necessity. The advancement in antiseptics, antibiotics, anaesthesiology, x-rays and biocompatible alloys, internal bone fixation became a suitable solution for doctors and patients. The first closed osteosynthesis using an intramedullary device was performed in the beginning of the 20<sup>th</sup> century by Georg Schöne (Fig.1.) [Bart10].

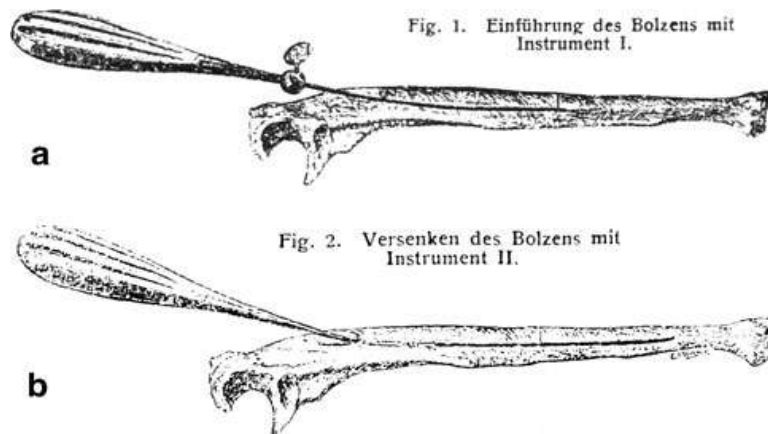


Figure 1: Beginning of intramedullary nailing [Bart10].

### 2.2.1. Intramedullary nailing.

Intramedullary nailing was previously not an accepted practice since it was thought to disturb the natural physiology of the bone marrow [Buhl19] until subsequent studies proved that periosteal blood supply can sustain the nourishment and physiological function of the bone. The advancement in flexible reamer technology enabled larger diameters of nails to be implanted into the intramedullary canal thus increasing stability by increasing the contact of the implant with the surface of intramedullary canal all throughout the length of the bone [Born14]. Interlocking screws assured the secure fixation of the nail inside the canal preventing it from longitudinal movement and rotation. A phenomenon called “stress shielding” was prevalent in the earlier nails because the loading forces passed through the nail, thus there was not much of physiological stimulation for bone to heal. The development of longitudinal slots allowed to introduce a slight movement of the nail inside the canal. This phenomenon is called “dynamisation” emphasized by Grosse and Kempf where the proximal part of the nail is fixed while the distal end is allowed to move freely.

### **2.2.2. Bone-compatible material.**

Besides the stainless steel, titanium is now the most widely used material in intramedullary nailing due to its toughness and its closer mechanical properties to the bone. However, titanium's mechanical properties remain slightly different from the bone [Lesi12].

Between nailing and plating, there is still some debate on which one is better to use on certain occasions and surgeon's preference is prevalent in those cases. Whilst, according to a study by Hu et al. [Hu19], the significant advantage of nailing was seen as there was less occurrence of malunion, acute superficial infection, better functional outcomes and less pain.

### **2.2.3. Long bone cases.**

The long bone osteosynthesis techniques are in permanent evolution. One of the techniques commonly used in Europe is to perform an osteosynthesis of the long bones is an intramedullary nailing. There are many advantages of this technique including an extra focal surgery, soft tissue preservation and anatomical accessibility.

#### **2.2.3.1. Femoral fracture.**

The global available statistics tend to show that the incidence of femoral diaphyseal fractures in Europe is 10/100,000/year [Bart13] and that intramedullary nailing is used in 54% of the cases, a plate and screw fixation is used in only 16% of the cases, the traction is used in 14% of the cases and external fixation accounts for 6% of the cases [Weis09]. Some older studies give a higher incidence rate that can be as high as 18.9/100,000/year for diaphyseal femoral fractures [Arne88]. The lower femoral fracture rates in recent years may be dependent on improvements in prevention of accidents and daily living but also in security improvements in case of motor vehicle accidents.

The fractures of some anatomical regions such as proximal femur traditionally treated by screw and plate fixation have now a tendency to be treated by intramedullary osteosynthesis [Yli12].

A study from Finland has shown that in 10 years between 1999 and 2009 the use of intramedullary nailing for the fractures of the proximal femur had almost 3 fold increase while the use of dynamic plate and screws has decreased two times [Yli12]. This is related to the introduction of modern intramedullary nails in Finland in 2005 – 2006.

The patients' age is quite variable and is gender dependent: median age at admission was found to be 67 (19–83) years. Men had a younger median age (27 years) than women (79 years). The female patients generated more admissions than male respectively 54% and 46% [Weis09]. The risk of femoral fracture was increased in men up to the age of 40 to 49 years and in women after 60 to 69 years. This is dependent on the mechanism of injury (high energy accident vs fall) [Weis09][Arne88]. This type of bimodal distribution (younger male in older female patients) is also described in another study evaluating femoral and tibial fractures [Bart13].

#### **2.2.3.2. Tibial fracture.**

The most injured long bone: incidence 14/100,000/year [Bart13] and 16.9/100,000/year (Fig.2.) [Lars15]. The incidence of tibial fractures can be very variable that might be due to regional differences, different time periods, different cultures and a lack of complete population observation [Lars15]. Males are more commonly affected (21.5/ 100,000/year), and the average age is 37 years with the highest frequency between the age of 10 and 20. Whereas women have a frequency of 12.3/100,000/year and have the highest frequency between the age of 30 and 40 [Lars15]. Although there is also a bimodal distribution as the mechanism of trauma is different. Those fractures at a later age are more related to osteopenia and osteoporosis. The mechanisms of injury and the energy of trauma are different in those 2 groups.

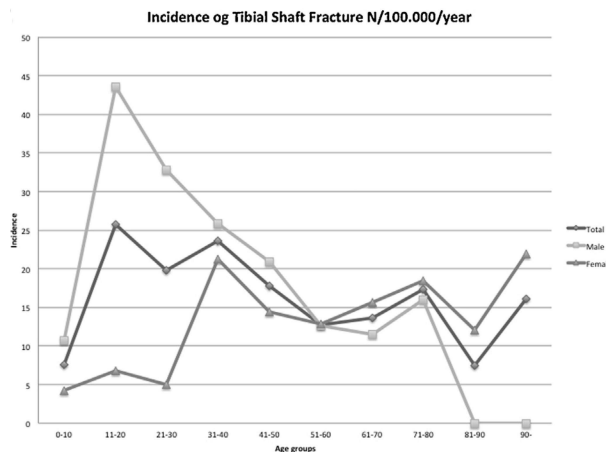


Figure 2: Incidence of tibial fractures [Lars15].

### 2.2.3.3. Peri-trochanteric and hip fractures.

Peri-trochanteric fractures are also often treated with short or long intramedullary nails. As the complexity of fractures at the proximal part of femur increases, the proportion of intramedullary nails is increasing, and the use of long versus short nails. [Matt18]. The intramedullary nails (short or long) were used 60% of cases as opposed to a plate with sliding hip screw that was used in 37% of cases [Matt18]. The total number of hip fractures in men and women in 1990 was estimated to be 338,000 and 917,000 respectively, a total of 1.26 million. As the incidence of hip fractures increases in ageing population and as the frequency of the intramedullary fixation itself increases as well, this surgical technique used for hip fractures can reach 2.6 million by the year 2025 worldwide, and 4.5 million by the year 2050 [Matt18].

The incidence of hip fracture varies considerably between different populations [Bjørø7]. An incidence of 1024/100,000/year for women over 50, and 452/100,000/year for men over 50 was reported for Norway between 1998 and 2003 [Bjørø7]. The extra capsular fractures account for about 40% [Quea14]. The relative proportion of extracapsular fractures also varies between 39% to 48% [Kara96].

This adds about 1 million patients/year by 2025 that could be treated by

intramedullary nailing in addition to femoral and tibial diaphyseal fractures.

#### **2.2.4. Conclusion.**

The long bone fractures are frequent. They are most often treated by intramedullary nailing. Though the numbers of diaphyseal femoral fractures in general population are declining due to improvements in transports security, the need to use the intramedullary nailing technique increases as this technique is more and more used to treat proximal femoral fractures which are frequent in ageing population and are especially related to osteoporosis.

Tibial fractures are also most often treated with intramedullary nailing techniques. This is the most frequently injured long bone the human body.

With constantly increasing numbers with increase of worldwide population, its ageing and technological developments allowing more frequent use of this technique, the use of intramedullary fixation in treatment of long bone fractures will remain very common and will continue to have an important impact on social and economic evolutions of modern society.

### **2.3. The bone development and healing at the bone/implant interface.**

#### **2.3.1. Bone formation.**

During the osteogenesis the bone formation starts within several weeks of gestation and continues in post-natal period until mid-twenties. Two ways how the bone tissue develops have been distinguished: intramembranous ossification, when the mesenchymal

tissue transforms directly into bone and endochondral ossification, when the cartilaginous tissue is replaced by the bone cells osteocytes [Gilboe]. Those different ossification patterns are observed in different anatomical regions, e.g. the skull undergoes an intramembranous ossification while endochondral ossification is typical for long bones (Fig.3.).

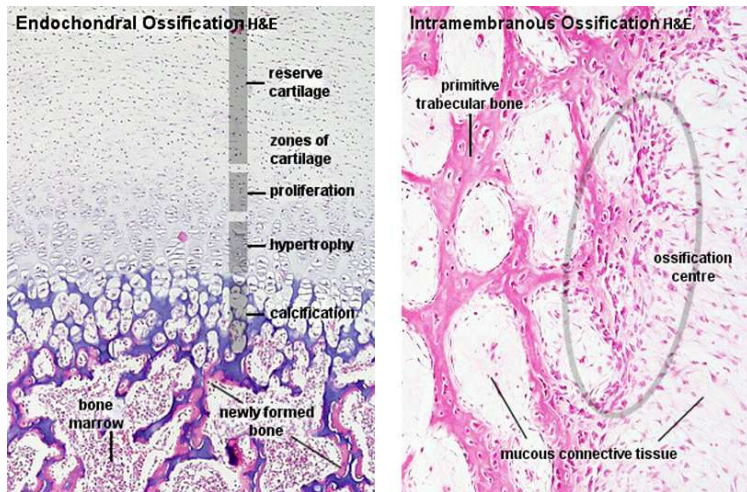


Figure 3: Endochondral and intramembranous ossification [Hill20].

During the endochondral ossification the ossification spreads towards the extremities from the centre of the long bone. When approaching the extremity the ossification meets the proliferating chondrocytes (cartilaginous cells) that form a growth plate allowing the bone to grow. This growth plate closes at a different age depending on the bone.

### 2.3.2. Bone healing.

Similar phenomena of ossification take place when the bone is healing. After the bone injury the fracture haematoma transforms into a granulation or scar tissue. The intramembranous ossification is seen as the osteoblasts at the periosteum start producing

the bone tissue. Adjacent to those areas undifferentiated mesenchymal cells later can be observed. As they proliferate, they start developing histological features of chondrocytes that produce the cartilaginous inter-cellular substance. Subsequently this area undergoes ossification to end the bone healing process [Bola92].

### **2.3.3. Bone remodelling.**

It is important to note that the bone substance formation is very closely related to its continuous transformation and remodelling. For the bone to remodel it has not only to undergo an osteogenesis but also some bone destruction. This is performed by osteoclasts, cells migrating from the blood vessels [Mano59] and capable to destroy the bone tissue if needed. The bone tissue permanently undergoes some resorption and reconstruction that is why it can remodel and get adapted to occurring strains and changing conditions. This allows the bone to develop, e.g. increase in diameter of a long bone as it undergoes some resorption of the inner part which is then replaced by bone marrow and a new formation of the bone tissue at the outer regions of it.

This remodelling also occurs as a result of bone reaction to strain improving its mechanical properties and increasing its resistance to mechanical load [Cart87][Lany85]. In fact, the bone is a mechanosensitive tissue and has an ability to react to mechanical stimuli. It can reshape in response to mechanical stimuli [Glat17]. It has been shown how the repetitive stress and strain in the bone can induce the cell proliferation, cell differentiation from mesenchymal tissue to bone, cartilage, or fibrous tissue. Intermittently imposed loading and the repetitive tensile forces would generate ossification. Hydrostatic compressive stress and high tensile strain is a stimulus for cartilage formation which later can undergo endochondral ossification [Cart98]. Similar phenomena take place during bone healing where the bone remodelling is an important phase [Orya15].

#### **2.3.4. Osteo-integration.**

This phenomenon also applies to the interface implant/bone [Loi16] and thus the interface between the locking screw and the bone. A surgical bone lesion takes place when the locking screw is put during the surgical procedure. Then the bone starts healing around it, but as the implant is still in place, and there are some strains passing through the locking screw it can be seen as a continuous bone sollicitation. Depending on the extent of this sollicitation it can become a bone growth stimulation or a continuous bone lesion if the micro-damage overcomes the bone regeneration capacity.

If the balance between the osteoblast and osteoclast activity occurs and if the attachments between the implant and the bone are established – an osteointegration takes place. This represents a foreign body equilibrium around the implant [Loi16].

If there is no equilibrium around the distal locking screw, the bone reconstruction around the screw may not be sufficient so the cyclic strain would cause a progressive resorption around the screw and loosening of it [Zell18]. It does not always compromise the overall fracture healing as a slight implant migration may enhance the compression and a better fragment contact at the fracture sight and enhance healing. However if the fracture is comminuted, i.e. with no longitudinal stability, this may lead to a complete fixation failure.



Figure 4: Distal locking screw failure. A) screw loosening and backing out. B) screw rupture [Wild20].

The biological and biomechanical phenomena occurring at the interface of the locking screw and the bone can involve either the bone resorption and screw loosening [Zell18] or the screw itself which can break [Whit95] due to repetitive strain (Fig.4.). This depends on many factors including the bone stiffness, its regeneration capacity, the fracture pattern and the mechanical resistance of the screw.

It has been shown that the locking screws can fail in up to 6% to 14% of the cases. Both proximal and distal locking screws can undergo failure. It is much more common in unstable fractures [Whit95]. A study [Grifo9] has shown that the average locking screw would not survive 1200 cycles of 2400N of peak loading. This study has evaluated the mechanical parameters of screws, not taking into account the screw/bone interface nor the bone biomechanical parameters.

### **2.3.5. Conclusion.**

The bone tissue is a tissue that has a capacity to react to mechanical stimuli and to reconstruct and remodel accordingly. This is related to a constant bone resorption by

osteoclasts and a bone substance production by osteocytes.

The biological phenomena occurring at the bone injury site resemble the osteogenesis during the healing process. This involves a haematoma transformation into the connective tissue and bone passing through a cartilaginous tissue phase in some cases.

There are some similarities of the bone reconstruction around the implant, e.g. the locking screw of the intramedullary nail. If the mechanical forces and reconstruction capacities of the bone are in equilibrium, there will be a normal course of bone healing at the fracture site, but if a disbalance occurs – the locking screw can become loose or break.

## **2.4. Surgery related problematics.**

The experience shows that a fracture fixation can be a real challenge to the orthopaedic trauma surgeon. The fracture configuration is always different and this needs to be specifically addressed. Therefore surgical techniques needed to be adjusted and adapted to every fracture. However, fractures are often treated in an emergency setting with a limited preparation time for such a surgery. The fracture treatment can be quite challenging especially if the surgical procedure is long, if it requires the position changing and involves several anatomical areas (e.g. polytrauma patient). That is why surgical technique and innovative technology that allows to shorten the surgery time, facilitates the use of instrumentation and improves the fracture fixation are extremely welcome.

### **2.4.1. Fracture treatment**

Fractured bones sometimes give some sequelae including such functional impairment as adjacent joint stiffness, pain, malalignment and deformity. A special care must be accordingly taken while treating bone fractures to restore the anatomy and make

the fragments heal in the best possible position and ideally – in the anatomical position. Several parameters are important to consider: the axis, the length and the joint surfaces' congruity and orientation in space. The fracture configuration can be very different ranging from a simple non-displaced fracture to comminuted, displaced, articular and unstable fractures.

### **2.4.2. Fracture treatment options.**

In order to treat bone fractures, the orthopaedic (Fig.5.) treatment is to immobilise the fractured limb for a certain period of time until the bone heals. It is indicated when the fracture is stable, non-displaced or with a small displacement and when this type of treatment would not result in a marked stiffness.



Figure 5: Orthopaedic treatment.

For a relatively small number of fractures , there is also a functional treatment (Fig.6.) when the bone heals itself because it doesn't need any immobilization or fixation, or the previous technique could not be implemented due to anatomical location [Sarm76]. Sometimes, immobilization is temporarily prescribed for pain relief. The percentage of bone healing is satisfactory while surgical procedure would expose the patient to some unnecessary risks.



Figure 6: Functional treatment.

For the other fractures, there are several types of surgical treatment: external and internal fixation. The external fixation consists of an external fixation device that remains outside of the body and holds the pins that are inserted into the bone through the skin. It enables to reduce the fracture, realign fragments but also sometimes to start mobilizing the limb quite early or sometimes they can be kept until the bone heals. The external fixators are often implemented when there is a marked soft tissue damage, bone, skin or other soft tissue loss which will later need reconstruction procedures. For polytrauma patients, external fixators (Fig.7.) stabilize multiple fractures while limiting the surgical injury known as “damage control” attitude. This allows to treat the patient rapidly and after the patient is stabilized, several days later adapt the best definitive treatment. The inconvenience is that the external fixation is exterior to the body and thus there is some risk of infection. It is also somewhat bulky and requires some adjustments in daily living. It doesn't always allow weight bearing.



Figure 7: External fixation device.

There are several types of internal fixation. Two major groups can be distinguished: screw and plate fixation and intramedullary fixation. The best surgical indication to use the plate and screws would be an unstable but not very comminuted fracture. As far as the screw and plate fixation is concerned, some dynamic compression (compression is achieved between fragments while tightening the screw) can be used while utilizing the plate holes' geometry (Fig.8.). The stability depends on the applied force of the plate against the bone. The advantage of this compression plate fixation is that the bone fragments can be compressed in way that it would allow a better bone healing.

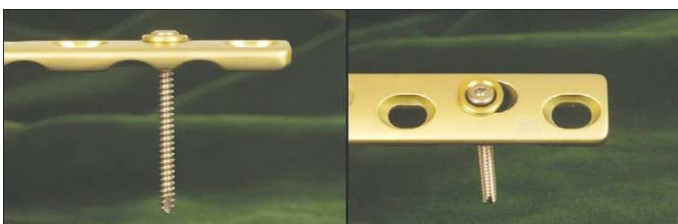


Figure 8: Dynamic compression plate.  
[www.aofoundation.org](http://www.aofoundation.org)

There were some important developments in recent years with appearance of

locking plates. They are used for internal fixation especially when the fracture is not very stable as they allowed to lock the screw into the plate which means that they will function as a mono-block: i.e. there is no movement possible between the plate and the screw after it is locked (Fig.9.). The best surgical indication for such locking plates would be comminuted, displaced fractures and sometimes fractures having bone substance loss but above all it would be unstable articular fractures that require to obtain the perfect joint surface alignment and congruency. The locking and dynamic compression plate features can be combined in one fixation device.

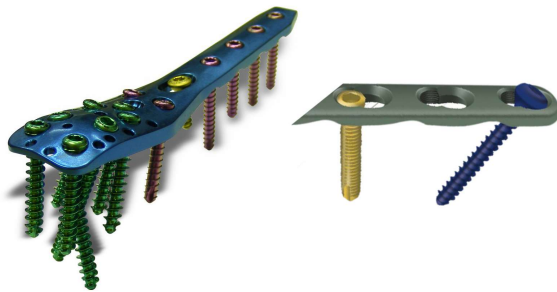


Figure 9: Examples of locking plates.  
[www.aofoundation.org](http://www.aofoundation.org)

The drawback of plate and screw osteosynthesis is a relatively large surgical approach, a fragment exposure that could eventually cut the blood supply to them and thus compromise the bone healing. Different anatomical layers must be crossed which puts these structures at risk of a lesion and if an excessive scarring occurs it can give a marked joint stiffness. When the fracture itself is exposed, fracture haematoma is evacuated. This haematoma is known to contain many active substances such as growth factors that would lead to quicker and better bone healing [Bola92] (Fig.10.).

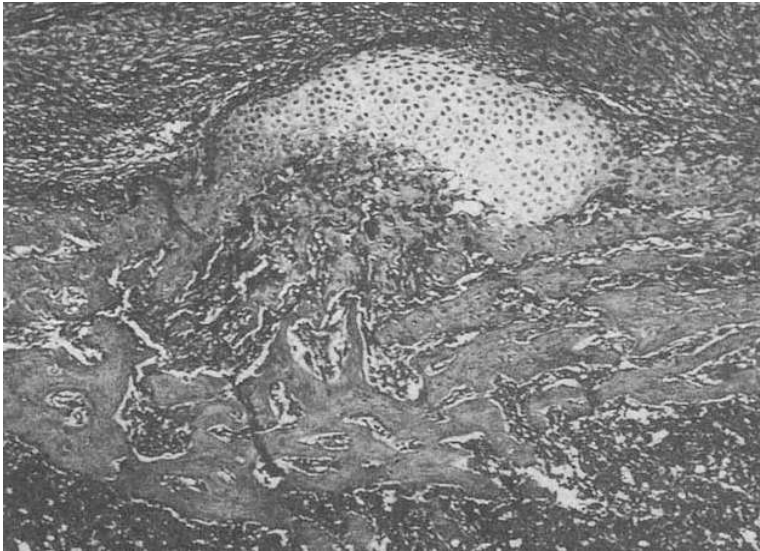


Figure 10: Importance of the fracture haematoma: cartilage cells that will later undergo ossification can be seen after 4 days following the subperiosteal injection of a TGF- $\beta$  (usually present in fracture haematoma) at a non fractured rat femur [Bola92].

There are some specific devices that allow to put the plate under the soft tissues without widely detaching or dissecting them. The plate is then fixed by screws percutaneously using specific guides. However, the plate is not in a good contact with the bone and the surgical technique doesn't always allow to reduce the fracture perfectly that is why it is considered as a kind of an internal fixator (Fig.11.).

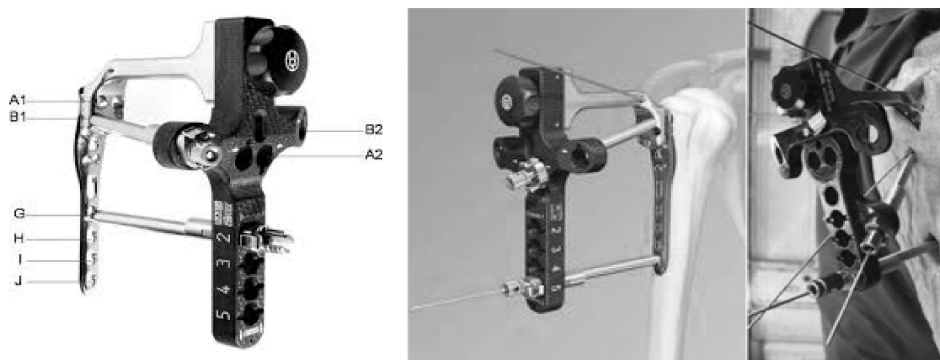


Figure 11: “Internal fixator”. [www.aofoundation.org](http://www.aofoundation.org)

Several other types of plates can be distinguished in relationship to how they work: neutralization plate (Fig.12) neutralizes the forces of torsion or bending while the fragments are fixed by inter-fragmentary screws; support plate stabilises fragments by not allowing them to move without fixing them by a screw; sliding screw plate, etc.

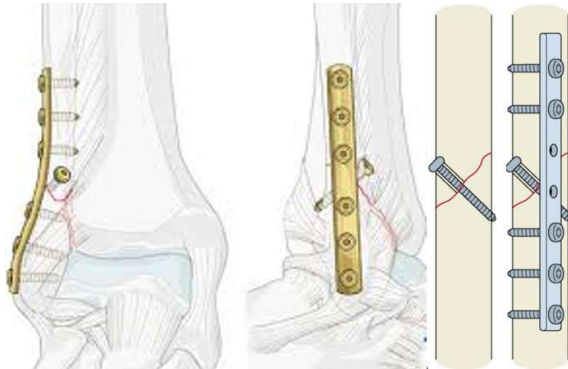


Figure 12: Example of a neutralisation plate. [www.aofoundation.org](http://www.aofoundation.org)

The intramedullary nailing is one of the most often used techniques for long bone fixation. It is a fixation device that is put inside a long bone into the intramedullary canal. It is usually locked proximally and distally with locking screws for stability. The intramedullary nail can be cannulated which is the most common type these days (Fig.13). This allows to use a special guide and reaming which lets better adapt the nail's diameter to the intramedullary canal and better contact with the cortical bone. The intramedullary nail can be put in the proximal to distal direction and vice versa.



Figure 13: Full and cannulated intramedullary nails.  
[periodictable.com/Items/022.4/index.html](http://periodictable.com/Items/022.4/index.html)

There are several parts of intramedullary nail: the proximal part where the handle and the impactor can be fixed. The proximal locking can be done through the holes in the handle using some drill and screw guides (Fig.14). The right position has to be found under the C-arm to lock the nail in relationship with anatomical landmarks. The middle part of the nail is the longest part and corresponds to the bone diaphysis. It is usually slightly curved to be adapted to the shape of the bone. There are holes for distal locking screws in the distal part. The holes can be situated in the frontal and sagittal planes and allows to lock the nail in several directions if needed.

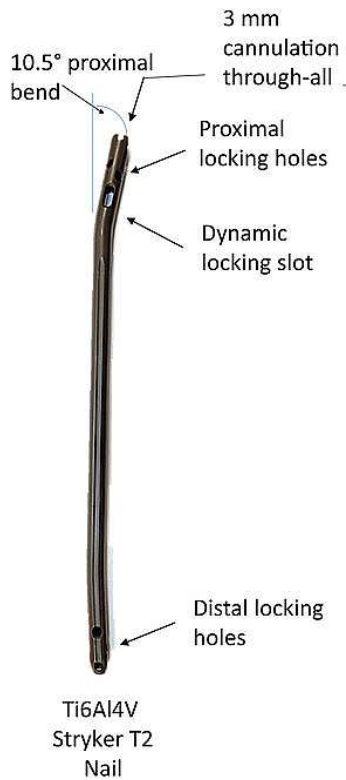


Figure 14: Parts of the intramedullary nail. (Adapted from [Hedg17]).

In most of the cases anterograde nail is used but sometimes a retrograde nail can be used in certain circumstances. The difference between the anterograde and retrograde (Fig.15) nailing is defined by the direction they are put : anterograde nail is put from proximal to distal direction, and retrograde – from distal to proximal. The surgical technique as well as challenges are similar. The choice between the two types is made in relationship with anatomical area.



Figure 15: Retrograde nail.  
[www.aofoundation.org](http://www.aofoundation.org)

The advantage of this internal fixation technique is a minimal surgical approach, absence of the fracture site exposure that allows to keep the fracture haematoma [Kola10] and preserves the biological factors that would enhance bone healing. The fragments are not dissected and exposed therefore the remaining blood supply not altered by the trauma itself stays intact enhancing the possibilities to heal in good conditions.

The inconvenience of this bone fixation method is that this is an extra focal fixation and that the surgeon cannot very well control the fragments' position and has to manipulate them while using external manoeuvres, traction or other indirect means in order to put them in a suitable position. The fracture reduction may not therefore be perfectly anatomical. There is no possibility to see and control other anatomical structures such as nerves, blood vessels, muscles and tendons while reducing the fracture. Then there might be interposition of these structures between the sharp bony fragments. This risk of damage needs to be evaluated before the surgery. The intramedullary nailing allows to align fragments but the rotations and the length control can be somewhat difficult and sometimes the surgeon must refer to the contralateral bone in order to obtain the measurements and to perform an appropriate fixation. If the fracture is not very

comminuted, the axial stability will be controlled by the direct contact between the fracture fragments and would allow immediate weight-bearing. In most cases this rotational and length control is insufficient and that is why the proximal and distal locking are necessary.

The intramedullary nail must not be extremely rigid as it must adapt its shape to the individual anatomy of every patient. It undergoes some deformation while it is being pushed down the intramedullary canal, allowed by the distal locking screw holes shifting. Due to the shifting distal locking holes, as the only external contact zone with the nail is at the proximal part of it, automatic distal locking using guides is not possible . Several surgical techniques exist and the most common one is a freehand locking when the surgeon is using x-rays in the operating theatre. Under x-rays the surgeon determines the position and direction of the locking hole, he has to drill through it and to put an appropriate screw in it. This can be easily done by an experienced surgeon but is sometimes time-consuming. The patient and the surgical team are exposed to ionizing radiation which can cause some specific health issues. Moreover, while attempting to drill and to put the locking screw through the distal locking hole, the bone around it can be damaged thus compromising the stability, the fragment position and the possibility of anatomical healing. Nowadays, there is a lack of understanding about the biomechanical behaviour at the interface between the bone and the distal locking screw and the risk of the potential bone damage that can arise because of malalignment of this screw.

## **Conclusion.**

There are many ways to treat a broken bone. This includes surgical and orthopaedic or non-surgical techniques. All of them have their advantages and drawbacks. One of the most commonly used technique of the bone fixation is the intramedullary nailing. The advantages of this technique include the limited exposure and thus, less soft tissue damage, preservation of haematoma in the fracture area containing growth factors which

improves the fracture healing. It almost always requires proximal and distal locking. While proximal locking can be easily done using aiming devices attached the proximal part of the nail, the distal locking is more complicated as the locking holes shift because of deformation of the nail. The distal locking is most often achieved using a free hand technique.

## **2.5. Surgical technique of intramedullary nailing and nail related problematics.**



Figure 16: Choosing the entry point that would allow good nail alignment inside the bone. [www.aofoundation.org](http://www.aofoundation.org)

To perform an intramedullary nailing the patient's positioning is key as the position would allow to reduce the fracture and have an comfortable accessibility to the entry point of nail (Fig.16). Very often the surgeon has to use a traction table. The reduction is performed at the same time as the intramedullary guidewire is being put into the medullary canal (Fig.17). It is done by external manoeuvre as the guidewire has to go into the distal fragment's medullary canal. Then the reaming can be achieved. This allows

to increase the intramedullary canal's diameter which enhances a better nail and cortical bone contact and to have less resistance when the nail is put into the medullary canal.

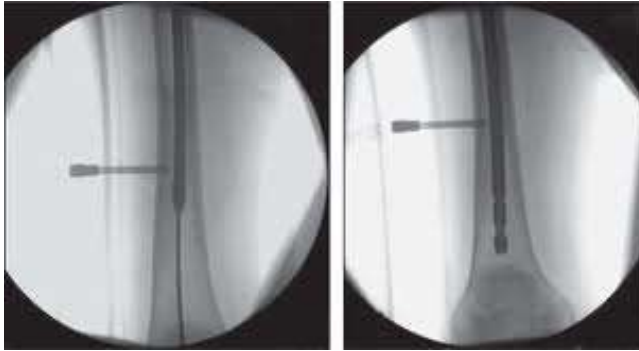


Figure 17: A guidewire put an the medullary canal with the reamer and the nail.

The reaming guidewire has a slightly different shape and has to block the reamer at the end. It has to be changed and replaced by another guidewire before the nail is put in the medullary canal when the reaming is done. The nail can be put over the guidewire and its position and length is controlled by the C-arm using x-rays. When the suitable position is found, the guidewire is taken away and the proximal locking can be done. It is done using a guide handle that is attached to the proximal part of the nail (Fig.18). This can be easily performed as the deformation of the nail is negligible at this area. Therefore locking holes are not shifted.

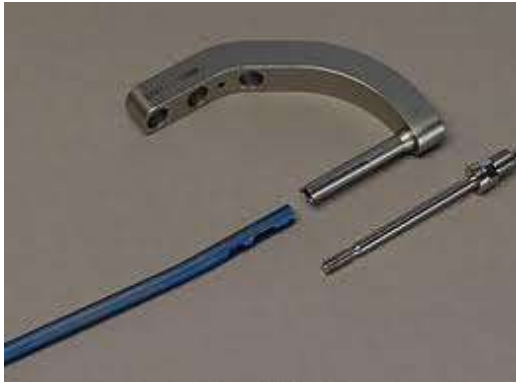


Figure 18: Nail and guide handle.

[www.aofoundation.org](http://www.aofoundation.org)

The situation is different for the distal locking as the distal locking holes (Fig.19) are shifted and no automatic locking is possible with a simple guide handle attached to the nail.

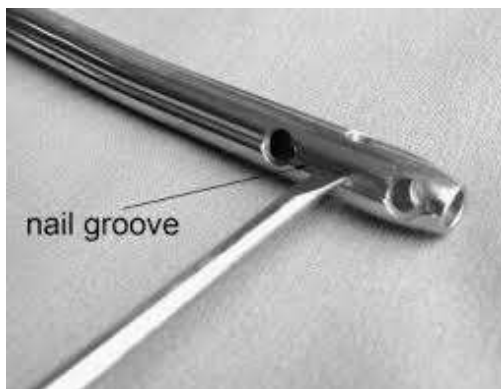


Figure 19: Distal locking holes.

### **2.5.1. Nail related problematics.**

The intramedullary nail cannot be very rigid as there is a risk of intraoperative fracture during insertion. The nail's shape and elasticity allow to adapt to the individual anatomy of every patient.

On the other side, the intramedullary nail used for osteosynthesis has to be sufficiently

solid in order to allow the early mobilization of the limb and to withstand certain strains as walking and weight-bearing.

Intramedullary nails are usually made of steel or titanium. The Young's modulus of bone is about 20GPa and the Young's modulus of titanium is between 110GPa and 114GPa [Guo09][Inam05]. The Young's modulus of steel is 200GPa. This difference in Young's modulus exposes the bone to the risk of a fracture during the surgical operation. The implant deformation is bigger for new bone similar alloys, such as titanium Ti2448, which Young's modulus of this alloy is 42 GPa [Guo09].

This intramedullary nail undergoes some deformation which is can be significant and may shift the distal locking holes by several centimetres. The observed deformation depends on how the implant matches the bone. A study that has evaluated almost 1000 femurs has found that there is quite a big mismatch between the shape of the femur and the femoral nails present on the market [Egolo4]. The study has evaluated the relationship of the radius of anterior convexity of the femur and the radius of the implants. They have found out that the average radius of the femur was 120 cm ( $\pm$  36 cm) and didn't depend on age. It depended on ethnic origin. The authors have found that the radius of anterior convexity of the intramedullary nails ranged from 186 to 300 cm, which means that they are much straighter and will undergo a substantial deformation while being put into the medullary canal [Egolo4]. This can also sometimes be a cause the anterior cortical bone fracture distally (Fig.20) [Egolo4].

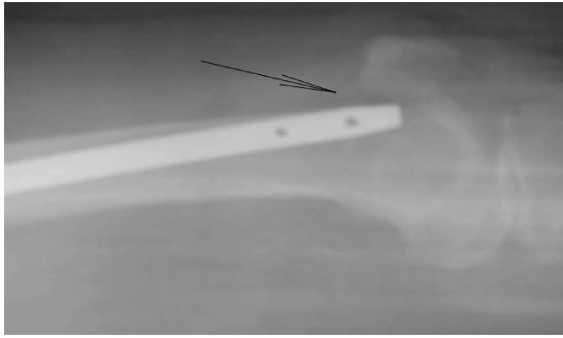


Figure 20: Fractured anterior cortical bone the distal femur [Egol04].

Studies have been made to evaluate the deformation of tibial and femoral nails in order to evaluate the lateral and dorsal translation and rotation around the longitudinal axis of the distal locking holes [Kret97\_1][Kret98]. The findings are summarised in the Table 1. Attempts to predict the displacement and the position in relationship with anatomical landmarks have been made. Radiographic-morphometric analysis was used for this purpose: distance between the distal locking holes and the anterior cortical bone was measured [Kret97\_2].

The authors concluded that the usage of the guide handle to lock the nail distally was impossible and found this locking technique insufficient. The variability of the position of distal locking holes shown in these study suggests that the distal locking based on the hypothetical position of the locking holes in relationship to anatomical landmarks can be difficult even though this method can give some value in predicting the position. The studies showed that the displacement of the distal locking holes was greater in femoral nailing. This is probably related to the anatomical differences but also to the greater length of the intramedullary nail and the greater stiffness of the femoral bone compared to the tibia. These studies explain the difficulty to perform the distal locking of the intramedullary nail. This is the reason why the automatic locking using a guide handle attached to the proximal part of the nail doesn't allow to be confident in locking as this

locking device doesn't take into the consideration the deformation of the intramedullary nail.

Table 1: Distal locking hole displacement in literature.

Study	Bone	Tested feature	Locking hole dorsal displacement	Locking hole lateral displacement	Torsion
Krettek et al. 1997. [Kret97_1]	Tibia	Locking hole displacement	7.8+/-5.8 mm	4.5+/- 3.5 mm	0.3+/-0.7°
Krettek et al. 1997. [Kret97_2]	Tibia	prediction of the position of distal locking holes in relation with anatomical landmarks	Range 14.3mm	Range 19.2mm	“minimal”
Krettek et al. 1998. [Kret98]	Femur not cannulated 9mm nail	Locking hole displacement	3.1 mm+/-4.3 mm	18.1+/-10mm	0.1°+/-0.2°
Krettek et al. 1998. [Kret98]	Femur cannulated 13mm nail	Locking hole displacement	0.4 mm+/-9.8 mm	21.5+/- 7.9mm	10°+/-3.1°

## Conclusion.

Surgical technique of intramedullary nailing requires good knowledge of anatomical landmarks as well as meticulous preoperative planning which includes the position of the patient, the eventual use of the traction table, position of the C-arm and good surgical skills.

The proximal locking can be performed relatively easily using the aiming guides attached to the nail. There are some difficulties to perform the distal locking of the intramedullary nail as the locking holes shift while the nail is put into the intramedullary canal. This is related to the nail and the bone discrepancies as well as the nail elasticity and plasticity. The prediction of the position of the distal locking holes is difficult as there is

quite a big variability. This is most commonly done using a free hand technique which requires certain experience and skills. This technique can be done relatively easily by a skilled surgeon but it can be very difficult for the beginner as the learning curve can be relatively long.

### **2.5.2. Distal locking. Existing aiming techniques.**

The most frequently used surgical technique for the distal locking is a freehand technique (Fig.21) that rely on the C-arm and x-rays in order to situate the distal locking holes. The surgeon must put the drill bit in front of the locking hole and in the centre of it. When x-rays are done, the aspect of the locking hole must be round. This indicates that the x-rays are perpendicular to the nail and parallel to the locking hole. This allows the surgeon to put the drill parallel to the beam of the C-arm and the find the needed direction to drill. No x-ray can be performed while the drilling device or the hand of the surgeon are in field, due to shadow, that would make the locking hole no visible. So the final direction of drilling is chosen in relationship of the C-arm position. The drilling direction has to be in line with the tube. The advantage of this technique is that there is no need to use any other specific device.

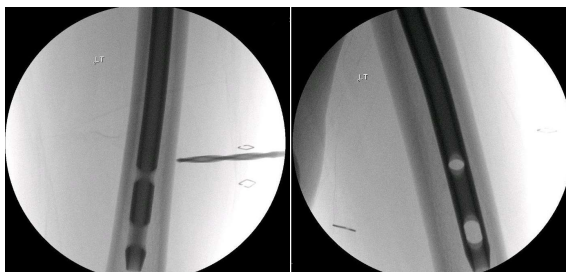


Figure 21: Freehand technique.

In order to reduce the human experience dependant errors, an “H” - shape guide

has been proposed (Fig.22). An outside identical intramedullary nail is put in parallel to the intramedullary nail already put inside the bone. This technique allows to situate the holes longitudinally but doesn't take into account any translation or rotation of the nail as it undergoes some deformation while being put in the intramedullary canal [Ster96].

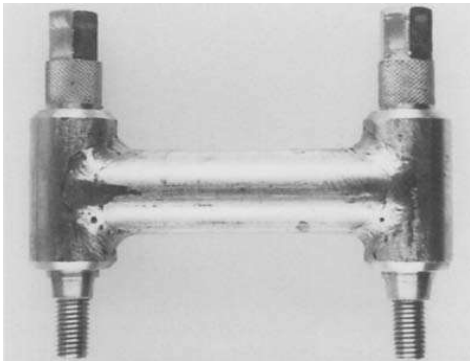


Figure 22: "H"-shape guide.

Another guide - a shifted guide has been proposed to more easily find the second hole (Fig.23). When the position of the first locking hole is found, the drill is kept in the whole and the shifted guide is mounted on the drill. This allows to find the second locking hole as the distance between the two holes is maintained. The surgeon still has to find the locking hole in the defined plane [Hash94].

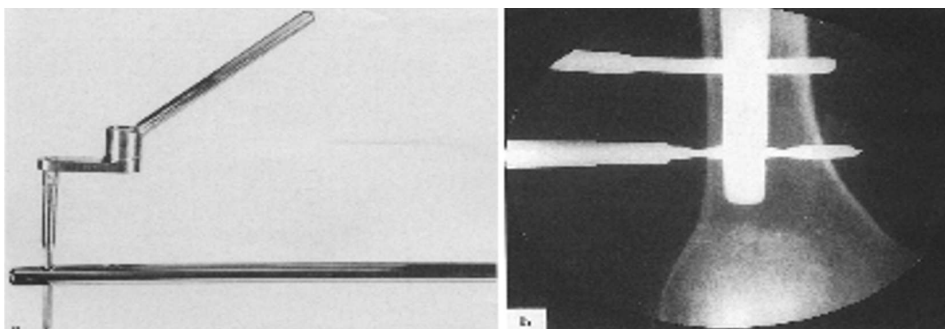


Figure 23: Shifted guide.

Two different mechanically stabilised guides have been proposed. One of them is fixed to the operation table. The operating technique requires to find the first locking hole

and centred (Fig.24) [Arleo8]. Then the aiming device is firmly fixed which allows to put in the remaining locking screws.

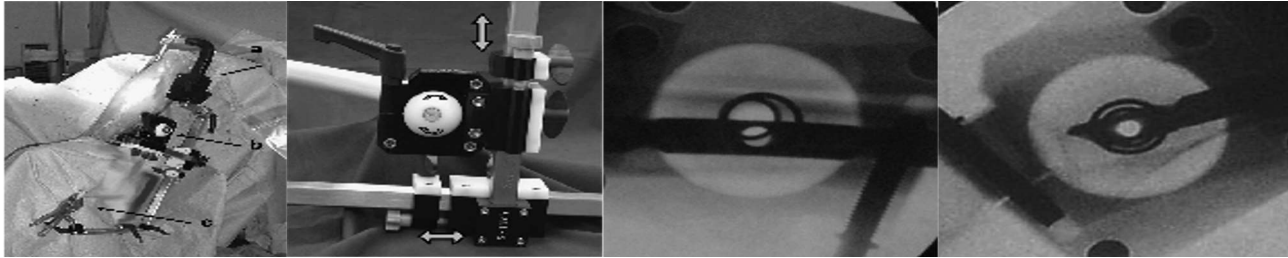


Figure 24: Stable guide, fixed to the operating table.

Another mechanically stabilized guide (Fig.25) [What06] is attached to the proximal and the distal part of the nail forming a rigid aiming device. The first locking hole is found using x-rays, after what the guide is fixed to the nail and stabilized. The drawback of those procedures is that one still has to use x-rays, when the first hole needs to be found. It resembles the freehand technique for the first hole where the guiding device will be fixed, and only then the surgeon is able to use an automatic locking. Finding of the first locking hole still requires the usage of x-rays which is finally very similar to the freehand technique.



Figure 25: Mechanically stabilised guide.

An experimental surgical technique using navigation (Fig.26) has been described as well [Micho8]. This is a computer assisted surgical technique where the sensors are put to identify the position of the bone (the shape of the bone identified beforehand by a CT scan). The direction of the fixation device can be guided by computer. The experimentation has shown some improved aiming of the locking holes. Nevertheless, this technique has some drawbacks including the sensor positioning, the error related to the position of the sensors and the definition of anatomical landmarks where the sensors have to be put. This difficulty occurs as the bone which has to be fixed is fractured so the bone fragments can be mobile as they lose contact between them and the anatomy is no longer normal.



Figure 26: Navigation. Experimental setting.

An improved freehand technique assisted by computer has been described (Fig.27).X This technique is similar to navigation, but does not attempt to identify the shape on the bone and its landmarks, but instead, while doing X-rays, it attempts to position a guide perpendicular to the locking hole. The computer shows the position while the surgeon manipulates the drill and the screw. It allows to limit the x-rays that is used to check and confirm that the chosen position of the guide is right. While using this technique there is an inconvenience that the guide is not stabilized, therefore when the position was found, the guide can still continue to move making the aiming somewhat inaccurate.

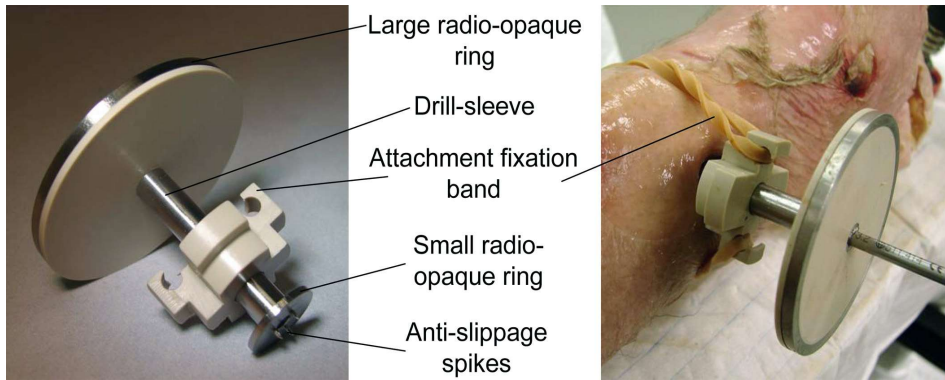


Figure 27: Computer assisted freehand technique.

There is a technique that uses the electromagnetic waves [Lang13] (Fig.28). This technique allows not to use x-rays. While using this technique, the surgeon puts a probe inside the nail which is attached to the computer. It allows a better positioning of the locking guide and a shorter operation time (Fig.29). It is a promising technique, however the authors describe some missed screws using this technique.

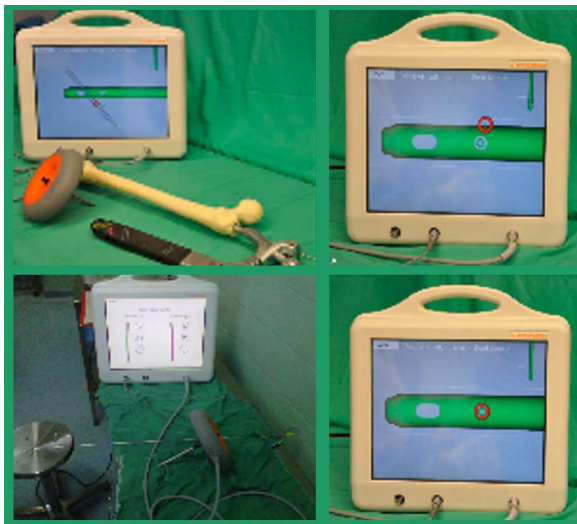


Figure 28: Device using electromagnetic waves.

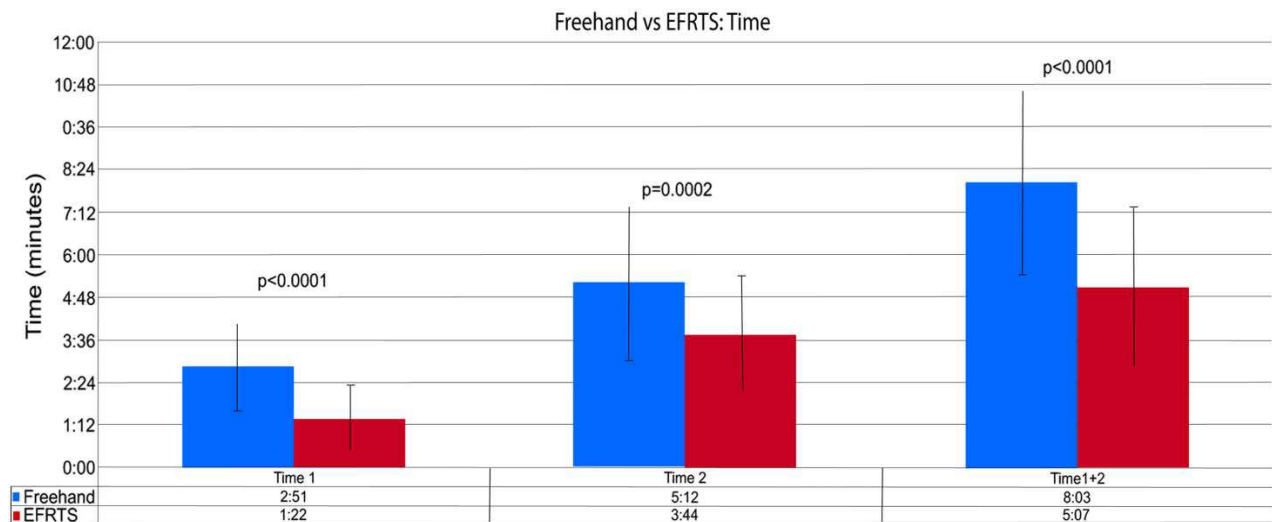


Figure 29: Time gain using the electromagnetic wave assisted in comparison to the freehand technique.

## Conclusion.

There are many different techniques to lock the intramedullary nail distally. They all have their drawbacks and advantages. The most frequently used technique is a free hand technique. Others either do not work very well or still must prove their efficiency.

The multitude of the aiming techniques described show the lack of superiority of one of them except the free hand technique which is seen to be the best at this stage. Nevertheless, this technique exposed the patient, the surgeon and the operating room personnel to ionising radiation that can cause potential health issues. The problematics related to ionizing radiation is more developed in Annex I.

## 2.6. Cortical bone density, strength, mechanical parameters and fracture propagation.

Mechanical strength of the bone is determined by the amount and properties of mineral substances (apatite) and organic matrix and their organization [Bosk99]. The

collagen fibres are very important to the bone strength. It has been shown that bone fragility can occur if there are some changes in collagen's biochemical structure and the fibres' cross-linking [Bail92], [Oxlu96], [Kowi97].

The genetic predisposition is an important factor for the bone strength and the bone mass [Smit73], [Poko87], [Dequ87], [Sowe86]. The twin studies [Smit73], [Poko87], [Dequ87], as twins have identical genetic information, have shown that there was no difference in the bone mass in homozygous twins but there was one in heterozygous twins. In another study that has evaluated women's bone mass in families [Sowe86] has found no statistical significance in resemblance of the bone mass, which means that genetic similarity, as opposed to identical genetic information, is not sufficient to have similar bone mass values.

Various classifications of different factors involved in the bone strength have been described [Caei13]. They include the whole bone structure, cortical and trabecular bone, osteons, molecular structure and mineral components. The microstructure such as the bone mineral density is important in mechanical behaviour of the bone. Some classification of the micro structural (from 10 to 500mm) bone features has been proposed: Haversian systems, osteons, single trabeculae; the sub-microstructure (1–10mm): lamellae; the nanostructure (from a few hundred nanometres to 1mm): fibrillar collagen and embedded mineral; and the sub-nanostructure (below a few hundred nanometres): molecular structure of constituent elements, such as mineral, collagen, and non-collagenous organic proteins [Rho98].

The bone mineral density implies a high degree of stiffness and would make the bone brittle while other factors that involve microscopical and macroscopical bone architecture would be responsible for the bone quality and for about 20 to 40% of the bone strength [Caei13].

The fracture propagation depends on different forces involved. The lesion force

must overcome different forces in the fracture area in order for the fracture to originate and propagate.

The resistance of the bone also depends on the orientation of the specimen and the orientation of the collagen fibres. It is different when the position of the specimen changes during the mechanical testing [Caei13]. The bone resistance to fracture or the crack toughening mechanisms are strongly dependent on the orientation of the crack propagation: the fracture toughness of long bones is considerably lower if the crack propagates along the long axis of the bone rather than perpendicular to it [Pete05].

The bone resistance to mechanical load of compression is higher than to any other type of load [Keav94].

The mechanical properties of the whole bone are a function of its macro-structure, i.e. its tubular structure and its density while the mechanical properties of a small cortical bone fragment more depend on its micro-structure: the orientation of the osteons and bone density. Not only the quantity of mineral substance is important for mechanical properties but also the substance itself. It has been shown that in the case of Paget's disease the lower carbonate-to-phosphate ratio is the cause of lower stiffness and hardness of 14% and 19% respectively [Zimm15]. The loss of orientation of Haversian structures reduces the stiffness and enhances plastic deformation seen in this disease [Zimm15].

Porosity and mineralisation explain 84% of the variation in stiffness in the cortical bone and has influence on the elastic modulus [Scha88], [Curr88]. It has also been shown that the elastic modulus is dependent on volume of the bone tissue and geometry of the bone specimen [Scha88].

The human cortical bone has shown different values during compression tests: resistance 167 – 213 MPa, Young's modulus 14.7 – 34.3 GPa [Reil74], [Burn76], [Ceza90], [Cupp04].

The bone resistance is often related to the quantity of mineral substance and the

ratio of it to the porosity in a certain volume (bone density)[Kell90].

It has been shown that the bone resistance to fracture was dependant on bone mineral content and bone mineral density [Aers98]. Though there are some differences en different species, there is a strong relationship between those parameters.

There are some variations regarding the bone density and bone resistance to fracture in different species. Those parameters are summarised in Table 2 and Fig.30 (both adapted from [Aers98]).

Table 2: Trabecular bone parameters [Aers98].

Species	Human	Dog	Pig	Cow	Sheep
	(n=4)	(n=5)	(n=6)	(n=6)	(n=6)
<b>BMC (mg)</b>					
Mean	76.3	173.1	173	232.7	236.1
Range	(45.8-110.6)	(138.1-221.3)	(162.7-192.9)	(193.1-294.6)	(212.4-273.1)
<b>vBMD (mg/cm<sup>3</sup>)</b>					
Mean	178	340	373	449	437
Range	(98-270)	(297-390)	(348-441)	(342-536)	(400-477)
<b>Fracture stress (N/mm<sup>2</sup>)</b>					
Mean	1.21	6.12	2.4	5.67	13.22
Range	(0.08 -2.40)	(4.32-7.78)	(1.70 -3.76)	(1.98 -9.28)	(9.30-15.79)
n indicates the number of examined cylindrical cores per species (one or two per subject).					

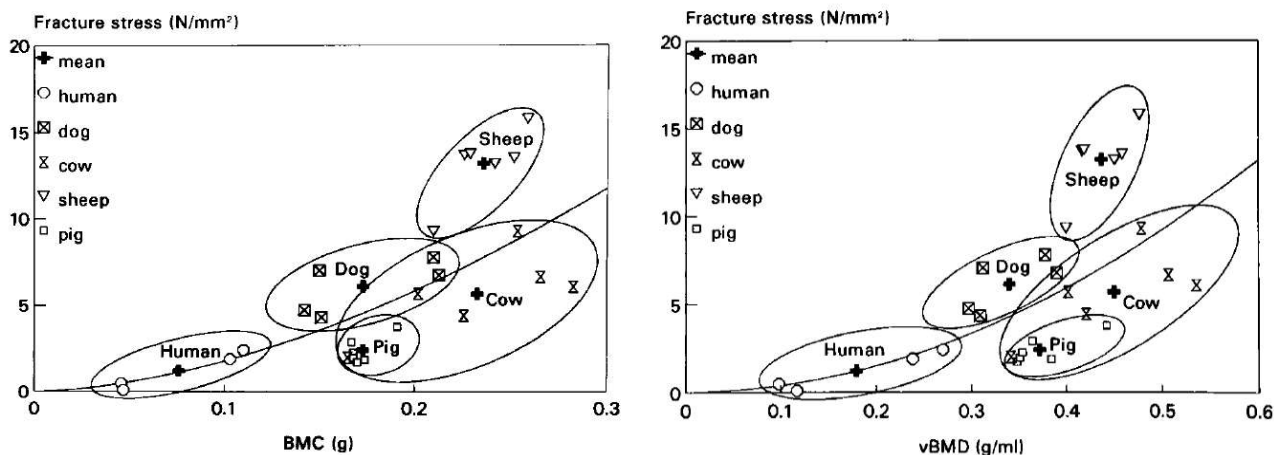


Figure 30: Trabecular bone resistance to fracture (BMC: bone mineral content; vBMD: volumetric bone mineral density) [Aers98].

A study has shown that the micro-porosity had negative correlation with the bone strength of the cortical bone and the bone mineral density had a positive correlation with the bone strength [Wach01\_1][Wach01\_2]. The mechanical parameter that was best predicted by those two parameters in this study was yielding stress. The specimen compression in a transverse plane was done in this study [Wach01\_1]. The bone structure is anisotropic, so the results of this study may be difficult to compare to other studies as most of them use compression models in longitudinal direction. Another study using a micro indentation techniques has shown that the porosity is a significant but often weak determinant of macroscopic tensile, compressive and torsional mechanical properties of human cortical bone [Mirz16].

The bone geometry has an important role in mechanical behaviour on the bone. The resistance of bone and its relationship to the bone geometry is different depending on what forces are applied. The resistance to bending and torsional forces would increase with the the bone diameter of the long bone while the resistance to compressive loading depends on the cross-sectional area of the bone [Boux06].

The energy per area was found to be strongly dependent on collagen fibres and their orientation with respect to the loading axis [Pete05][Zimm15]. If the fracture propagation

continues parallel to the collagen fibres, much less of energy ( $110 \text{ J m}^{-2}$ ) is needed the crack to continue. The energy needed doesn't change a lot up to  $50^\circ$  and then increases rapidly to reach the maximum ( $9,920 \text{ J m}^{-2}$ ) when the lesion force is perpendicular to the collagen fibres in the bone (Fig.31) [Pete05]. It is interesting to note that when the crack in the bone propagates along the collagen fibres, the crack path is straight and smooth, which is typical for brittle fracture. When the crack crosses the collagen fibres, the crack path is uneven, which is more common in quasi-ductile fractures [Pete05].

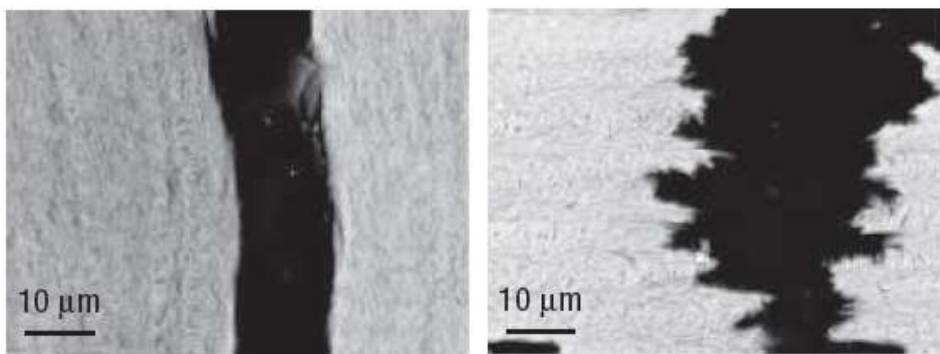


Figure 31: Crack extension parallel and perpendicular to the collagen fibres [Pete05].

In addition the bone toughening to fracture has been described in this is dependent on different phenomena occurring in the fracture area.

It has been shown that depending on the orientation a “crack bridging” (Fig.32) phenomena can be observed. This is related to the microstructure of the bone, alignment of the osteons and collagen fibres [Nallo3]. The unbroken area between the cracks is called a ligament bridging. Often it is associated to extensive microcracking around. It happens when the main crack is in the direction of the osteons and can substantially increase the bone resistance [Nallo3].

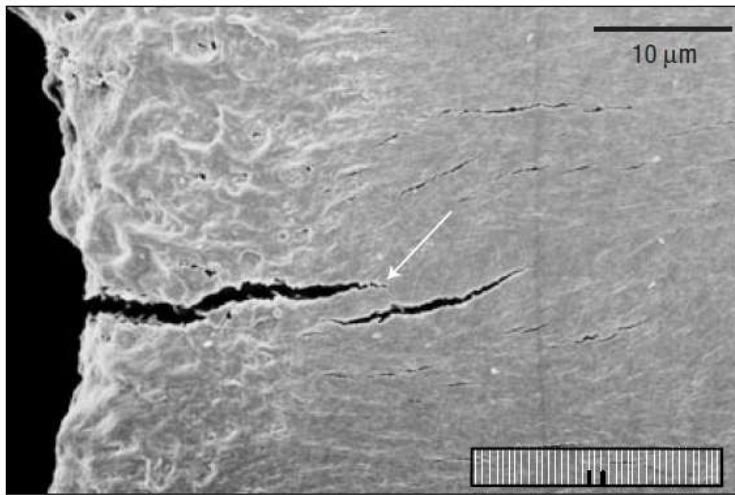


Figure 32: Bridging [Nallo3].

Collagen bridging can be distinguished as well. It is another form of bridging and it can be seen at a much smaller scale. The collagen fibres that are stretched between the two fragments contribute to the increase in the resistance (Fig.33).

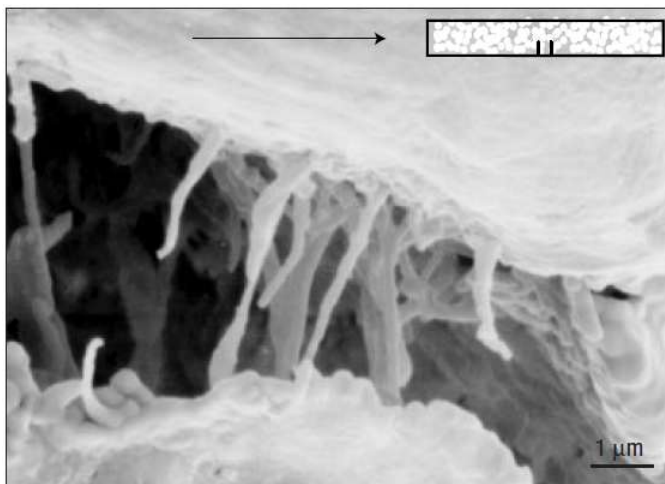


Figure 33: Collagen bridging [Nallo3].

Non-collagen proteins also increase the bone toughening to fracture by several mechanisms. One of them is sacrificial bonding. During the separation the energy is dissipated through the sacrificial bonding mechanism [Morg15]. This mechanism involves non collagenous fibres which interact with  $\text{Ca}^{2+}$  forming and reforming bonds. This

dissipates energy and increases the fracture toughness of bone [Morg15]. The non collagenous proteins osteocalcin and OC and osteopontin are directly associated with mineral or mineral–collagen complexes. Osteocalcin has been shown to bind strongly to the bone mineral hydroxyapatite and it complexes with and links to collagen through osteopontin. Osteocalcin’s ability to link the mineral and organic components of bone renders it a strong candidate for serving a mechanical function in bone (Fig.34) [Atha12] [Morg15]. Dilatational bands are distinct ellipsoidal voids ~100 nm in size that form due to the deformation of non collagenous protein complexes embedded within bone’s rigid mineralized matrix.

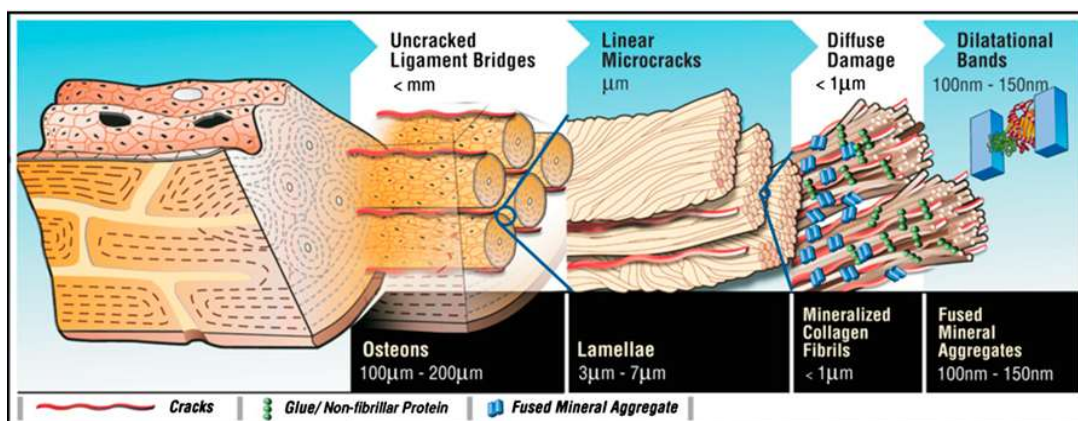


Figure 34: Bone hierarchy and dilatational bands [Atha12].

Other microscale toughening mechanisms have been described including viscoplastic flow [Fant05], microcracking, crack deflection [Pars01], [Pete05] and blunting [Nallo05]. There are also some suggestions that the microcracking is dependent on the osteon remodeling is a the soft the newly formed osteon has some influence in redirecting the microcracking towards a more solid osteon [Guo98]. There is also a hypothesis that the size of of the crystals found in the bone matrix can have a role in fracture propagation as in the bone of young individuals the ratio between the newly formed small crystals and the large crystals is higher than in the osteoporotic bone. The crystals in the osteoporotic bone

are larger and therefore the bone becomes more brittle as there is a deviation from the ideal composition. The crystal size imbalance is related to the deterioration of mechanical properties [Auga06]. The newly formed osteons and smaller crystals in the bone matrix are found in a remodelling bone. The remodelling of the bone is much more common in very young individuals. It is thought that the structure of the bone as the result of this remodelling is therefore more resistant to fractures [Mart93].

Moreover, the bone strength or its resistance to fractures depends also on the on the length of the crack as the bridging occurs when the crack is longer than the distance between the fragments. Therefore, the crack-growth resistance can be variable depending on the length of the crack [Koes08]. At the same time the direction of the fracture driving force is important. It has influence on the bone toughening. The toughness may reach the values of  $25\text{MPam}^{1/2}$  over the first  $500\mu\text{m}$  of cracking in the transverse direction. In contrast, corresponding fracture in the longitudinal orientation requires far lower driving forces, as the stress rises between 1 and  $2\text{MPam}^{1/2}$  when the crack extends to the first  $500\mu\text{m}$ , and then approaches  $5\text{MPam}^{1/2}$  as the crack extends beyond  $500\mu\text{m}$  [Koes08].

## **Conclusion.**

Mechanical parameters of the bone depend on different factors including mineral substance or apatite, organic substances as collagen fibres, the volume and geometry of the bone tissue. Those components are related to the biology of every individual and has a genetic predisposition. The bone tissue resistance is different in different direction as it depends on the micro-architecture: orientation of osteons and collagen fibres.

There are many different barriers for the fracture to propagate. They are seen at macroscopic level (geometry of the bone, quantity of mineral substance, bone mineral density), at microscopic level (orientation of Haversian structures and collagen fibres, apatite crystal size), at molecular level (non collagenous proteins, dilatational bands) and

also phenomena of bone toughening phenomena during the fracture process (crack bridging, collagen bridging, viscoplastic flow, microcracking, crack deflection and blunting).

The bone's structural elements, different phenomena that take place during the bone lesion and their interaction makes the occurrence of fracture and its propagation in the bone tissue a very complex event.

## **2.7. Experimentation and mechanical loading.**

To study the phenomena related to a local loading experimental models had to be created. The literature review was done to gather the existing data and analyse the experimental models created before. Several major groups of the experimental bone fracture models in vitro were found: compression [Zhao18], traction [Kane03], torsion [Bruy00][Reil75] and bending [Lotz91][Choi90][Choi92] forces were used to analyse the fracture propagation in the experimental specimens. A certain amount of data could be retrieved regarding different experimentation patterns and data obtained. Most of the studies that analysed the compression mechanisms used parallel compression platens for this purpose. The entire bone specimen is put in between the platens (Fig 35.)



Figure 35: Usual experimentation setting [Zhao18].

The stiffness reported in different studies using compression models was between 15GPa and 20GPa [Zhao18]. Most of the time, the femur (Human or Bovine) was used as a tested bone during those experimentations. The data regarding elastic modulus and the bone tissue used were summarised in Table 3.

Table 3: Elastic modulus and the bone tissue

Authors	Type of loading	Type of bone	Apparent Young's Modulus	Bone
Murdoch et al. [Murdo4]	compression	cortical	27GPa	Human tibia
Bayraktar et al. [Bayr04]	compression	cortical	19.9GPa	Human femur
Yu et al. [Yu11]	compression	cortical	13.0 - 17.5GPa	Bovine femur
Reilly & Burstein [Reil75]	compression	cortical	17.9GPa	Human femur
Mirzaali et al. [Mirz16]	compression	cortical	18.9GPa	Human femur
Evans [Evan76]	compression	cortical	13.6 - 19.2GPa	Human femur
Currey [Curr88]	compression	cortical	19.4GPa	Bovine femur

Those and subsequent studies were built in a way that they used a global response of the specimen to mechanical loading. It could be an entire bone or a bone fragment tissue that underwent some mechanical compression. The best of our knowledge, there were no experimental models analysing the local strain phenomena that take place around a metallic rod placed over a cortical bone, so it was not clear what the apparent stiffness during the local loading would be, when rupture would occur, whether it would be preceded by a plastic phase and what the values would be.

## **Conclusion.**

The data found in literature shows that biomechanical experimentations involved the studies of the global response of the specimen to mechanical compression. The relevant studies that are important to this work are those using compression loading of the cortical bone. The most of them cited here used specimens extracted from human or bovine femur. The Young's modulus of those specimens was between 13GPa and 27GPa.

No studies could be found dealing with a local strain that occurs between a metallic rod and the cortical bone under mechanical compression.

## **2.8. Hertz Theory of Cylindrical Contact.**

This part was done in collaboration with master student Felix Camagay.

Before a fracture occurs, there is an intensification of stress at the surfaces in contact. Initially, upon application of load, the two bodies (bone and metallic cylinder in this case) in contact experience elastic deformation, then sometimes a plastic deformation and eventually a rupture occurs. The Hertz theory for linear elastic deformation is applied to the very initial stage. In this theory, Hertz analysed the behaviour of 2 spherical bodies that are pressed one onto another [Hert96]. Quadratic functions were used to deduce a system of equations that are called the Hertz' equations of elliptical bodies in contact. The figure below (Fig.36) represents the two elliptical bodies in contact and with different radii and material properties.

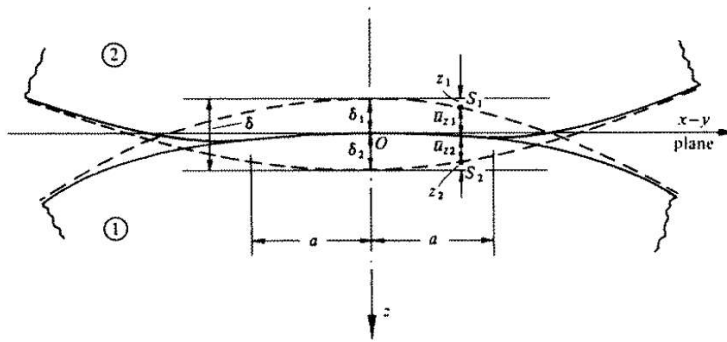


Figure 36: Two elliptical bodies in contact [John85].

Derivations from the Hertz theory were done for specific applications such as hardness testing and rolling contact of bearings. The point-point configuration is mostly used in material hardness testing. In this specific study, the metallic rod and the diaphyseal bone can be represented by the cylindrical-flat configuration of Hertz' theory, where the analytical solution is described by Schmid [Schm14], Brewster [Brew76] and Johnson [John85]. The metallic rod is of a known radius and the surface of the bone which the rod is in contact with is of infinite radius ( $r = \infty$ ; flat). When a cylinder is lying flat on the surface without any force, it can be assumed that the contact between the elements are similar to a line with effective length equal to the length of the rod touching the surface (Fig.37). The diagram shows a cylinder in contact with a flat surface. In this study, the rigid body is the rod and not the surface.

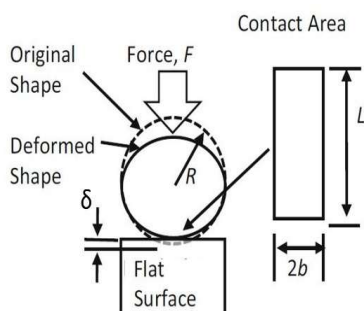


Figure 37: Cylinder in contact with a flat surface.

When two cylinders with radii  $R_1$  and  $R_2$  are in contact, an effective radius  $R_C$  and

elastic modulus  $E_c$  are described for the whole system. These effective parameters take into consideration the radius, Poisson ratio  $\nu$  and elastic modulus  $E$  of each material (1 and 2).

$$R_c := (R_1^{-1} + R_2^{-1})^{-1} \quad E_c := \left[ \frac{1 - \nu_1^2}{E_1} + \frac{1 - \nu_2^2}{E_2} \right]^{-1} \quad (1,2)$$

As the cylinder is being pushed deeper into the bone, an elastic half-width  $b$  becomes the concentration of contact. The half width  $b$  increases as the  $\delta$  increases (Fig. 37). The half-width is important as the deflection of the materials depend greatly on this parameter. It also dictates the range of applicability of the mathematical model to be used in analysing the elastic-plastic-fracture mechanics of Hertz contacts. The analytical solution of the deflection per unit force is shown below. Adapted from the Modern Tribology Handbook [Bhus01] which was obtained from Johnson [John85]:

$$b := \left[ \frac{4 \cdot P \cdot R_c}{\pi \cdot E_c} \right]^{\frac{1}{2}} \quad (3)$$

where  $P$  is the force and  $R_c$  is the radius of contact and  $E_c$  is the elastic modulus of the whole system.

It is important to note that in these cases, transformations are done to the effective elastic modulus and radius depending on the loading configuration.

## Plastic Deformation

Yielding begins as soon as the elasticity of the material ceases and as the force required to deform the material does not change significantly compared to the increase that can be seen in elastic deformation. It is important to identify the yielding onset point or the critical point where the yielding starts: the yield point or the yield strength.

Commonly, the yield strength is identified to be at the 0.2% of the strain offset to the right from the line of elastic modulus. The following table (Table 4) shows the yield strength from different sources:

Table 4: Yield Strength Values

Yield Strength (MPa)	Loading Configuration	Model	Source
107.9 ± 12.3	Uniaxial Tensile	Human Cortical	Bayraktar et al. [Bayr04]
174.3 ± 32.1	3-pt Bending	Canine Cortical	Autefage et al. [Aute12]
121.0 ± 11.0	Uniaxial Tensile	Human Cortical	Wolfram and Schwiedrzik [Wolf16]

These values are obtained from uniaxial loading and three-point bending. Contact stresses are mostly defined by shear stress thus the yield strength values cannot be directly obtained by uniaxial tests. Numerous studies have analysed the beginning of the plastic yield curve but the most prevalent of them are based on the maximum shear stress theory (Tresca criterion) and the distortion energy theory (Von Mises criterion). The following two studies by Green and Wang & Zhu discuss both criteria for yield strength and have suggested analytical solution for predicting the critical values for occurrence of yielding (Fig.38).

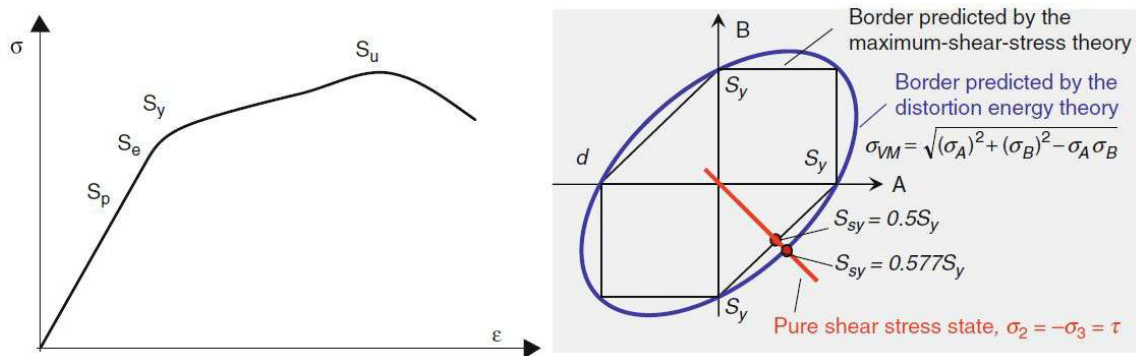


Figure 38: a) Diagram of regular stress strain diagram identifying critical points, and b) Diagram of von Mises and Tresca criterion. Adapted from Wang and Zhu. [Wang13].

### **Critical Yield Point by Green.**

Green [Gree05] determined the effect of different Poisson ratios on the greatest elastic phenomena for cylindrical and spherical Hertzian contacts. Although most metals have the Poisson ratio of  $\nu=0.3$ , his work identified the range  $0 \leq \nu \leq 0.5$  and compared different results.

Using the von Mises criterion for yielding, Green looked for an analytical solution of the critical yield point of cylindrical contact.

### **Critical Yield Point by Wang and Zhu.**

According to Wang and Zhu [Wang13], the contact stress field can be evaluated by either maximum shear stress or the von Mises stress. Both the maximum shear stress theory and distortion energy theory are commonly used to find the yield point of a material. The first one is more conservative while the second is more convenient to use. Their study also describes spherical and cylindrical contact but their approach uses software to pinpoint the location of maximum stresses inside the material. The location of maximum shear stress is identified in terms of  $b$ , which is the cylindrical contact half-width.

The maximum von Mises stress inside the material with Poisson ratio  $\nu=0.3$  is at about  $z=0.703b$  below the surface and the yield pressure at  $p_o=1.792S_y$ . For the Tresca criterion, when  $\nu>0.243$ , the maximum stress in the material is at  $z=0.786b$  below the surface. It was also found that the pressure at yield point is at  $p_o=1.667S_y$ .

### **Fracture Initiation.**

If the loading continues, a material will undergo fracture. It is known that a crack is initiated by a shear stress as opposed to a normal stress because the shear stress is related to high surface fatigue. Therefore the shear stress calculations are important when dealing with fractures. Predicting the fracture initiation of the bone is difficult since its density is

not uniform throughout the volume and it is an anisotropic material. Regarding the bone's anisotropy, bone's fracture properties were studied by Libonati and Vergani using bovine bone [Libo14] in perpendicular directions using three-point bending. As mentioned earlier there may be differences in the bone's behaviour when it comes to a fracture: it can either be ductile or brittle. Griffith's strain energy theory for ductile fractures states that the bonds at the crack tip must be stressed to failure and that for an increment of crack extension, the amount of strain energy released must be greater than or equal to what is required for the surface energy of a new crack to occur (Fig.39)[Fischo7].

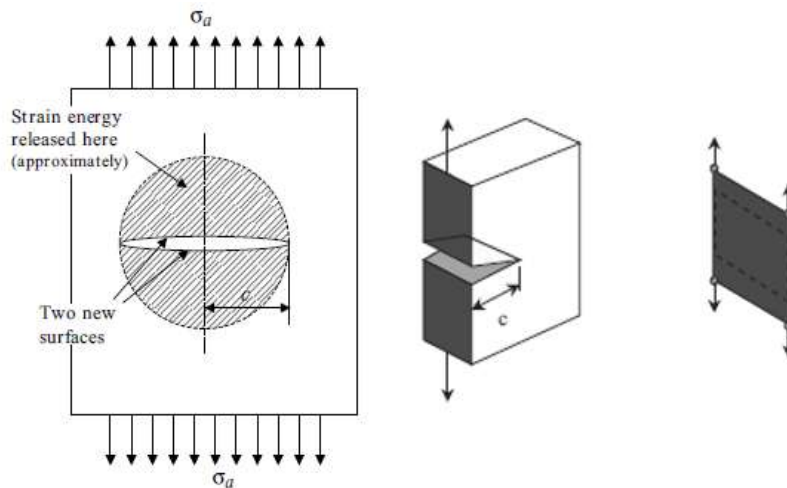


Figure 39: Fracture initiation.

Brittle fractures, on the other hand, are more complicated to analyse since the occurrence of a fracture is not limited to a criterion as opposed to Griffith's and a more statistical approach would be more adequate. This analysis is based on the hypothesis that fractures come from a material's surface imperfections and that will dictate the probability of a fracture. With this hypothesis a two-parameter Weibull distribution can be used.

Another consideration when it comes to fracture of bone substance, is that the bone is considered to be a quasi-brittle material. According to Bazant [Baza04], quasi-brittle

materials are materials in which the fracture process zone is dependent on the scale of the cross-section of the material, meaning that material fracture properties change if the material is large or if it is small. A study of the fracture properties of bone as a quasi-brittle material on the microscale was published by Wolfram and Schwiedrzik [Wolf16].

### **Conclusion.**

The initial interaction between a metallic rod and a bone during compression can be in accordance with the Hertz's theory of contact between cylindrical bodies. If the compression of two cylindrical bodies continues half-width of contact becomes the concentration of contact. If it continues further, a crack can be initiated by a shear stress as is related to high surface fatigue. Predicting the fracture initiation of the bone is difficult because the bone is an anisotropic material.

### **General conclusion and objectives.**

The literature review has shown that the long bone fractures remain rather frequent in general population despite some recent improvements regarding transports security. One of the most frequently used the techniques of fixation is an intramedullary nailing which requires proximal and distal locking. As the nail undergoes some deformation when it is put into the medullary canal the locking holes of the nail distally shift which makes the automatic locking using a guide attached to the nail handle impossible. The technique that is used in most of the cases to lock the nail distally is a freehand technique. This requires some skills and experience. The intramedullary nail has to withstand cyclic strains until the bone heals therefore the mechanical stability is very important. This requires for the bone substance to remain sufficiently strong during the healing especially around the distal locking screw if the fracture has an unstable pattern.

The literature review has dealt with some general aspects of the bone substance, it's

resistance and fracture propagation patterns. It was shown that the bone has a complex structure and has multiple levels of resistance to the fracture and its propagation in order to limit the bone lesion and stop further propagation. Those levels include macroscopical geometrical shape and structural trabecular organization but also microscopical alignment of collagen and non-collagen fibres, mineral substance crystals and even some molecular interactions.

The literature review has outlined the studies that have dealt with the mechanical parameters of the bone experimentally. No studies were found dealing with the local strain and phenomena occurring at the interface of the metallic rod and the cortical bone. This allowed to expect some new information to emerge from this scientific work.

## **2.9. Synthesis, aims and objectives of this thesis.**

The literature review has defined the social and economical impact of the long bone fractures and the predictable evolution of it. Various publications on long bone fixation techniques with the emphasis on intramedullary nailing have been discussed. The challenges related to the implant design, surgical techniques, treatment objectives and problematics related to ionising radiation used in the operating theatre showed the importance of better understanding of the phenomena that take place at the distal locking screw during the procedure and after it: different aspects of the bone formation, healing and remodelling. No publication was found dealing specifically with the locking screw of the intramedullary nail and a long bone contact area.

The publications analysed in the literature review have outlined the essential aspects regarding the distal locking of intramedullary bone fixation that have to be taken into account in this dissertation. The aim of this dissertation is to better understand the

biomechanical phenomena occurring at the distal locking screw interface with bone when there is some compression loading on the screw and to explore what implications would be if the position of the locking screw is not perfect.

In order to achieve these goals two experimental protocols were created using and in vitro animal models.

The first one was a simplified model a local strain at the metallic rod and the cortical bone contact area and was designed to evaluate the phenomena that take place when the diaphyseal cortical bone is about to rupture under a local mechanical load. As it was not known beforehand when the metallic rod would induce a fracture, and also in order to understand what happens just before the fracture occurs, three groups of 15 specimens were used with different displacement imposed to the rod. Precise medical imaging was used before and after the experimentation in order to evaluate different parameters including the geometrical shape of the bone and the bone matter density in distinguished areas under the metallic rod. The medical imaging after the experimentation was done with a purpose to evaluate the extent of bone damage, the fracture propagation and then relate to the specimen parameters. This was the first step before studying similar parameters in a more realistic setting that was done in the second experimental model.

Another protocol was designed to analyse the influence of the position of the screw in relationship with the nail and regarding the strain and bone damage under a compression load that is the result of the position. Three groups of 6 specimens were used in this part of the study with a locking screw positioned differently in different planes. The purpose of this second phase of experimentation was to create an experimental model that would examine the phenomena around the distal locking screw, put perpendicularly to the nail axis and also to study how the phenomena change when an error is introduced in the direction of the distal locking screw.

### **3. Mechanical behaviour of the cortical bone under local loading**



### 3. Mechanical behaviour of the cortical bone under local loading

#### **3.1. Introduction.**

As it was described in the literature review, the intramedullary fixation is one of the most frequently used methods of osteosynthesis in the modern orthopaedic and trauma surgery for long bone internal fixation [Weis09][Yli12]. This surgical technique involves inserting a metallic rod into the medullary canal of a long bone. This fixation is meant to realign the bone fragments and maintain them in a wanted position until the bone heals.

In the most cases, locking screws inserted distally and proximally are used in order to ensure the suitable fixation of this intramedullary device [What06]. If the fracture has a stable pattern, i.e. oblique non comminuted fracture, the longitudinal alignment would be sufficient to guarantee a good bone stability. If the fracture is comminuted and has multiple fragments, the locking device must be used to have a suitable longitudinal and rotational stability [Köse00]. In such a case before the bone consolidation occurs, all the forces would go through the distal locking screw if there is any mechanical loading, e.g. walking. There are few studies analysing the forces and strains passing through the distal locking screw and the relationships between these forces and potential bone damage.

As it was seen in the literature review, it is important to understand what happens when the bone undergoes a local mechanical loading. So, the purpose of this experimental work was to analyse the phenomena occurring at the contact area between the metallic rod and cortical bone under local loading. The goal was to better understand what forces are involved at this area, what is the mechanical behaviour of the bone and the metallic rod under mechanical loading, how the bone can be damaged and what is the damage pattern if the forces come to a limit of rupture.

## **3.2. Material and Methods.**

### **3.2.1. Specimens.**

Forty-five long bone cylinders were harvested from ewe femoral mid-shaft. The specimens measured 65mm in length and were about 20mm in diameter. A particular attention was paid to obtain parallel cuts. The lower cut was made at the junction area of metaphysis and diaphysis. The specimens were kept frozen at -20°C in vacuum sealed plastic bags. The samples were slowly defrosted for 12 hours at +5°C before being exposed to the room temperature prior to mechanical testing to not altered the biomechanical properties [Shaw12].

### **3.2.2. Pre-experimental Imaging.**

All the specimens were scanned using a microCT (SCANCO MicroCT 100 - cubic voxel: 17.2µm) before experimentation.

These pre-experimental microCT scans were performed to identify the bone geometry: cortical bone width, radius of femoral diaphysis (Fig.40) and cortical bone surface area in a microCT slice. It also permitted to assess the microstructure in specific areas and to look for a possible bone damage. The latter could potentially influence the fracture pattern, experimental curves, the results and subsequently could later possibly explain the mechanical behaviour.

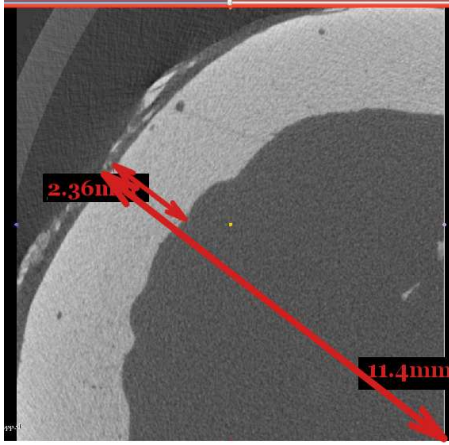


Figure 40: Measurements of the femoral shaft radius and cortical thickness

For those purposes, the harvested bone cylinder was manually divided into 13 evaluation zones of several millimetres: thinner zones just under the metallic rod and thicker zones at the bottom. A representative microCT slice in the middle of every zone was chosen. The thickness of a slice was defined by the microCT scan resolution. The slice was defined in relationship with the distance from the metallic rod, the first of them starting 1mm beneath the rod; it was situated in the middle of each zone and was considered representative. Eight slices with an increment of 2mm were chosen in the upper part of the cylinder, followed by two slices with 5mm increment, then one slice with 7.5mm increment and two slices with 13mm increment at the bottom (Fig.41). The image was then divided into four parts that were called NESW (north, east, south, west) for identification purposes (Fig.41) the centre coinciding with the centre of the intramedullary canal or the centre of inner cortical bone circumference.

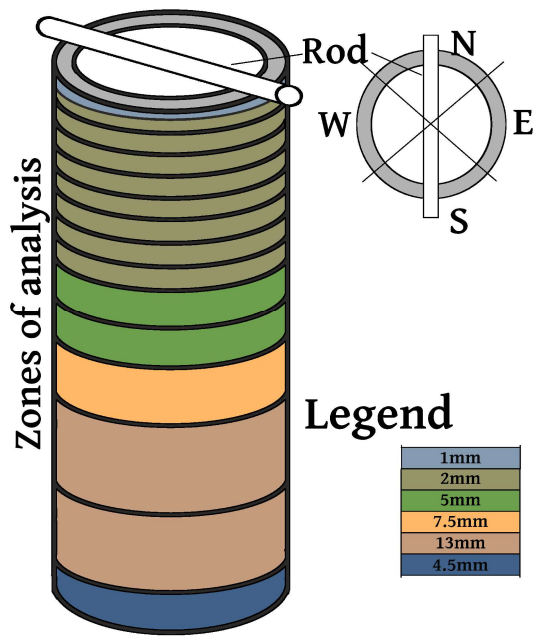


Figure 41: Position of the rod on the specimen and definition of zones of analysis.

The quantitative imaging analysis was performed using the 3D Slicer© software using the pre-experimental microCT scans (Fig.42). It is an open-source platform for medical image informatics, image processing, and three-dimensional visualization. It was created with a support from the US National Institutes of Health and a worldwide developer community.

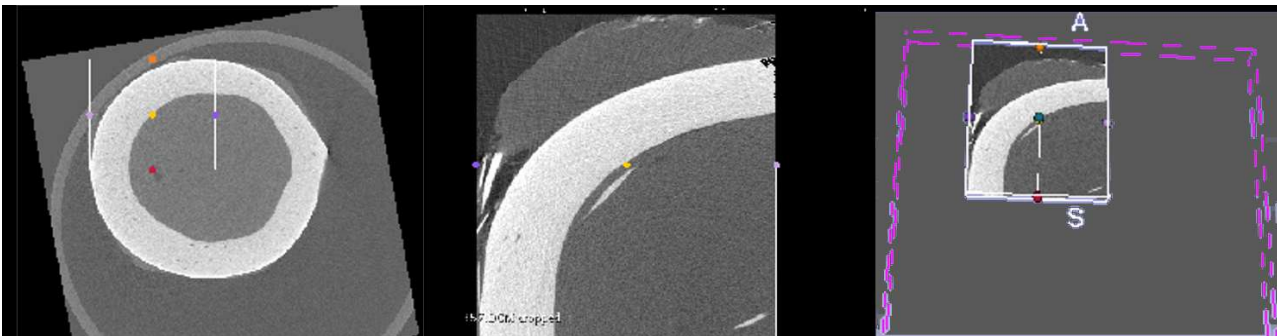


Figure 42: Defining the region of interest for BT/TV calculations.

The BV/TV ratio was calculated automatically using the Slicer 3D software after an automatic segmentation adjusted for bone substance (Fig.43).

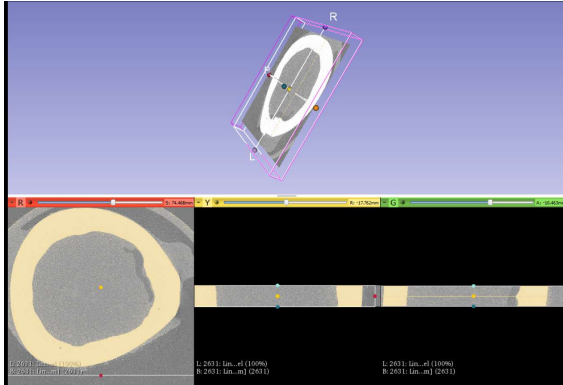


Figure 43: Segmentation adjusted for bone substance.

The BV/TV allowed to calculate the effective average cortical area  $Seff = BV/TV \times S$  (where S is an average cortical area).

### 3.2.3. Mechanical testing.

A 4mm diameter metallic rod was centrally placed on the top side of each specimen in a medial to lateral direction. Forty five quasi-static compression (1mm/s) were performed using an Instron 5566 machine (Fig.44). Specimens and rod were preloaded by about 1N before compressions.

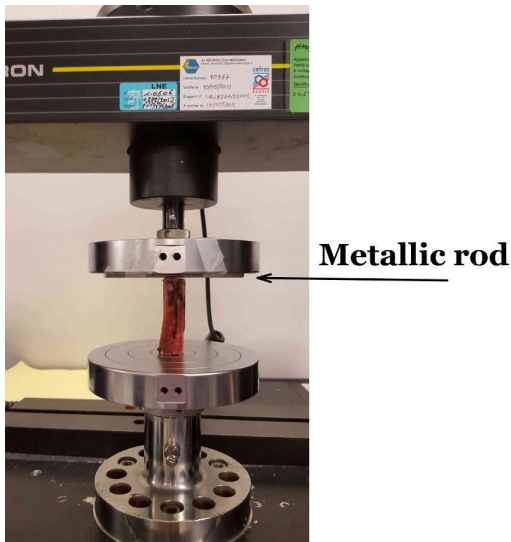


Figure 44: Experimentation setting.

Specimens were divided into 3 groups of 15 specimens, defined by the maximal displacement imposed to the rod (Table 5). Force-displacement evolutions were recorded.

Table 5: Experimental groups

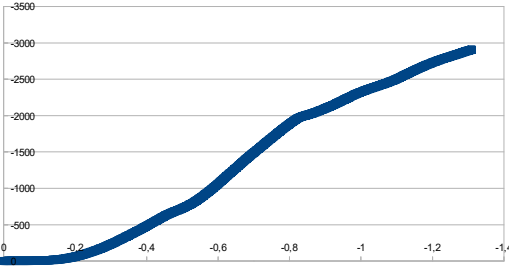
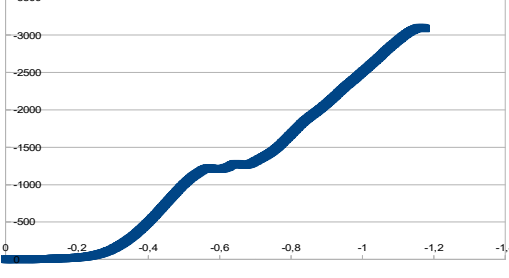
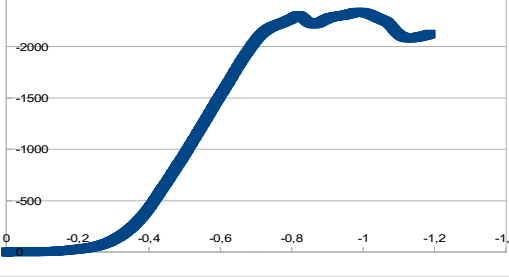
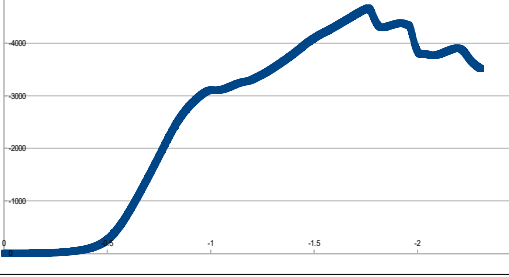
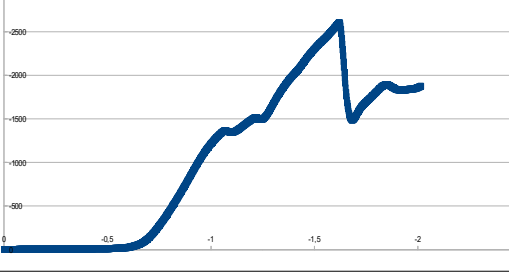
	Group 1	Group 2	Group 3
Maximal displacement	0.97 mm	1.95 mm	3.9 mm
Number of specimens	15	15	15
Equivalent strain	1.5%	3%	6%

### 3.2.4. Mechanical Data Analysis.

The experimental curves were classified depending on their shape. To precise the curve description, a notion of a *crack* as opposed to a *fracture* has been introduced. The limit between a crack and a fracture was defined as 1kN. If a drop in a curve exceeded 1kN it was considered as *fracture*, if it didn't – as *crack*.

Ten types of curves have been identified. They are summarised in a Table 6 below.

Table 6: Curve types.

Typical Force (N)-Displacement (mm) evolution	Description	Arbitrarily chosen abbreviation
	Linear behaviour	L
	Double Linear behaviour	2L
	Linear behaviour with Yielding	L + Y
	Double Linear behaviour and Yielding	2L + Y
	Double Linear behaviour and Crack	2L + Crack

	<p>Double Linear behaviour with Crack and Yielding</p>	$2L + \text{Crack} + Y$
	<p>Double Linear Behaviour with Crack and FRacture</p>	$2L + \text{Crack} + \text{FR}$
	<p>Double Linear behaviour with Yielding and FRacture</p>	$2L + Y + \text{FR}$
	<p>Double Linear behaviour with FRacture</p>	$2L + \text{FR}$

If a major rupture was identified (eight specimens), the further curve was discarded as it was considered not reliable (Fig.45).

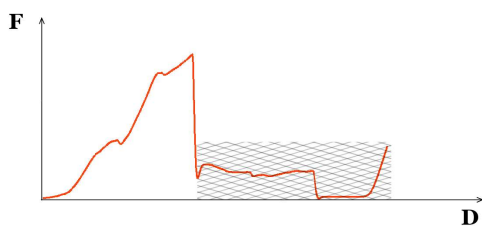


Figure 45: Discarded part of the curve.

To assess the mechanical behaviour several parameters were obtained from the curves:

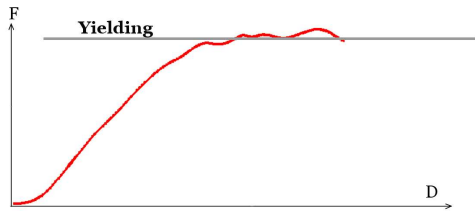


Figure 46: Yielding.

- The yielding point characterized by its force  $F_{\text{yield}}$ , the yield strength (curves: L+Y, 2L+Y, 2L+Crack+Y, 2L+Y+FR), It was defined as an intersection of the curve and a line with 0.2% offset (Fig.46, 47).

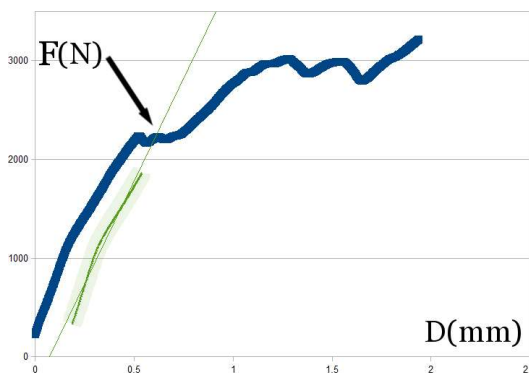


Figure 47: Yielding strength (arrow) using 0.2% offset.

- The rupture point characterized by its couple (Displacement, Force) : (Drupt, Frupt) (Fig.48).

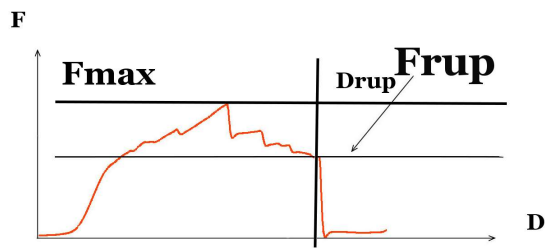


Figure 48: Bone damage before the complete rupture seen in this curve.

- The maximum point characterized by is force  $F_{max}$  (Fig.48).

Sometimes the  $F_{rup}$  coincided with  $F_{max}$  (Fig.49a, 49c), but sometimes not, as the specimen underwent some local damage before complete rupture (Fig.48).

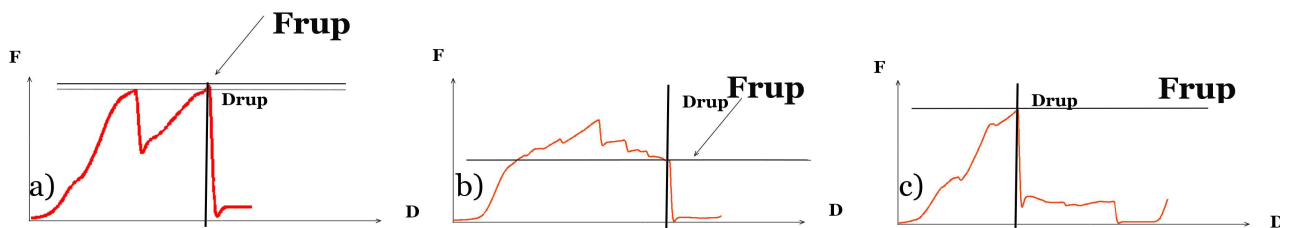


Figure 49: Force to rupture ( $F_{rup}$ ) and distance to rupture ( $D_{rup}$ ).

- The apparent stiffness  $k_0(N/mm)$  for every group was calculated using a method of least squares after having selected 50% in the middle of the ascending part of the curve (Fig.50).

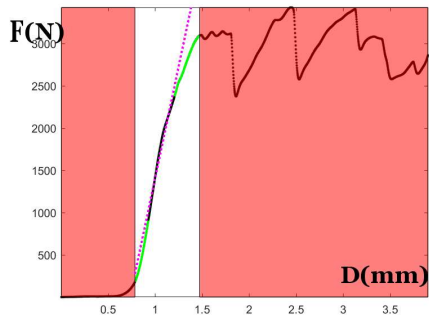


Figure 50: Apparent stiffness calculation.

- The mechanical behaviour in the Force/Displacement curve and microCT analysis allowed to calculate apparent elastic modulus  $E_{app}$  of the specimen. It was calculated using known parameters: stiffness ( $ko$ ), the length of the specimen ( $L$ ) and the average cross-sectional area ( $S$ ).

$$E_{app} = \frac{ko}{S_0} \times L$$

### 3.2.5. Post-experimental imaging.

All the specimens were scanned again by a microCT scanner after the experimentation using the same parameters (SCANCO MicroCT 100 - cubic voxel: 17.2 $\mu$ m).

The post-experimental microCT scan was used to evaluate the bone damage and the fracture patterns as well as the length of the fracture line propagation. As it was already known after the experimentation – the position of the metallic rod could be related to the geometry of every specimen and therefore the fracture propagation could be related to the calculated the BV/TV ratio in each specific segment.

As the position of the specimen in the microCT scanner's tube before and after the experimentation was different, the orientation of nearly every microCT slice had to be

digitally turned to make the positions match. To achieve that, anatomical landmarks on the microCT images had to be compared and the rotation angle measured. After that the image could be transformed using the 3D slicer tools to the image applying the chosen rotation angle.

The bone damage evaluation after compression included description of fragment line propagation if any fracture occurred (Fig.51), an assessment of comminution at the contact area with the metallic rod and fragment migration (separation distances between the fragments).

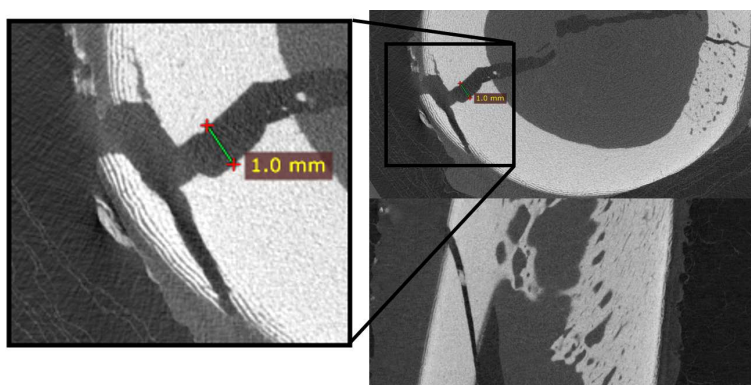


Figure 51: Measurement of fragment displacement and fracture propagation length.

Any comminution or bone chip was assessed as well as the distance between the major fragments was measured. The distances were classified as very large (over 1.2mm), large (0.8-1.2mm), medium (0.4-0.8mm) and small (less than 0.4mm). Yielding zones were also identified. A *fracture score* was defined from 1 to 5 depending on those distances at each zone of evaluation.

In order to better describe the extent of damaging force, an overall *fracture score* for each specimen was calculated by adding all the attributed values. This allowed to have a score that took into account the fragment displacement and the fracture length altogether.

The length of the fracture line propagation in relationship with the defined regions was recorded. This evaluation allowed to have a volume map of fracture propagation and

its pattern in relationship with the position of the metallic rod (Fig.52).



Figure 52: Example of pattern of rupture obtained from MicroCT analysis. Colours relate to the size of crack for the pattern of damage.

### 3.2.6. Relationship between the data obtained in microCT and curve analysis.

The relationships between the microCT data, fracture pattern and different mechanical parameters were then studied.

The correlation between the fracture score and different parameters including stiffness ( $k_0$ ), BV/TV, effective average cortical area were studied.

The relationships between geometrical features (radius of the bone, cortical thickness effective bone area and BV/TV were also investigated.

The variability coefficient in BT/TV in every segment was calculated in order to relate to a fracture propagation.

The Pearson's correlation test was used to evaluate the correlations between these different parameters with significance value of coefficient set at 0.8 [Akog18].

### 3.3. Results.

#### 3.3.1. Qualitative and quantitative curve analysis.

A linear behaviour was observed at the beginning of all the loading curves. Different data regarding parameters as stiffness ( $k_0$ ), apparent elastic modulus  $E_{app}$  and  $F_{max}$  are summarised in Table 7. The average stiffness was  $4155 \pm 1654$  N/mm (mean  $\pm$  standard deviation), the average apparent Young's modulus was  $1.52 \pm 0.54$  GPa (mean  $\pm$  standard deviation).

Table 7: Average values of different parameters classified by types of curves.

	Number of specimens (G1, G2, G3)	Average stiffness $k_0$ (N/mm)	Average $E_{app}$ (GPa)	Average $F_{max}$ (with or without rupture) (kN)	Average $F_{rup}$ (kN)	Average fracture line length (mm)	Average fracture score
L	8 (8, 0, 0)	3494	1.33	2.64		2.8	3.4
2L	3 (1, 2, 0)	3882	1.66	3.49		10.3	11
L + Y	3 (2, 1, 0)	3731	2.09	2.79		10	10,7
2L + Y	5 (0, 4, 1)	3392	2.10	3.86		12.5	13
2L + Crack	15 (4, 7, 4)	4429	1.26	3.10		20.5	16
2L + Crack + Y	2 (0, 0, 2)	4010	1.52	3.64		39	29
2L + Crack + FR	4 (0, 1, 3)	4709	1.16	2.96	2.6	42.3	75.5
2L + Y + FR	1 (0, 0, 1)	1795,8	4.08	2.66	2.7	45.5	86
2L + FR	1 (0, 0, 1)	1685,1	8.08	3.99	4.0	32.5	59
2L+ Crack + Plateau+ FR	3 (0, 0, 3)	4582	1.93	4.33	4.2	47.3	71.7

The yielding occurred in 11 of 45 specimens. As far as different displacement groups are concerned, the most yielding curve types were observed in the group 2 (equivalent strain 3%): 5 of the total of 11, while there were 4 yielding types curves in the group 3

(equivalent strain 6%) and 2 in the group 1 (equivalent strain 1.5%). The yielding started when the force on average equalled  $2557 \pm 566$  N (mean  $\pm$  standard deviation) and at the displacement of about  $1.3 \pm 0.46$  mm (mean  $\pm$  standard deviation). Only 1 of 11 specimens that had undergone yielding showed subsequent total rupture. It happened in the group 3 (highest displacement).

A complete rupture occurred in 9 of 45 curves. Only one of them occurred with an yielding phase. The average  $F_{max}$  (if fracture occurred) was  $3500 \pm 885$  N (mean  $\pm$  standard deviation).

The force-displacement curves and their types are presented in Annex II.

### 3.3.2. Imaging.

The MicroCT performed before and after the local mechanical loading experimentation has allowed to calculate the BV/TV, to measure the cortical bone width and calculate the cortical bone area of a slice. In order to gather the information regarding the differences between groups, average BV/TV, cortical bone width and cortical area were calculated (Table 8).

Table 8 : Average BV/TV, cortical bone width and cortical area

	Group 1 (1.5%)	Group 2 (3%)	Group 3 (6%)
Average BV/TV of all specimens	0.926	0.932	0.941
Average radius of all specimens (mm)	10.4	10.8	10.6
Average cortical thickness of all specimens (mm)	3.09	3.18	3.07
Average cortical bone section area of all specimens (mm <sup>2</sup> )	171.5	181.9	174.6

It has also allowed to evaluate the fracture propagation length. The data is summarised in Table 9. However, the microCT imaging after the experimentation of local mechanical loading showed some bone damage in all the specimens whether it was some

comminution at the contact area or a far descending bone fracture.

Table 9: Fracture propagation length and fracture score. The overall fracture propagation score was greater in a greater displacement group.

Group	Average fracture line length (mean ± standard deviation) (mm)	Average fracture score (mean ± standard deviation)
G1	9.6±14.6	8.1±7.5
G2	18.1±14.5	19,47±19,78
G3	33.7±19.8	46.9±30.3

The  $\mu$ CT analysis allowed to evaluate the bone damage after the experimentation.

Different patterns could be identified (Fig.53, Fig.54).

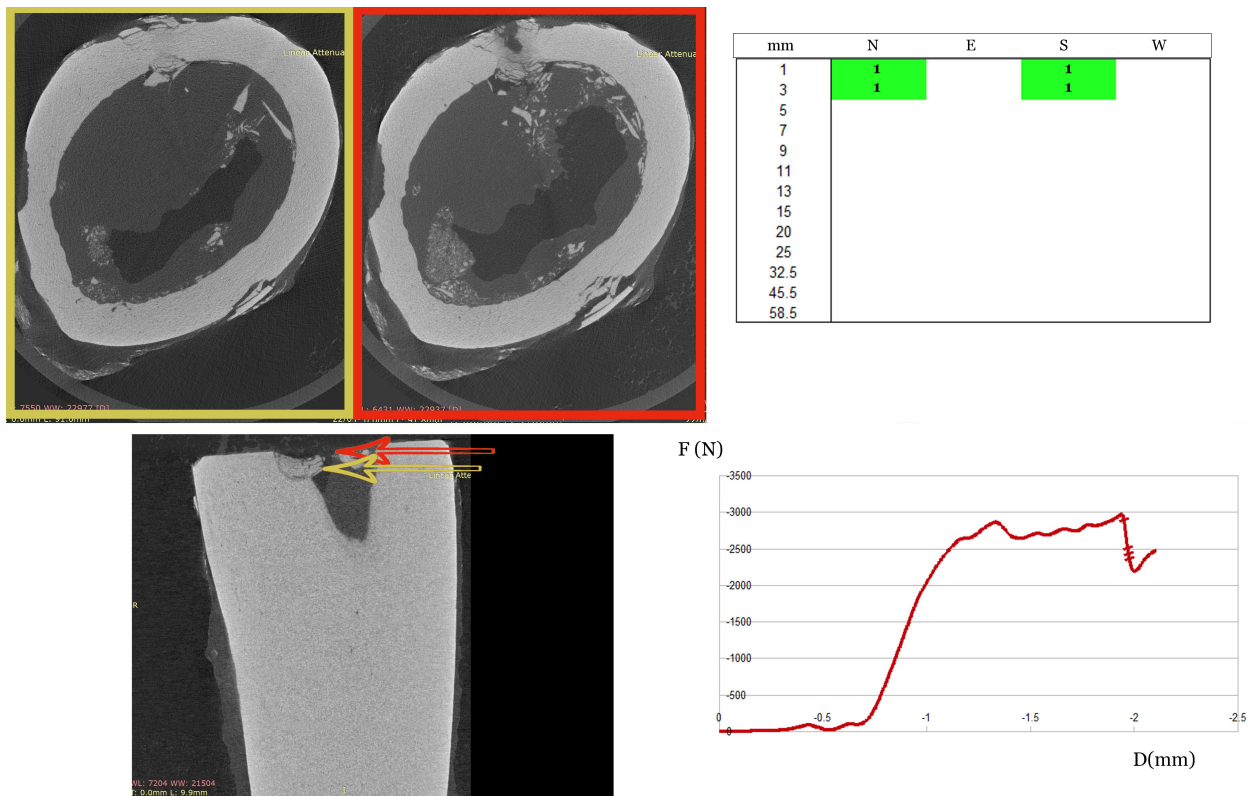


Figure 53: Bone damage as yielding phenomenon seen in the curve. There is more comminution and fragment displacement in the upper part of the specimen and less bone damage in the area where the metallic rod stopped. Yielding in this case is related to a local bone damage. Note the absence of major fracture.

The bone damage in Fig.54 is reflecting a fragile rupture in the curve. There is a large displacement, some comminution and bone damaging in the upper part of the specimen. As the fracture goes down, there is less comminution and displacement. The fracture line reaches the opposite side of the specimen.

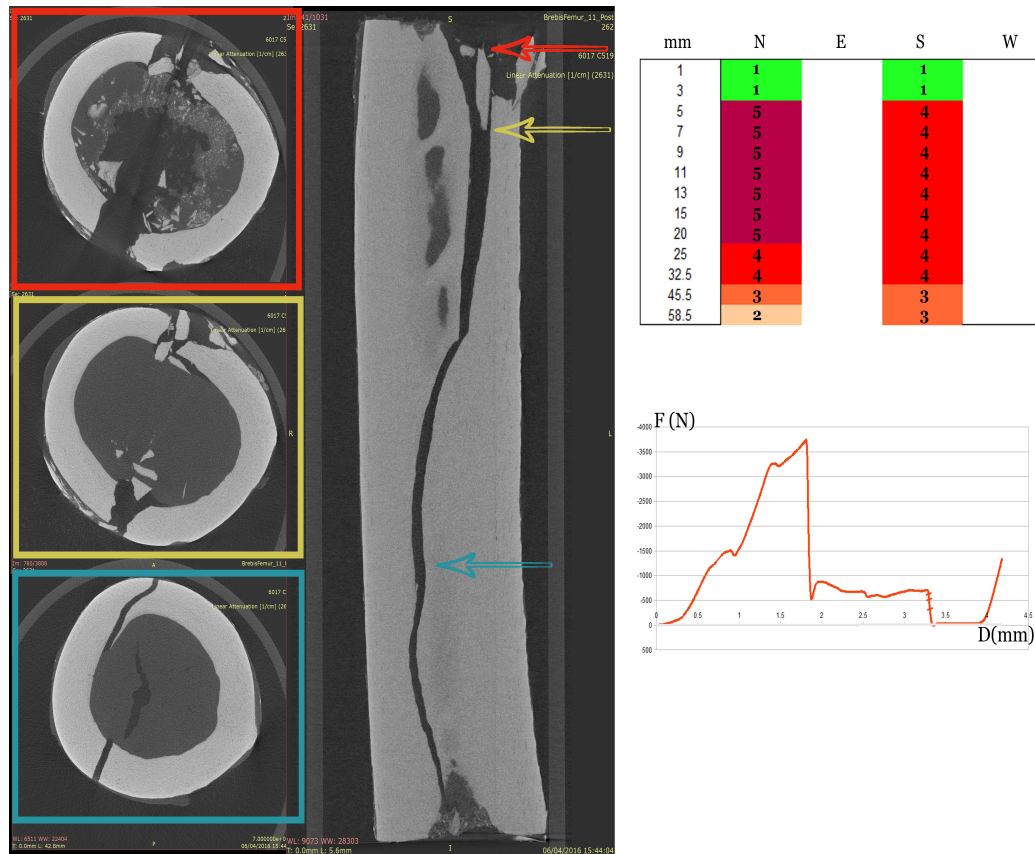


Figure 54: Bone damage reflecting a fragile rupture in the curve.

### 3.3.3. Correlation between the imaging and the mechanical parameters.

The results combining mechanical parameters and imaging data are summarised in Annex III.

The geometrical parameters of the specimens didn't show any correlation between them except the correlation between the cortical thickness and effective bone area.

The fracture line propagation length, the fragment displacement, the two or a single cortical bone involvement was linked to different shapes of the curves (Fig.55).

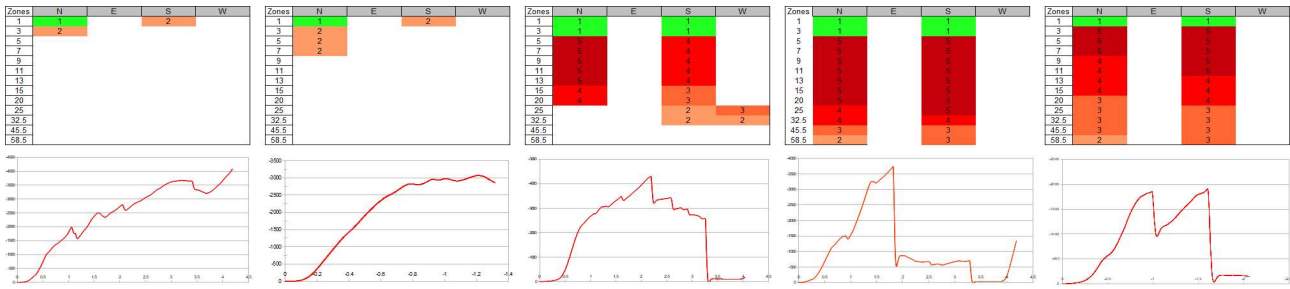


Figure 55: Examples of fracture propagation and mechanical behaviour (typical curves).

Most of the specimens that showed a fracture propagation line beyond 5mm had two cortical bones involved in the fracture.

There was much less fracture line propagation in the yielding group. The fracture propagation length seen on microCT scans in this group was on average  $19.6 \pm 16.4$  mm (mean  $\pm$  standard deviation). The average fracture score in the group showing yielding type of the curve was 21.

When a total rupture was seen in a curve, the microCT showed at least one cortical bone rupture in most cases with a longer fracture line propagation. The fracture propagated in those specimens for  $43.22 \pm 13.17$  mm (mean  $\pm$  standard deviation). The fracture propagation cartography with segmental BV/TV is presented in AnnexIV.

The average BV/TV ratio in segments containing a fracture (seen in the microCT) in relationship with the fracture gap is summarised in Table 10.

Table 10: BV/TV ratio in segments containing a fracture (seen in the microCT) in relationship with the fracture gap.

	gap between fragments					
	overall	comminution /yielding	small (less than 0.4mm)	medium (0.4 to 0.8mm)	large (0.8 to 1.2mm)	very large (more than 1.2mm)
BV/TV (mean ± standard deviation)	0.934±0.034	0.932±0.034	0.931±0.035	0.940±0.038	0.937±0.028	0.926±0.030

The overall average BV/TV ratio in segments without a fracture was found to be  $0.933 \pm 0.029$  (mean ± standard deviation), the overall average variation coefficient of BV/TV in segments containing a fracture was 0.028.

There was no correlation between the BV/TV and the fracture propagation score, no correlation between the variability of the BV/TV in the segments under the metallic rod and the fracture propagation score, no correlation between the variability in BV/TV in all the segments and the fracture propagation score.

### 3.4. Discussion.

#### 3.4.1. Experimental method.

Human bone models share numerous features with animal models such as prediction of fracture mechanism. The animal models can be very accurate. Animals such as rabbit, dog, sheep, goat and pig are often considered in such experiments [Pearo7]. Dog, sheep or goat are often good candidates for implant testing. Due to the sheep and goat's similarity to human bone size and other properties on the micro and macro scale, either one could be considered in a study. Also, since the two are food producing animals, performing tests proved to be less critical in the public's eye compared to companion

animals such as dogs. There were some considerations of availability of the specimens. In this study, ewe specimens were used. An experimental model was applied in this study. Although the mechanical properties depend on the age of the animal, the ewe femoral bone was chosen as it can show similar mechanical properties to the human cortical bone [Pearo7]. It is important to note that despite similarities to the human bone, the ewe bone samples differ in terms of the bone mass and the balance between the quantity of mineral substance and proteins. In fact, the dry bone weight in human femoral bone is 61.3% while in sheep it is 63.4%, the quantity of total protein is 49.2 $\mu$ g/mg in dry in human femoral bone, while it is 80.7 $\mu$ g/mg sheep [Aers98]. That is why there may be some differences in mechanical properties and mechanical behaviour between the ewe and the human femoral bone. It has been shown that resistance to fracture was greater in ewe than in human trabecular bone [Aers98].

To mimic natural conditions a rod was placed in a lateral to medial direction at the metaphyseal area. A metallic rod as a simplified model of a screw was chosen for mechanical testing and local strain analysis in order to simplify the experimental setting and to have less variables and thus to have an easier investigation of the phenomena under the rod. A threaded cortical screw would have had a much more complex contact interaction. The rod used instead of a screw may have limited the reproduction of the screw mechanics, but has allowed to simplify the metal-bone interface and has reduced the variables that might have intervened in calculations such as the screw shape or the screw thread pattern.

A quasi-static loading has been chosen for the experimental mechanical compressions. The velocity of 1 mm/s is compatible with a quasi-static loading definition for bone [Toen14].

### **3.4.2. Discussion of the results.**

#### **3.4.2.1. Mechanics.**

Mechanical properties of the bone are quite close to the data found in literature where in one study the mean apparent elastic modulus obtained by spherical indentation was 9.9GPa, and compression apparent elastic modulus was 4.42GPa [Boug18]. The average Young's modulus for femoral shaft is 18.6GPa [Cupp04]. The  $E_{app}$  was 1.5GPa $\pm$ 540 (standard deviation) in this study. There are quite a lot of variations in the data found in the literature. It has been shown that the elastic modulus in the growing trabecular ovine bone can vary from 0.67GPa to 1.2GPa [Nafe00]. Moreover, sheep have seasonal bone variations [Wanc15]. The differences between this study and studies found in the literature can be explained by the sheep age and seasonal variations, but also by the design of experimental settings. The studies found in the literature evaluated a bone segment's Young's modulus in contrast with this study that aimed to evaluate local mechanical loading. The mechanical loading in this study was done using the interposition of a metallic rod which may have influenced the results as mechanical phenomena such as described by Hertz in the surface contact theory but also a localised yielding [Stra99] may have occurred.

The linear mechanical behaviour was observed in the beginning of all curves. A large number of force-displacement curve types show the complexity of the phenomena that take place at the metallic rod and bone surface contact area. There is certainly a combination of multiple factors such as anisotropic features of the bone, surface contact, other factors that may have had influence on bone resistance (not evaluated in this study) such as protein concentration, collagen fibres' direction and finally, which is more obvious - the displacement distance defined by the protocol.

It is important to note that the bone rupture mostly occurred when the equivalent strain was 3%-6%. There were less fractures observed when the equivalent strain was 1.5%.

The average  $F_{max}$  was higher in the curves that showed a fracture ( $3605 \pm 946N$ ) than those that showed cracking ( $3099 \pm 810N$ ) or yielding ( $3422 \pm 702N$ ). This may be related to the fact that if some bone damaging occurs, stress changes are irregular with increasing strain, so that a wavy line is created in the curve (Fig.56). Some increase in stress can be enough to cause the proportional limit to be exceeded, but it is not sufficient to induce a total rupture. Under this force the material begins to flow and the structure undergoes some reorganisation with microfractures and cracking, and the first plastic deformation occurs. This area in which the material flows and microfractures occur lies between the upper and lower limit of this part of the curve (Fig.56). The highest point in this part of the curve is the point accompanied by an initial, sudden loss of quality. As a result, the stress required to continue to strain the material reduces immediately and reaches the lowest point.

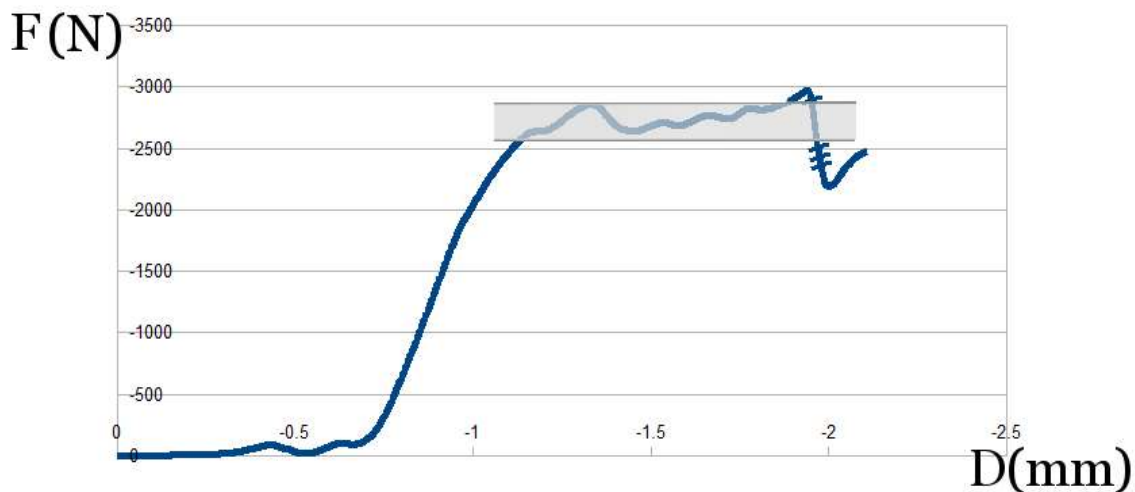


Figure 56: Micro-fractures seen in this curve.

This study shows what strain can put the bone at risk of a fracture at the distal locking screw area. This experimental study has evaluated a single quasi-static rod

compression effect on a bone. The situation can be different in a natural setting where more cyclic compressions and bone reconstruction can be observed.

#### **3.4.2.2. Discussion of the imaging results.**

The microCT scanning is an appropriate imaging for the bone damage analysis [Ding15][Wach01]. It has been found that there was a strong correlation between the bone mineral density (BMD) and mechanical strength [Auga98]. Though the BV/TV and the bone mineral density are not quite the same parameters, they are related. There was no correlation between the BV/TV and mechanical parameters in this study because the study design and the boundary conditions were different. The study that has found a strong correlation between the BMD and mechanical parameters used 12mm bone cubes harvested from different areas [Auga98] as opposed to an interposed metallic rod on a cortical bone cylinder that was used in this study.

The microCT scanning has allowed to evaluate the pre-experimental bone shape and the bone damage in post-experimental scans. They have shown different fracture propagation patterns that are discussed below.

#### **Pre- and post-experimental imaging.**

The pre-experimental images were evaluated for any bone damage that could possibly influence the results. This local bone damage was related to bone preparation during the diaphyseal extraction process (Fig.57). This did not always have a clear influence on the results.

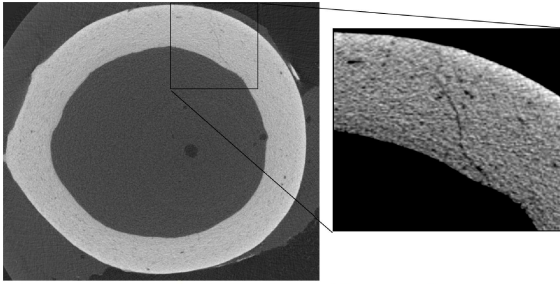
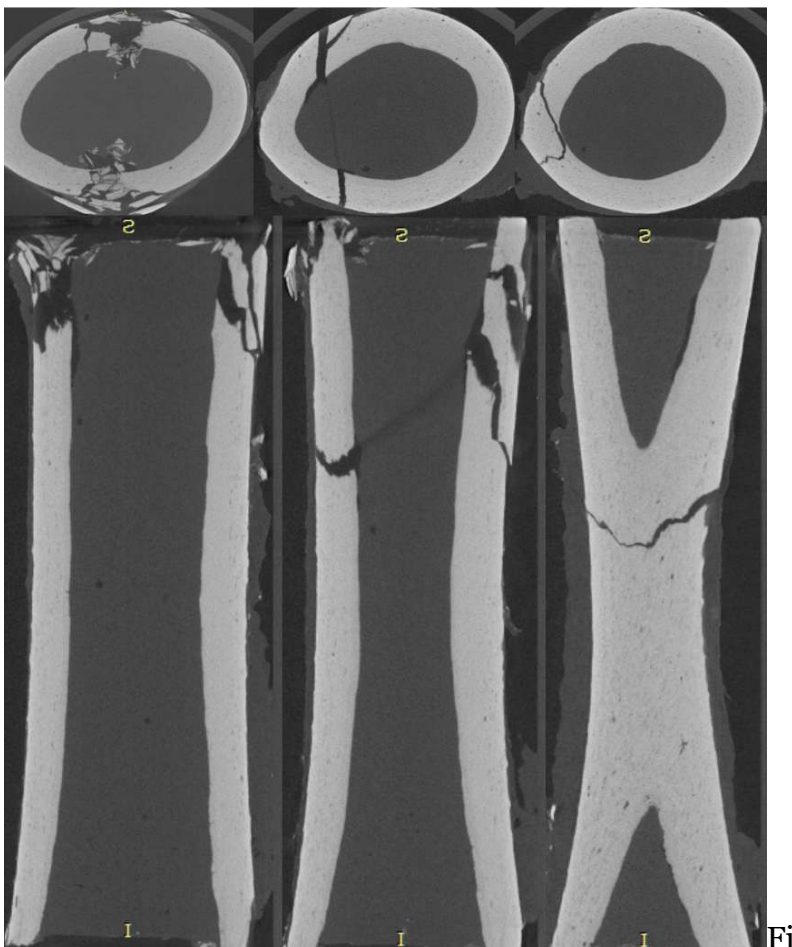


Figure 57: A slight local bone damage could be seen in pre-experimental MicroCT scan.

Several features including the bone damage pattern, comminution, fracture propagation length if present were looked for in post-experimental MicroCT scan images (Fig.58). The criteria to describe those features had to be chosen arbitrarily as there were no references in the literature describing this type of local strain experimentation.



### **BV/TV and fracture propagation.**

There was no difference in the BT/TV ratio in segments having a fracture line and those segments which remained intact, nor there was a difference in BV/TV in segments with different fragment displacement gaps. In fact, the fracture line had a clear tendency to propagate in a longitudinal direction just underneath the metallic rod suggesting that the direction of fracture propagation was not quite related to the relative quantity of bone substance in any adjacent segment, but it was more related to the bone structure: direction of osteons' alignment, direction of collagen fibres, etc. This is in line with the literature where it has been shown that the energy required for bone fracture to appear was different in different directions [Caei13][Nallo3][Pete05][Zimm15].

### **Correlations.**

An attempt was made to find any type of correlations between different parameters but couldn't be found. This may be due to the complexity and variability of mechanical behaviour at the local contact area between the metallic rod and the cortical bone. It was impossible to find correlations between the mechanical parameters and the imaging as the mechanical parameters, including  $F_{max}$ ,  $F_{rup}$ , type of the curve varied a lot making it difficult to find any particular type and relate it to the data extracted from imaging (e.g. BT/TV, fracture propagation length, fracture score, etc.). Taken into account the variability, larger groups of specimens could have possibly given statistically significant correlations. Some specimens had quite unexpected mechanical behaviour or different parameters and had different values than others so they were further discussed separately.

### Particular specimens.

1) The specimen number 8 from the 1st group (1.5% displacement) showed much higher than average stiffness, less than average BV/TV, but had the fracture line that propagated down to 20 mm while the type of the curve was of L+Y (Fig.59).

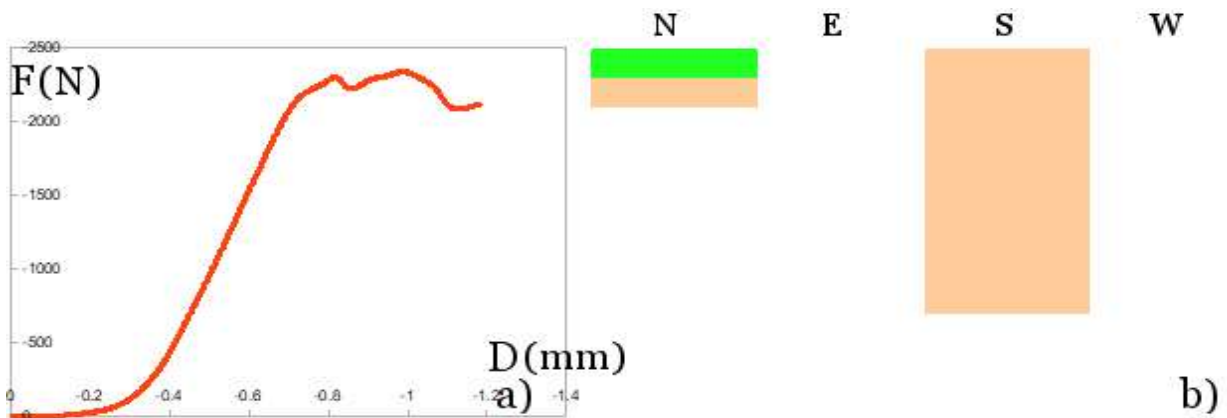


Figure 59: L+Y type of the curve, specimen Nr.8, 1st group.

When re-examining the proximal part of the specimen before the experimentation, it was seen that there was some initial bone damage, the fracture lines propagating up to 5 mm distally (Fig.60). The metallic rod later was placed in the area where one of the fracture lines was seen in the pre-experimental micro-CT scan. There was some comminution in the very proximal part with visible debris.

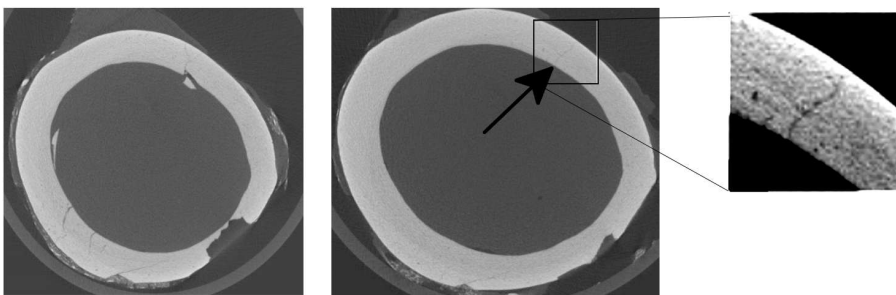


Figure 60: Proximal bone damage (specimen 8, 1st group).

There was a nearly 5 mm bony defect at the distal part that extended longitudinally for about 1 mm (Fig.61).

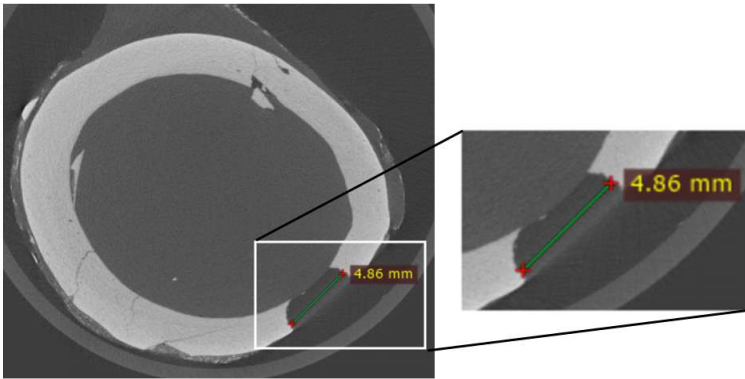


Figure 61: A nearly 5 mm bony defect.

There were some tiny fracture lines seen in the specimen before the experimentation in the area where the metallic rod was placed.

Although the metallic rod was not placed in the area of the defect at the distal part of the specimen, it could have had some influence on the shape of the curve.

The cuts were parallel and therefore there was no or minimal positional adjustment during the compression experiment. The cuts were made in almost perpendicular to the longitudinal axis of the specimen and the alignment of the specimen was satisfactory (Fig. 62).

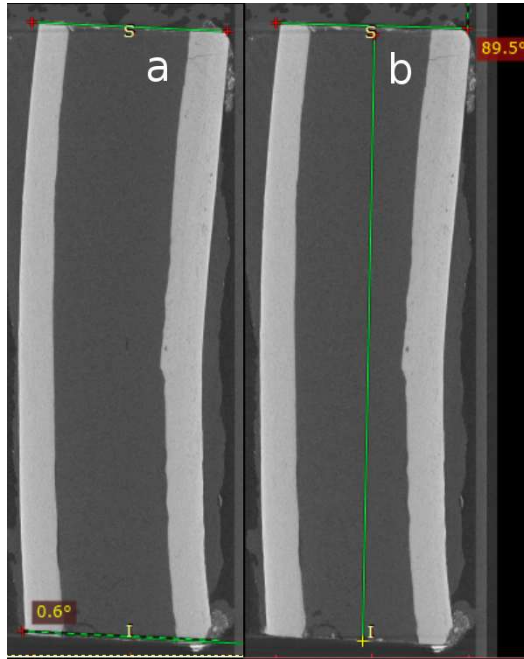


Figure 62: a) Parallel cuts. b) Satisfactory alignment (specimen 8, 1st group).

2) The specimen Nr.9 from the 1st group (1.5% displacement) showed higher than average stiffness, higher than average BV/TV, and had the fracture line that propagated down to at least 58.5 mm (i.e.: almost the whole length of the specimen). The type of the curve was of fragile rupture. This fracture was incomplete and again showed an increase in force after a drop in the curve. This corresponds to only one cortical fracture as it was confirmed in the post-experimental micro CT scan (Fig.63).

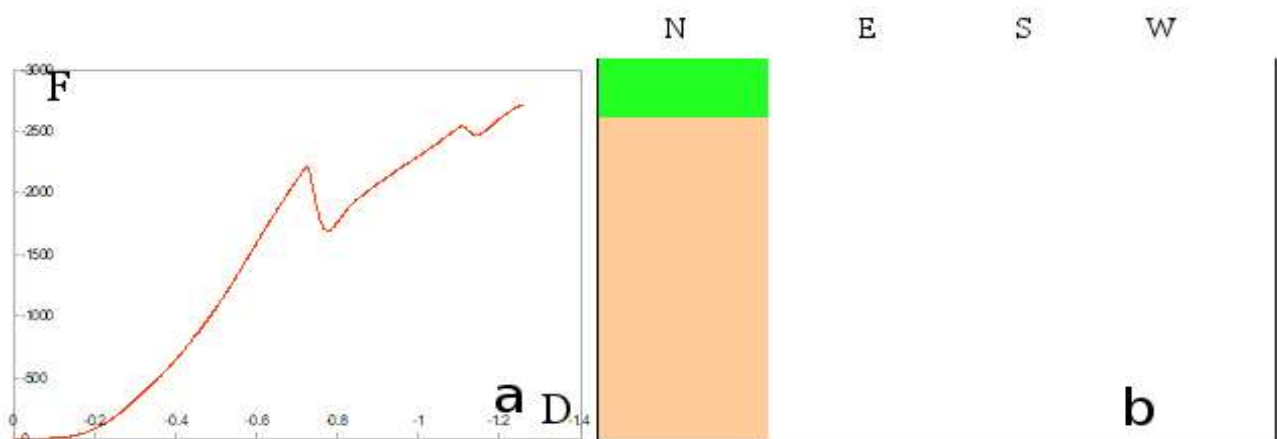


Figure 63: a) Force/displacement curve, specimen Nr.9, 1st group. b) Mapping of fracture lines.

Having had a closer look at the specimen, it was found that some bone damage could be seen on initial pre-experimental micro CT. The pre-experimental fracture line extended for about 12.5mm (Fig.64) at the proximal side and for about 8mm at the distal side (Fig.64). There was some damage and cortical bone loss at both sides.

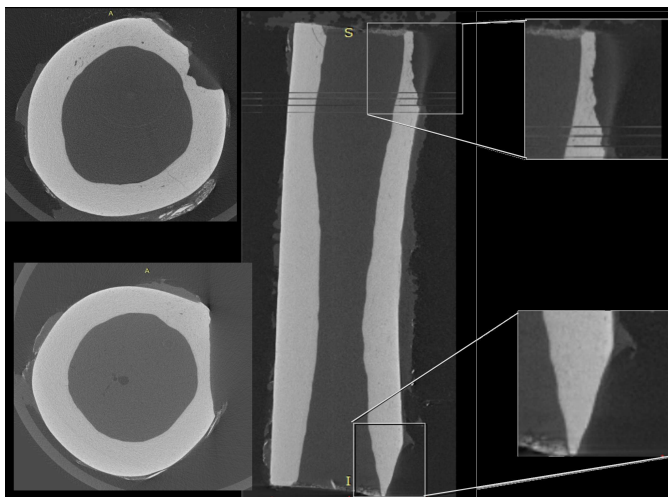


Figure 64: Proximal and distal end damage, note damage on both proximal cortical bones.

The proximal and distal cuts of the specimen were not quite parallel and thus, not quite perpendicular to the longitudinal axis of (Fig.65).

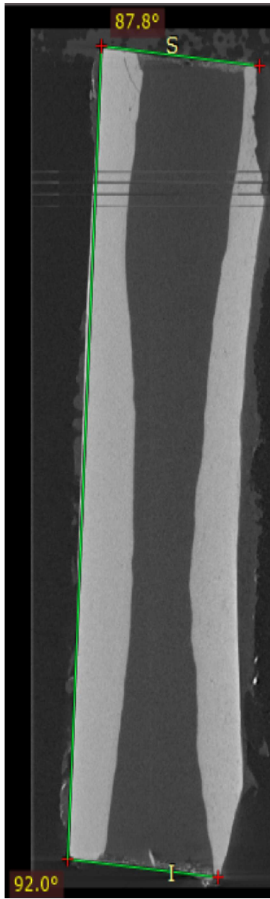


Figure 65: Slight misalignment of proximal and distal cuts.

3) Specimen Nr.3 from the 2nd group (3% displacement) had the shape of the curve of yielding showing no complete rupture but several small incomplete ruptures (Fig.66).

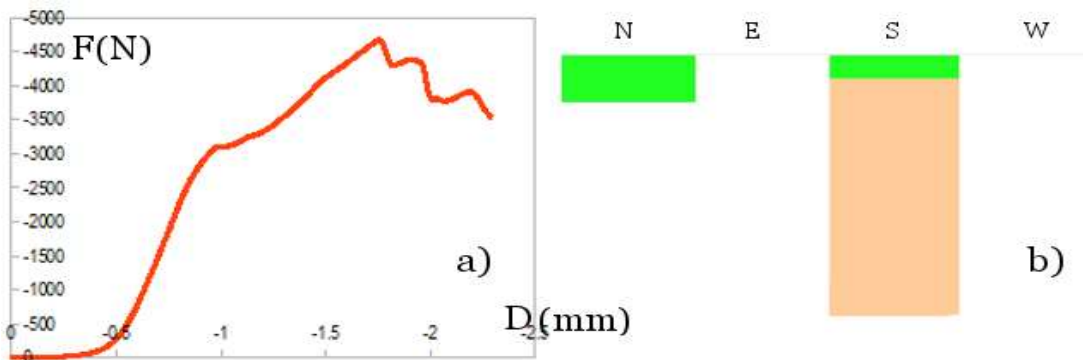


Figure 66: a) 2L + Y type of the curve, but showing several small ruptures, specimen Nr.3, 2nd group. b) Mapping of fracture lines.

The fracture line has been found going down up to 32.5 mm in the micro-CT scan after the experimentation. The BV/TV ratio was less than average, this specimen had a very high stiffness. There was a very slight cortical bone damage seen on the pre-experimental micro CT scan (Fig.67).

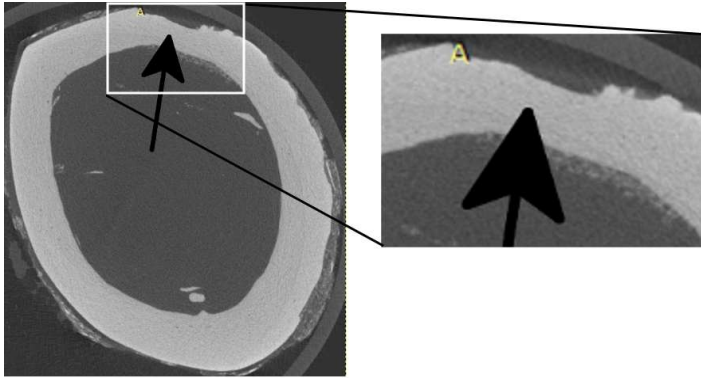


Figure 67: Slight cortical bone damage, specimen Nr.3, 2nd group.

There was also a  $4^\circ$  misalignment between the proximal and distal cuts and this might have had some positional adjustments and some influence on the shape of the curve. One of the cuts was well aligned and was perpendicular to the longitudinal axis (Fig.68).



Figure 68: a) 4° Misalignment (note a blood vessel entering the bone). b) alignment with the longitudinal axis, specimen Nr.3, 2nd group.

While further analysing this specimen in the post-experimental micro CT scan it became clear that the comminution extended for about 2 mm (Fig.69).

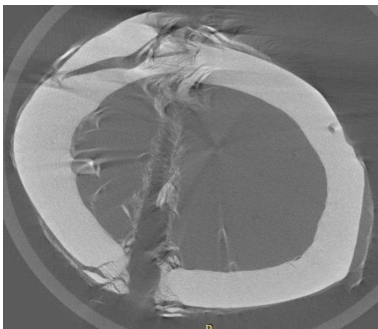


Figure 69: Comminution of the post-experimental micro CT scan, specimen Nr3, 2nd group.

The length of the cortical bone fracture corresponded to the bone chip detached from the proximal cortical bone but it didn't involve the whole thickness of the cortical

bone (Fig.70). The length involving the full thickness of the cortical bone was 2mm. This corresponds to the yielding patent of the curve.

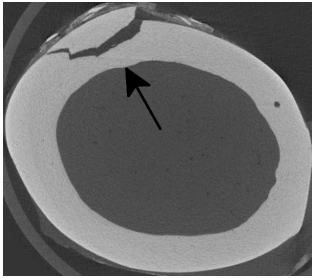


Figure 70: The bone chip detached leaving some of the cortical bone intact, specimen Nr3, 2nd group.

4) Specimen Nr.5 from 2nd group (3% displacement) showed a 2L+Crack type force/displacement pattern (Fig.71), although the fracture line under the metallic rod seen the extended for only 3mm.

This specimen had less than average stiffness and a bit higher than average BV/TV.

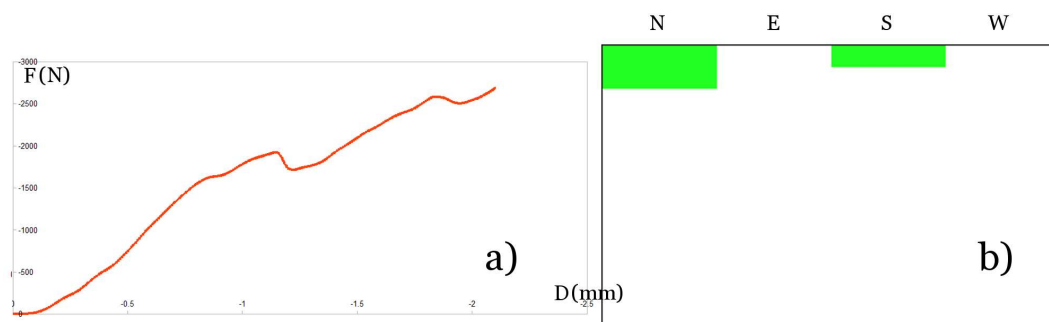


Figure 71: Small incomplete fracture seen in the curve (a) and fracture mapping (b), specimen Nr.5, 2nd group.

It was seen in the pre-experimental micro CT scan that there were some fracture lines up to 6.5mm at the distal part of it, there was some comminution as well (Fig.72).

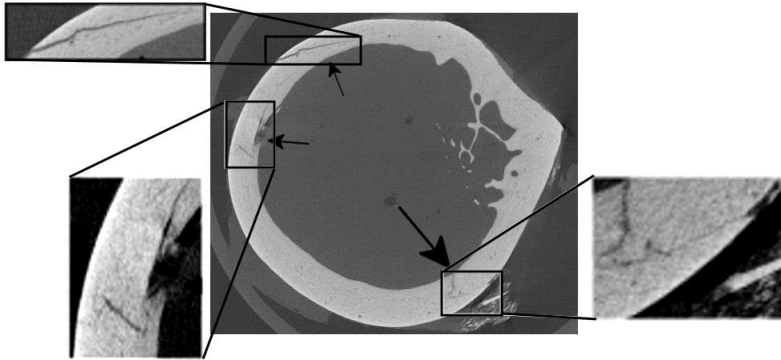


Figure 72: Fracture lines up to 3mm, specimen Nr.5, 2nd group.

While examining the distal part of the specimen in the post-experimental micro-CT scans procedure that those fracture lines slightly extended to up to 7mm (Fig.73). This shows that a fracture extended at the distal part of the specimen but not at the proximal part where the metallic rod was placed. This explains the fracture pattern of the force/displacement curve, but also relatively small fracture propagation under the rod.

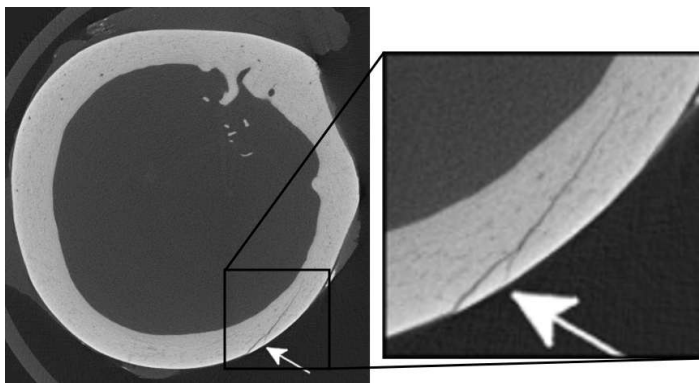


Figure 73: Fracture extension in post-experimental micro CT scan at the distal part of the specimen Nr.5, 2nd group.

The alignment of the cuts proximally and distally was considered satisfactory. The cuts were perpendicular to the longitudinal axis of the specimen (Fig.74).

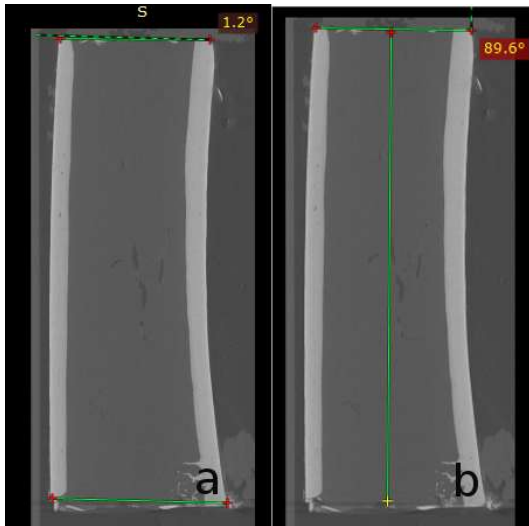


Figure 74: a) Proximal and distal cuts almost parallel. b) The cuts were perpendicular to the longitudinal axis, specimen Nr5, 2nd group.

5) Specimen Nr.13 in the 2nd group (3% displacement) showed 2L+Crack pattern in the force/displacement curve, it had relatively high stiffness, and average BV/TV, it showed a long fracture propagation line that extended for at least 32.5 mm (Fig.75).

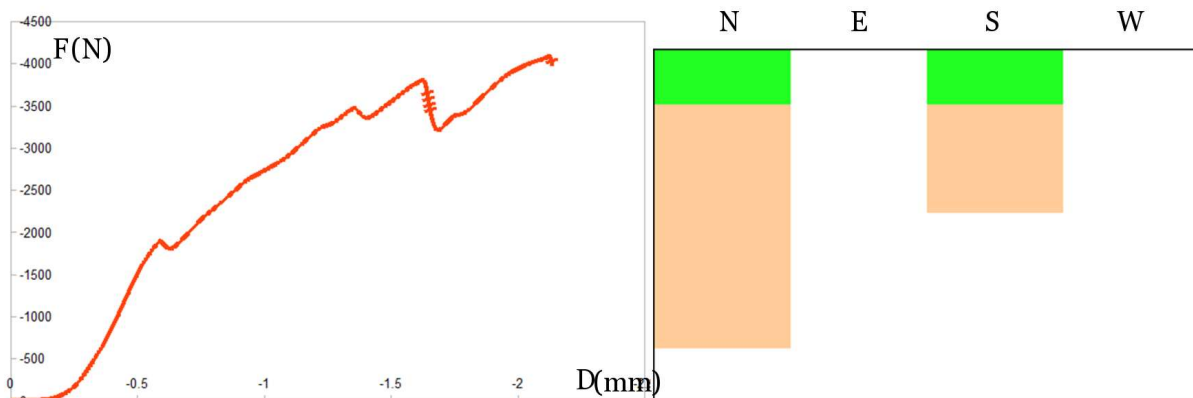


Figure 75: 2L + Crack type of the curve but showing several small incomplete fractures.

While analysing the pre-experimental micro CT scan it was seen that the specimen had some damage at the distal part of it with some fractures extending up to 3 mm (Fig.76).

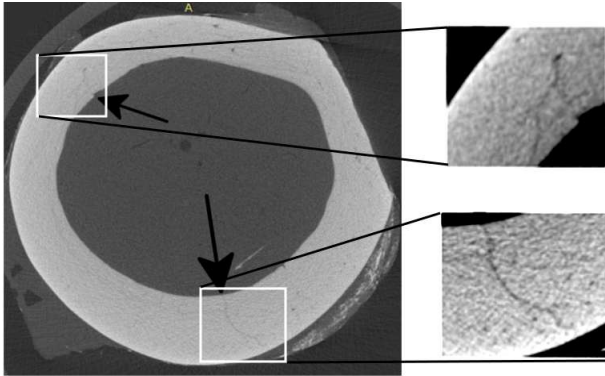


Figure 76: The fractures seen in the pre-experimental micro CT scan, specimen Nr. 13, 2nd group.

Although the two fractures (proximal and distal) identified in the post-experimental micro CT scans remained apart, there was a gap of only 10 mm left between them in the post experimental micro CT scan (Fig.77).

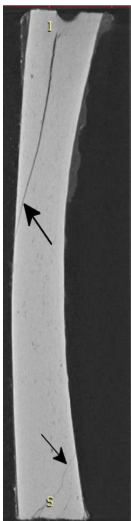


Figure 77: Proximal and distal fracture lines seen in the post-experimental micro CT scan, specimen Nr.13 in the 2nd group, the distal line was seen in pre-experimental micro CT scan.

6) Specimen Nr 14 in the 2nd group (3% displacement) showed a high fracture score of 83. The fracture line extended distally with a rather big distance between the fragments resulting in a high fracture score.

The force-displacement curve also showed signs consistent with a brittle fracture

(Fig.78).

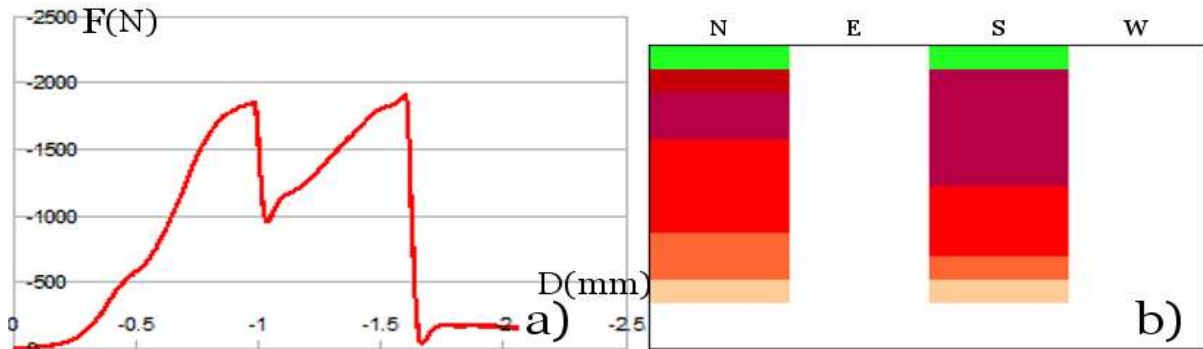


Figure 78: a) 2L+Crack+FR fracture type of the curve. b) Fracture mapping, specimen 14, 2nd group.

There were very few signs of comminution or bone damage at the contact area in the post experimental microCT scan. The fracture looked very brittle with swift fragment separation (Fig.79) and a considerable distance between them.

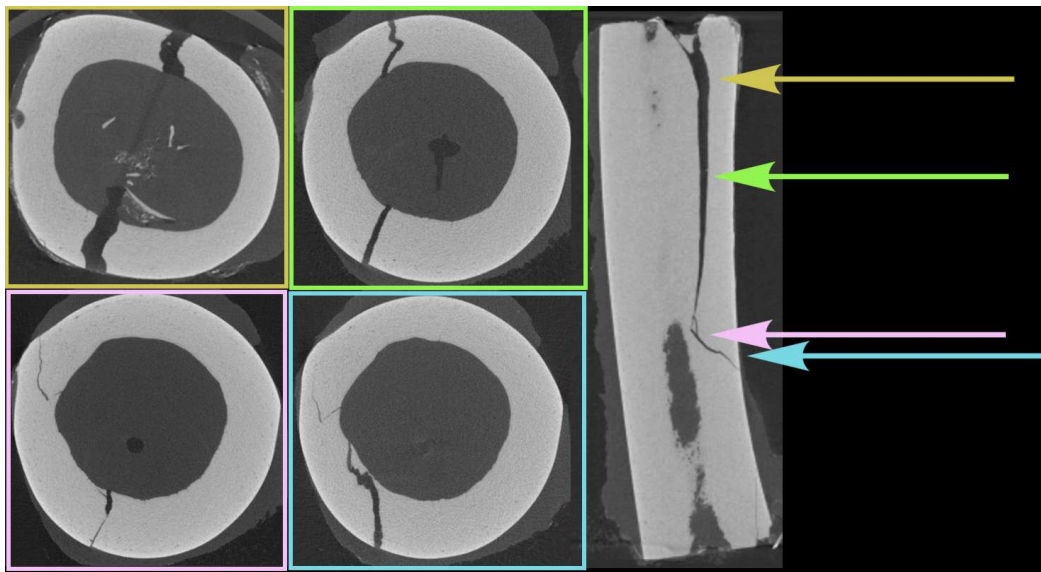


Figure 79: Brittle fracture. Note little signs of local bone damaging at the contact area.

7) Specimen Nr. 9 from the 3 group (6% displacement) had a 2L+Crack force/displacement curve pattern, had low stiffness, higher than average BV/TV, and had the fracture line extended up to 45 mm.

There were several drops seen in the force/displacement curve which corresponds to some incomplete fractures while the global form remained comparable to a plastic deformation (Fig.80).

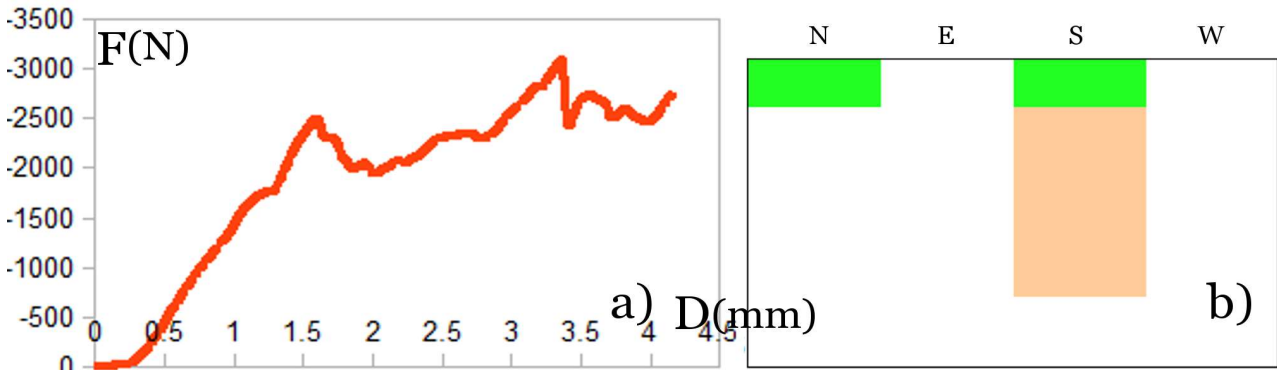


Figure 80: a) Several drops in the force/displacement curve showing incomplete fractures. b) fracture mapping, specimen number 9, 3rd group.

The fracture seen in pre-experimental micro-CT scan that extended to 10mm at the distal part of the specimen. This fracture became more displaced in the post-experimental micro-CT scan (Fig.81) There was no major damage at the proximal part of the pre-experimental micro CT scan.

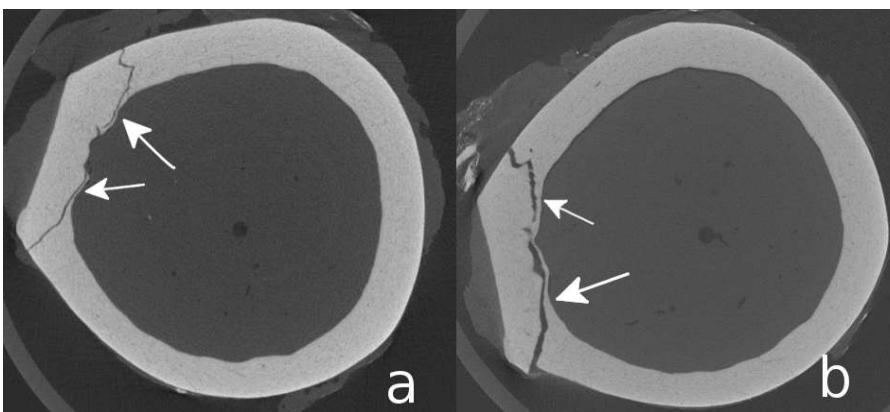


Figure 81: Fracture lines in pre-experimental micro CT scan (a). The same fracture with greater displacement (b), specimen Nr.9, 3rd group.

The proximal and the distal cuts were well aligned and parallel, they were perpendicular to the longitudinal axis (Fig.82).

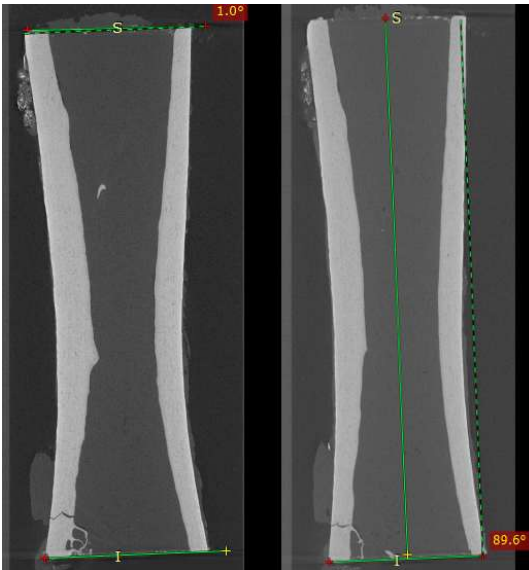


Figure 82: Satisfactory alignment, specimen 9, 3rd group.

The full cortical fracture involved one cortical bone while the other had some comminution extending for several millimetres (Fig.83).

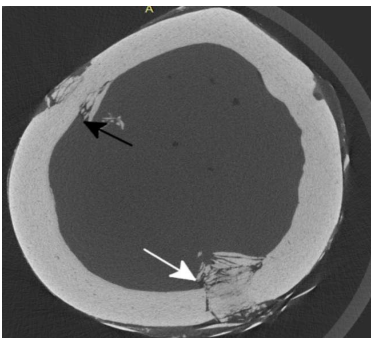


Figure 83: Comminution (black arrow) and a cortical fracture with communication (white arrow), specimen Nr.9, 3rd group.

8) The specimen Nr.12, 3rd group (6% displacement) showed a 2L+Crack+Y pattern in the force/displacement curve though it had fracture propagation line extending distally

for at least 44.5 mm. This specimen had higher than average stiffness and lower than average BV/TV.

The force/displacement curve showed a global pattern of plastic deformation but there were several drops in the curve showing that there were several incomplete fractures (Fig.84).

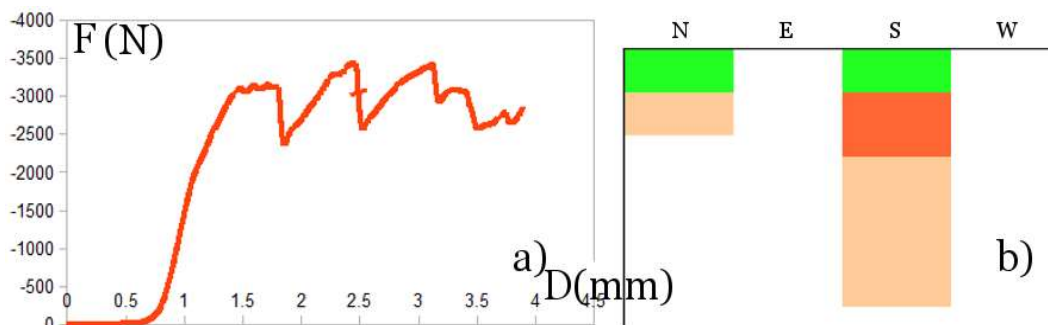


Figure 84: Incomplete fractures seen in the force/displacement curve, specimen Nr.12, 3rd group.

There was a bony defect extending for about 3 mm at the proximal part of the specimen in the pre-experimental micro-CT scan (Fig.85).

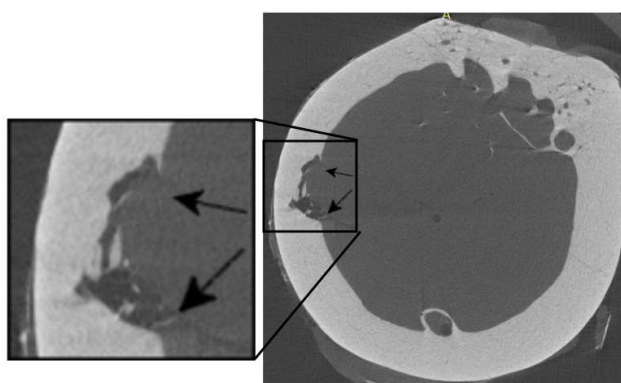


Figure 85: Bony defect extending for about 3 mm at the proximal part of the specimen Nr.12, 3rd group.

It was also a tiny fracture line seen on the opposite side, i.e. distal end that extended

for about 4mm (Fig.86).

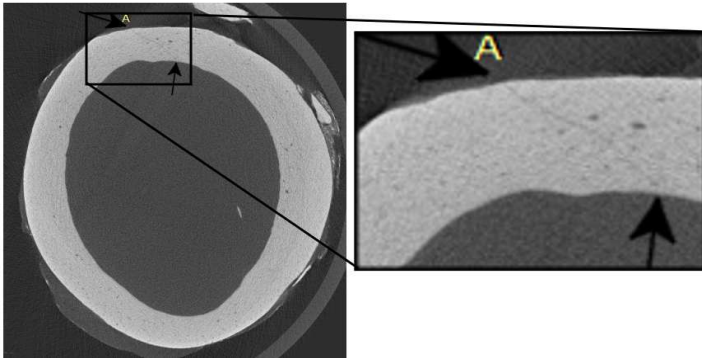


Figure 86: A tiny fracture line seen on the opposite side, distal part, specimen Nr.12, 3rd group.

The distal and proximal cuts were not quite parallel, they were done with an angle of about  $5^\circ$ . There was also some degree of misalignment between the cut and the longitudinal axis of the specimen (Fig.87). This may have generated some additional strain on one of the cortical bones.

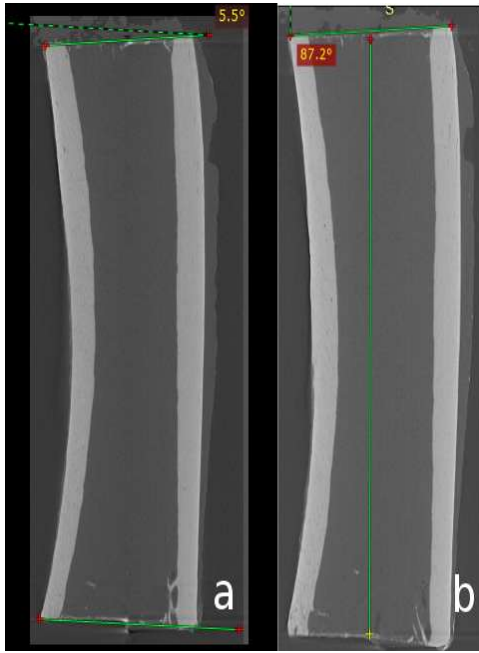


Figure 87: a) 5° Misalignment of the proximal and distal cut. b) Misalignment of the cut and the longitudinal axis, specimen Nr.12, 3rd group.

Moreover, the distal cut made during the preparation was a bit uneven (Fig.88) with a prominent bone fragment. This small fragment was fractured during the experimentation therefore causing a drop in the force/displacement curve.

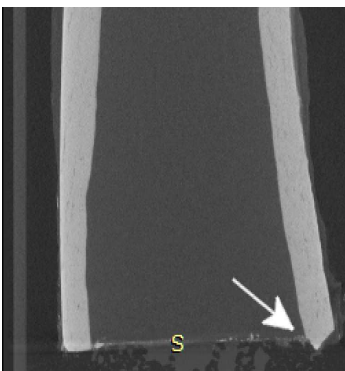


Figure 88: A small fragment seen at the distal part of the specimen Nr12, 3rd group.

The fracture line seen the in the post-experimental micro CT scan didn't have any

connection with previously described fracture lines. It was independent, was present in a different region, was just under the rod and propagated longitudinally (Fig.89).

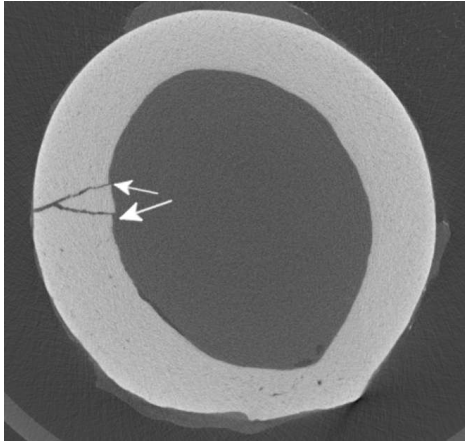


Figure 89: Fracture line seen in post-experimental micro CT, specimen Nr.12, 3rd group.

9) The specimen Nr. 14 from 3rd group (6% displacement) showed also a yielding pattern in the force/displacement curve (Fig.90) still showing some incomplete small fractures, it had a less than average stiffness, higher than average BV/TV, and had the fracture propagation up to at least 32.5mm.

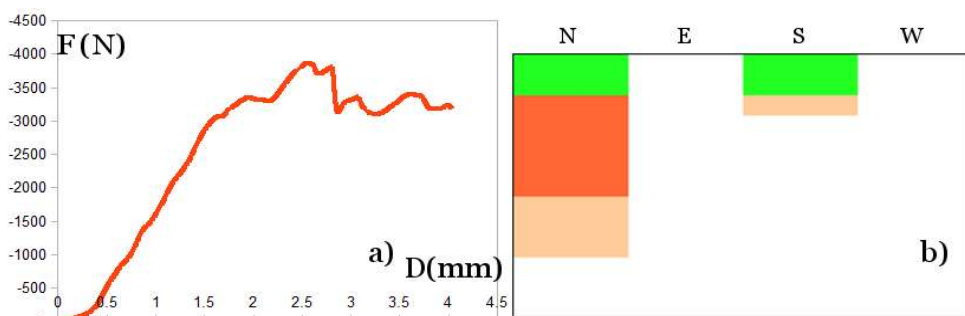


Figure 90: a) Force/displacement curve and mapping (b) specimen Nr.14, 3rd group.

The alignment of the proximal and distal cuts was satisfactory as well as the

alignment of the cuts in relationship with longitudinal axis (Fig.91).

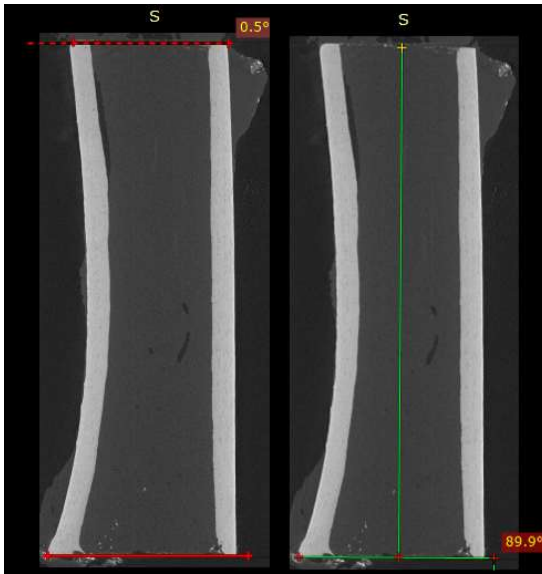


Figure 91: Proximal and distal cuts are parallel and aligned with the longitudinal axis, specimen Nr.14, 3rd group.

There was no major bone damage at the proximal end of the specimen in pre-experimental micro-CT scan. There was some damage found in the distal area of the specimen in the pre-experimental micro-CT scan. Some fracture lines extended for at least 4mm (Fig.92).

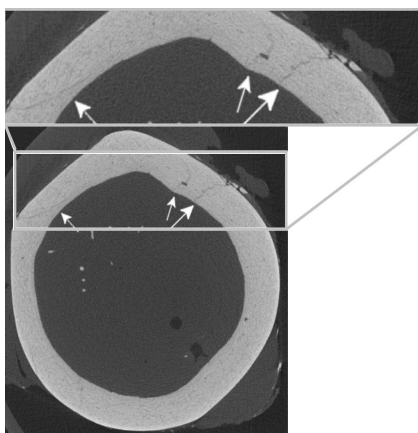


Figure 92: Pre-experimental bone damage, specimen Nr.14, 3rd group.

There was a major extension of those fracture lines seen in the pre-experimental micro-CT scan after the compression experimentation. The same fracture lines at the distal side of the specimen after the experimentation extended for at least 11mm (Fig.93).

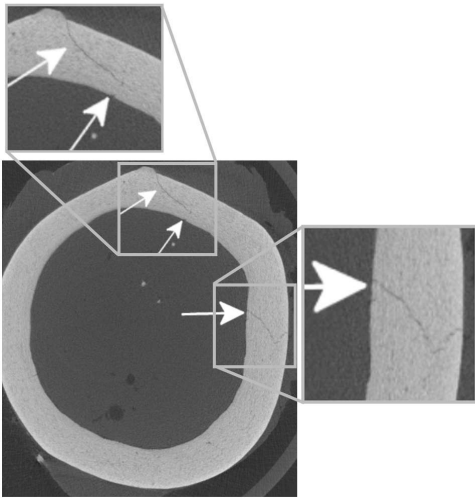


Figure 93: Extension of the fracture lines at the distal part of the specimen Nr. 14, 3rd group.

There was another fracture line propagating from and the metallic rod seen proximally, but there was no connection with fractures coming from beneath. The proximal and distal fracture lines didn't join each other. However this may have had some influence in the force/displacement curve as it showed a global pattern of yielding with several drops indicating several incomplete fractures (Fig.94).

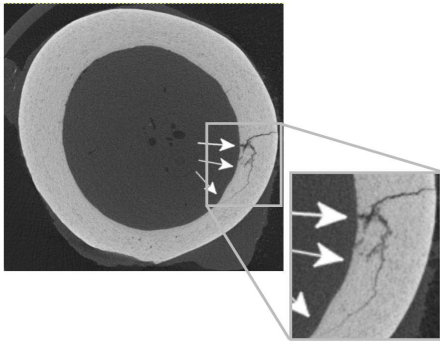


Figure 94: Fracture line propagating down from the metallic rod, specimen Nr14, 3rd group. It is interesting to note that this fracture line disperses laterally within the cortical bone at the very distal part of it.

### **3.4.3 Conclusion.**

In conclusion, different phenomena take place during the process of fracture including linear behaviour, plastic deformation, and the fracture itself, but also phenomena related to the surface of contact. They may be present to different extent therefore the global mechanical behaviour and thus the shape of the curve is defined by the predominant phenomenon.

Several specimens were problematic because of the bone damage during the extraction of the bone cylinders from the ewe's femur. Therefore, the biomechanical behaviour and imaging findings were altered. Some of them showed incomplete fractures and combined the mechanical behaviour a choice had to be made as to what category of the curve it had to be attributed.

### **3.4.4. Mathematical analysis of the contact area.**

This part was done in collaboration with a Master student Felix Camagay.

#### **Introduction. Failure Hypothesis.**

Development of bone fracture is a complex event as several phenomena take place

at the same time at the same time. It is even more so when a metallic rod is interposed between the compression machine and the bony cylinder. At the very beginning of every force-displacement curve a non-linear part that resembles an exponential curve could be seen (Fig.95).

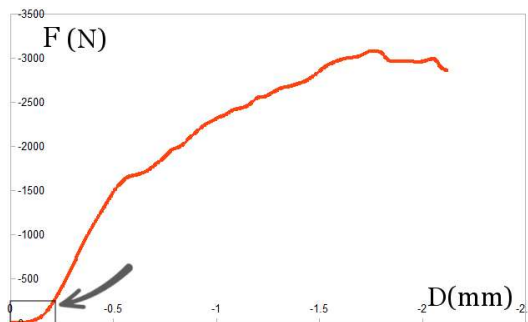


Figure 95: A non-linear beginning of the curve (arrow).

It was hypothesised that other than specimen's positioning, local contact phenomena could explain this part of the curve. In this case, Hertz's contact theory between two cylinders could be applied. One of the cylinders would be the metallic rod with known radius and another cylinder would be the specimen with a radius approaching infinity as the metallic rod lays over the bone specimen.

Several configurations can be distinguished at the interface between the bone and the metallic rod while it undergoes local loading (Fig.96).

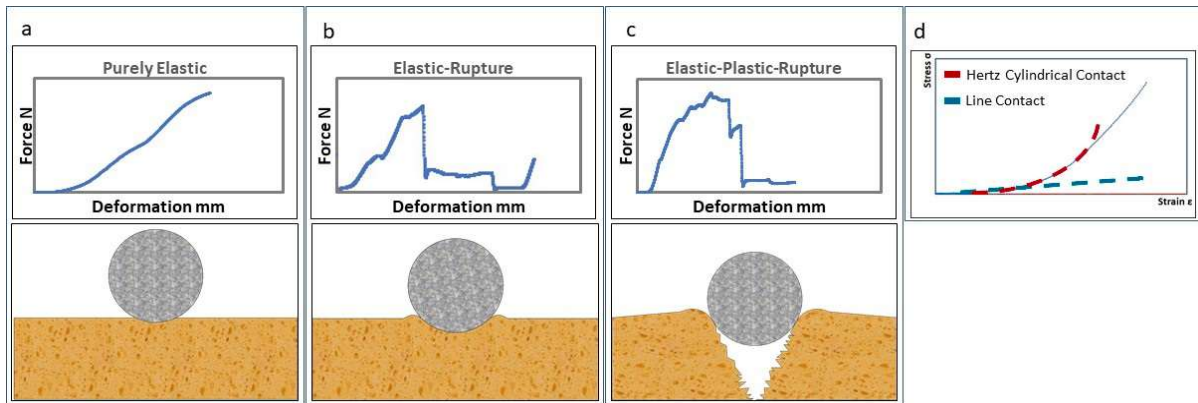


Figure 96: Loading configurations: a) elastic behaviour, b) elastic behaviour with rupture, c) elastic-plastic behaviour with rupture. The curve d) represents a very initial part of an obtained curve (grey), theoretical calculated curve related to Hertz's theory (red dotted curve) and theoretical curve of linear behaviour (blue dotted curve).

Initially, the metal rod and the surface of the bone are in contact with each other, which denotes the zero (0) point in the displacement scale. As soon as a load is applied, the bone undergoes linear elastic deformation. This was seen in all of the groups. Although in general the mechanical behaviour in the beginning was linear, it was not at the starting point of a curve for a fraction of a mm (estimated 0.05-0.15mm) of displacement (Fig.97).

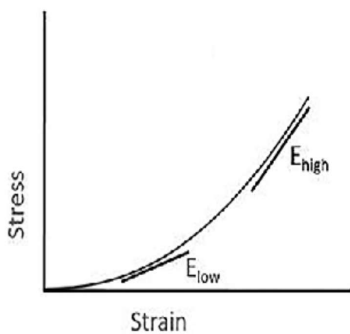


Figure 97: Elastic non-linear behaviour. Adapted from [Wang16].

As this phenomenon was observed in all curves, it was important to include this in the study.

The explanation could be related the Hertz contact theory. This theory could apply

in the beginning of loading. As the rod is pushed deeper into the bone, there is some stress distribution because of increase of contact area, that is why a different curve which is similar to the normal linear elastic curve can be observed. This happens because the stress is more evenly distributed throughout the bodies in contact and the observed phenomena are not related to the contact theory.

The study by Ghaednia, et al. [Ghae17] presented analytical solutions for the stresses involved in elastic-plastic deformation in cylindrical contact. After plastic deformation (Fig.96c), a rupture occurs. Though not all of the specimens underwent a rupture, it is important to note that if the rupture takes place, it can be with or without a plastic deformation. It can therefore be assumed that there is a different bone fracture mechanism: ductile (with plastic deformation) and brittle (without). The assumption can be justified as the bone is anisotropic and its resistance varies depending on its density and other features of structure such as osteon alignment, collagen fibres' orientation, etc.

### **Using a Mathematical Model to Fit the Experimental Data - Validation by Curve Fitting.**

In order to apply the Hertz theory on the elastic region of the experimental curves, a semi automatic curve fitting program was made using Octave, which is a freeware version of Matlab [Eato19]. The aim of the curve fitting was to determine what the modulus of elasticity is obtained by the analytical solutions presented in the previous section, and also to determine the range at **which** this solution is applicable to the curve. According to the literature, the Hertz theory only applies to about 10-20% of the elastic range. To begin with, certain assumptions were made. It was assumed that the radius of the bone is infinite since it is a surface. The elastic modulus of the metal rod is also considered infinite since the modulus of steel is much higher than that of the bone. The thickness of cortical bone in

contact with the metal rod, based on the micro-CT scans is about 3mm, thus the effective length of contact between the rod and the cortical bone is 6mm. Since the loading configuration is considered plane stress, the working Poisson ratio is negligible. Therefore, the effective elastic modulus of the system is equivalent to the elastic modulus of the bone (Table 11).

Table 11: Assumptions on Curve Fit Values.

	Metal	Bone
Radius	2mm	inf
Poisson Ratio	0*	0*
Young's Modulus	inf	20 GPa**
Length of Contact 6mm		

\*plane stress

\*\*assumption based on literature, which is the initial condition for curve fitting

The working equation of the curve fitting was also tailored for running effectively in Octave. The curve fit equation was obtained as follows:

$$\delta_1 := P \cdot \frac{1 - \nu_1^2}{\pi \cdot E_1} \cdot \left( 2 \cdot \ln \left( \frac{4 \cdot d_1}{b} \right) - 1 \right)$$

$$\delta_2 := P \cdot \frac{1 - \nu_2^2}{\pi \cdot E_2} \cdot \left( 2 \cdot \ln \left( \frac{4 \cdot d_2}{b} \right) - 1 \right)$$

$$k := \pi \cdot 2 \cdot a \cdot \left[ \frac{1 - (\nu_1)^2}{E_1} \cdot \left( 2 \cdot \ln \left( \frac{4 \cdot d_1}{b} \right) - 1 \right) + \frac{1 - (\nu_2)^2}{E_2} \cdot \left( 2 \cdot \ln \left( \frac{4 \cdot d_2}{b} \right) - 1 \right) - \frac{1}{E_c} \right]^{-1}$$

$$E_c := \left[ \frac{1 - \nu_1^2}{E_1} + \frac{1 - \nu_2^2}{E_2} \right]^{-1}$$

The term  $1/E^*$  can be denoted as a single variable  $a$ , which can be post-processed after the curve-fitting. Making it a single variable instead of a fraction makes the Octave program run easier. To be able to fit the curve properly, it was considered to add an arbitrary variable for the a single-axis translation of the data, thus  $c$  is added. The final curve fitting equation is as follows:

$$\delta = \mathbf{a} \left[ \ln(4R) - 0.5 \ln \left( \frac{2PR}{\pi L} \right) - 0.5(a) - 0.5 \right] + \mathbf{c}$$

The initial condition for the value of  $a$  was supposed to be  $1/20e9N$  but the program could not find a real solution with this value. With the pre-determined and unchangeable values such as the radius  $R$  and contact length  $L$ , different values closer to 1 were tried until an initial condition of  $a=0.5$  succeeded. The initial condition for is  $c=0.000$ , where the variable  $c$  was used to align the curves. It was maintained to be very small with the idea that it should not significantly affect the behaviour of the main curve and it is only a small adjustment.

All of the 45 specimens were curve fitted. The code will run until the  $error^2$  between the original displacement and the curve-fitted value reaches 0.0001 ( $(\delta_{\text{experimental}} - \delta_{\text{predicted}})^2 \geq 0.0001$ ). This is only an arbitrary value which was determined to limit the analysis to a certainty.

The curve-fitting code consists of 3 main functions that 1) reads the experimental data from excel, 2) curve fits the data and 3) writes the curve-fitted data in a new excel file and creates a graph. The code asks first for the .xlsx file for input values, then asks the specimen numbers, then for the output .xlsx file where the data will be put. Refer to AnnexV for the code. The desired outputs of the program are the maximum displacement reached before the  $error^2$  reaches the maximum, the force at that displacement, the values of parameters  $a$  and  $c$ , and the computed modulus of elasticity  $E$ . Refer to AnnexVI for obtained curve fitting values.

## **Results.**

Five behaviours were registered after the experimentation: Elastic deformation, linear elastic and plastic deformation, elastic and plastic deformation followed by rupture, elastic deformation followed immediately by rupture, and elastic deformation followed by 2 consecutive ruptures were recorded. Since all the results presented a linear elastic deformation in the beginning of the test, a stiffness of  $2648 \pm 873$  N/mm was deduced. Rupture forces were recorded between 2000N and 4000N.

The loading was quasi-static as opposed to cyclical loading in a clinical setting. The data presents that even at 1mm to 4mm displacement a fracture can already occur. This suggests that after the surgery, such strain at the entry points of the distal locking screw would result in considerable internal stresses and ultimately, a fracture, which would compromise the bone fixation.

## **Validation by Curve Fitting.**

The results from the curve fitting program have been obtained. The **error<sup>2</sup>** of 0.0001 proved to be sufficient to calculate a curve that closely matched that of the original experimental curve and up to about 10-20% of the elastic curve (Fig.98). Almost all of the experimental data obtained such curve. As it can be seen in the figure (Fig.98), the experimental data points and mathematical model data points are very close to each other until around 0.15mm and the curves deviate as the graph moves toward positive infinity.

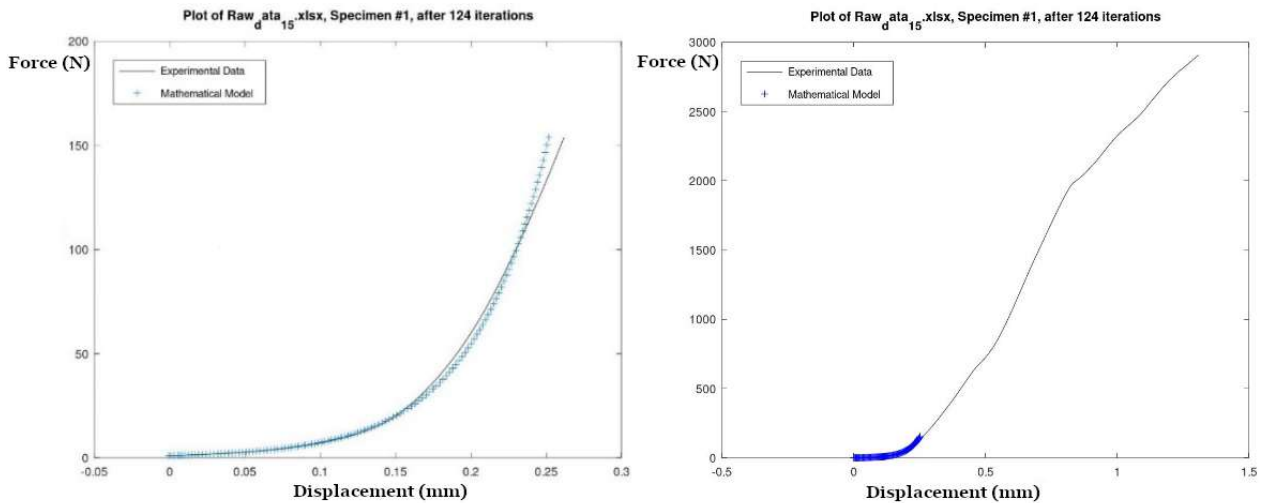


Figure 98: Example of Curve-fitted Graph of Experimental Data. a) Particular data set before reaching  $error^2$ , b) Extended graph of experimental data with curve-fitted graph.

Before the **error<sup>2</sup>** is reached, there is only 1 intersection between 0.2 and 0.25mm (Fig.98a) where the two lines meet before the mathematical model curve grows logarithmically. By this point, the original curve is seen to grow almost linearly (Fig.98b), similarly to linear elastic deformation mechanics in materials. This must be caused by the increasing amount of contact between the rod and the surface of the bone. As the contact area increases, the nature of contact transforms from being shear stress dependent into normal stress dependent. It approaches a configuration of a cylindrical shaft in a hole that is almost the same size as the shaft and loaded vertically downwards. In classical mechanics it is assumed that the hole will deform downwards and only the stresses parallel to the direction of force are taken into consideration – similar to the analysis of uniaxial loading. Using this guiding principle the stiffness of the linear elastic curve was recorded during the experimentation.

Table 12: Summary of Data Obtained.

Max Deflection (mm)	Max Predicted Deflection (mm)	Max Force Obtained (N)	Elastic Modulus (Pa)
0.18	0.17	121.6	12.3
0.17	0.16	78.6	8.8
0.10	0.09	12.4	16.9
0.15	0.14	70.9	12.6

As shown in Table 12 above, the average value of elastic modulus obtained was  $E=12.64\text{Pa}$ , the average maximum deflection and force were  $\delta=0.1468\text{mm}$  and  $P=70.8757\text{N}$ , respectively. The elastic modulus of such degree is very small to be realistic. The explanation for this is not quite obvious and further refinement of the working equations should be done. One of the hypothesis might be that the contact between the rod and the bone was not completely flat (e.g. the contact might be slightly slanted) thus only some of the surface was effectively in contact. To prevent this, a pre-loading was done before the actual recording was started but due to differences of the bone geometry, some specimens still experienced partial contact which resulted in double-spiking. Three specimens were excluded from the analysis since the application could not find a converging solution. The noise in the curve could be a possible explanation. See AnnexVI for the summary of results.

### Conclusions and Perspectives.

The curve fit equation was partially acceptable since the curve was shown to match a certain part of the elastic region and within the range described in the Hertz theory which is about 10%. Although the behaviour of the mathematical model might be a success, some parameters must be adjusted to better fit the acquired values and be more realistic. The obtained average elastic modulus value was not realistic as it should range at around 15-25GPa based on literature describing tests of uniaxial loading. Further research on the usage of the working equations must be done in order to match the values correctly.

After the curve fitting of the elastic region, the next perspective could be the plastic region of the curve and then fracture.

The effect of contact on bone is not very well studied, but some studies on contact using metals and other materials have been done. On some assumptions, comparison to metal could work but only to some extent since the bone has properties similar to composite materials. Understanding the contact mechanics of bone, being anisotropic and quasi-brittle, can lead to vast applications from ensuring safety precautions for bone the use of implants, and even non-bone applications such as composites.

### **3.5. Relationship between the curves and the imaging.**

There were no specific studies evaluating the contact area, different forces and potential bone damage at the distal locking screw and the bone interface to the best of our knowledge. Our experimental protocol and experimental model using an animal bone allowed us to evaluate those different parameters and correlate the displacement, the forces involved and the imaging which has allowed to get some more information about the potential bone damage at the distal locking screw.

Our protocol involved an animal bone cylinder and a metallic rod instead of the locking screw. The mechanical testing was quasi static compared to a cyclical solicitation in a clinical setting. Despite those drawbacks our study allowed us to identify the limit values of rupture and study the bone damage patterns as the displacement of the distal locking screw comes close to the limit value of rupture.

### **3.6. Conclusion.**

An experimental model was created. It allowed to investigate the potential bone damage around the distal cortical locking screw of intramedullary devices by identifying several microstructural damage patterns related to the mechanical behaviour. A simplified local strain model was used in this case. This model allowed to study different phenomena taking place during the process of fracture including linear behaviour, plastic deformation, and the fracture itself, but also phenomena related to the surface of contact. They may be present to different extent therefore the global mechanical behaviour and thus the shape of the curve was defined by the predominant phenomenon. A mathematical model based on the Hertz' contact theory was used to explain the non-linear behaviour seen the beginning of every curve.

Pre-experimental and post-experimental imaging allowed to identify the geometry of the specimens and calculate  $BV/TV$ , but also allowed to follow the fracture lines if they occurred. This has led to describe qualitative and quantitative parameters. This study allowed to identify the limit values of rupture and evaluate the bone damage patterns as the displacement of the distal locking screw comes close to the limit value of rupture.

More complete assembly was needed to approach clinical settings.

## **4. Experimental model of local strain at the bone and locking screw contact area**



#### 4. Experimental model of local strain at the bone and locking screw contact area

### **4.1. Introduction.**

As seen in the literature, sometimes occurs a distal locking screw misalignment that can have a negative impact on the final outcome of bone healing and fragment position [Sakao7][He22]. In order to better understand the phenomena that take place around the distal locking screw of the intramedullary nail and to get closer the real conditions another experimental work was done. The purpose of this experimentation was to create an experimental model that would examine the phenomena around the distal locking screw, put perpendicularly to the nail axis and also in line with the screw hole of the nail and how the phenomena change when an error is introduced in the direction of the distal locking screw. It is important to note that in clinical setting it is not always easy to put the distal locking screw perfectly, that is why some angulation is often present. It is not clear if this has any clinical impact and it is not known if some angulation can compromise the fracture fixation and how the bone resistance changes if it does at all.

### **4.2. Material and Methods.**

#### **4.2.1. Specimens.**

Eighteen long bone cylinders were harvested from the ewe femoral mid-shaft. The specimens measured 65mm in length and about 20mm in diameter. A particular attention was paid in order to have parallel cuts. The lower cut was made in the junction area of metaphysis and diaphysis. The specimens were kept frozen at -20°C in a vacuum sealed plastic bags. The samples were slowly defrosted for 12 hours at +5°C before being exposed to the room temperature prior to mechanical testing.

#### 4.2.2. Mechanical testing.

An experimental model of distal intramedullary nail locking was created. The nail was custom made in order to comply with the experimental model (Fig.99).

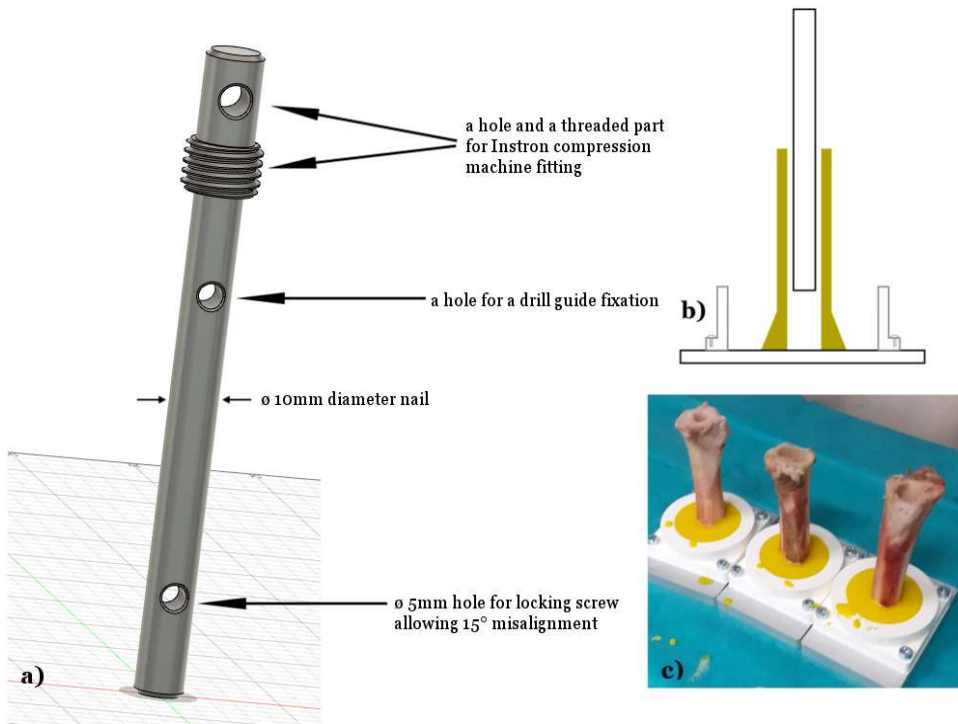


Figure 99: a) Custom made nail. b) Diagram of specimen orientation before embedding. c) The specimens were fixed and embedded in polymethyl methacrylate.

The lower part of every specimen was fixed and embedded in polymethyl methacrylate in a way that the intramedullary canal's direction is perpendicular to the transversal plane (Fig.99c). In order to achieve this a 10mm metallic rod was inserted in the specimen and oriented vertically beforehand. This allowed to have the longitudinal alignment and avoid major friction during the experimentation.

Three experimental groups of 6 specimens were created.

A metallic cylinder of 10mm of diameter was inserted into the intramedullary canal of each specimen in order to mimic the intramedullary nailing. The 1cm diameter, which is

less than the average ewe's femoral canal's diameter (21.2mm in this study) was chosen in order to minimise and avoid any friction that might distort the results. A hole, perpendicular to the axis of the cylinder in the frontal plane was created beforehand.

A metallic screw with a diameter of 3.5mm was put through the bone and through the cylinder hole in a medial to lateral direction in every specimen. This hole was created in a way that it could allow a 15° error of aiming in the frontal and transversal planes.

A guide was created and printed with a 3D printer. This guide allowed to drill a hole in the bone in a defined direction passing through the locking hole of the nail (Fig.100).

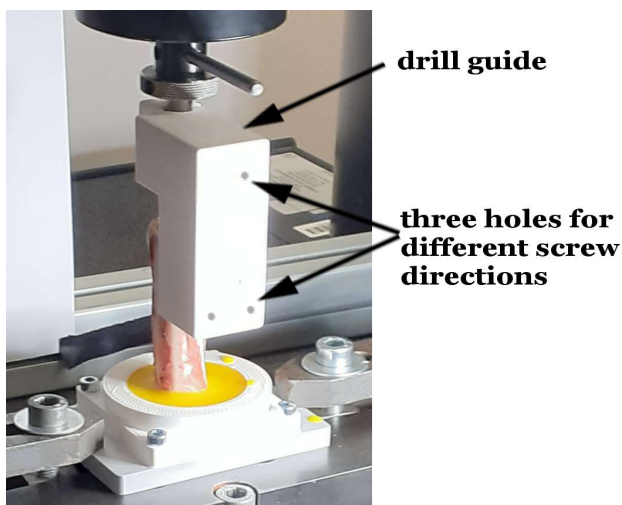


Figure 100: Drilling direction guide.

Specimens were divided into 3 groups defined by the angle of aiming. The locking screw was inserted perpendicularly to the axis of the nail and in the frontal plane in the group 1 which served as a control group (Fig.101a).

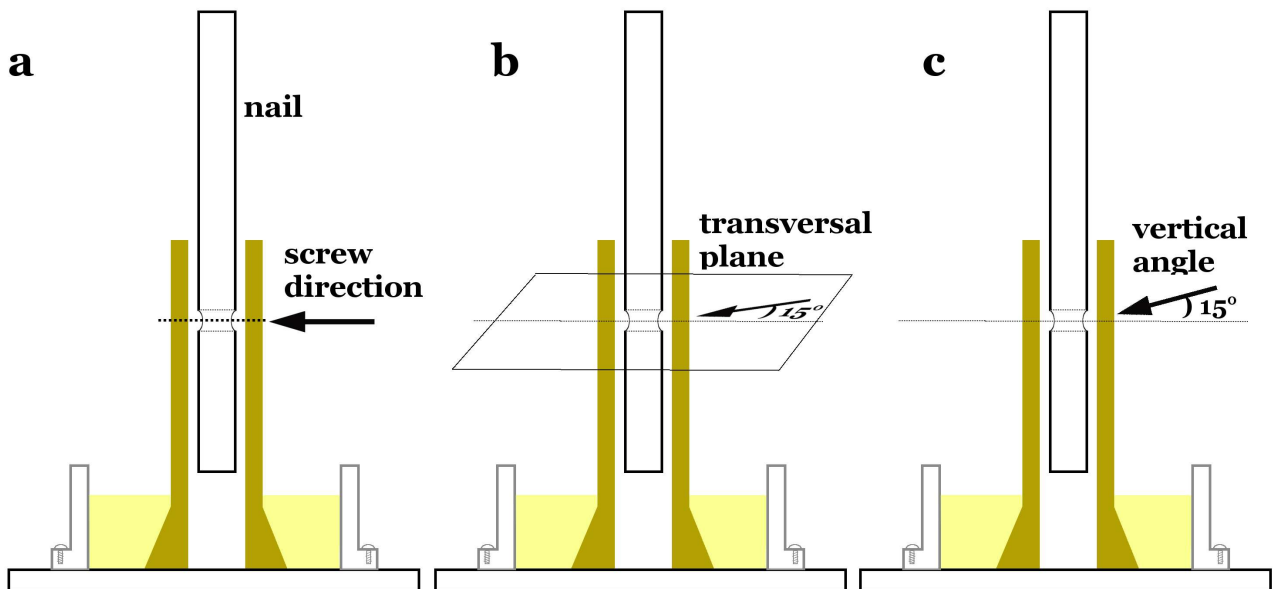


Figure 101: a) Group 1: locking screw was inserted perpendicularly to the axis of the nail and in the frontal plane. b) Group 2: locking screw inserted perpendicular to the axis but with  $15^\circ$  angulation the transversal plane. c) Group 3: locking screw was inserted in the frontal plane with  $15^\circ$  angulation to the axis of the nail.

The locking screw was inserted perpendicular to the axis of the nail but with  $15^\circ$  angulation in relationship with the direction of the locking hole in the transversal plane In the group 2 (Fig.101b.). The locking screw was inserted in the frontal plane with  $15^\circ$  angulation to the axis of the nail in the group 3 (Fig.101c).

Quasi-static compression (0.5mm/min) experimentations were performed using an Instron 5566. Specimens and the cylinder were preloaded by about 1N before compressions. The force-displacement evolutions were recorded.

The experimentation was recorded on video in a way that the two ends of the screw remained visible in order to correlate the visual data to the curve.

#### 4.2.3. Mathematical analysis.

In order to analyse the experimental data a simple mechanical model was proposed (Fig.102).

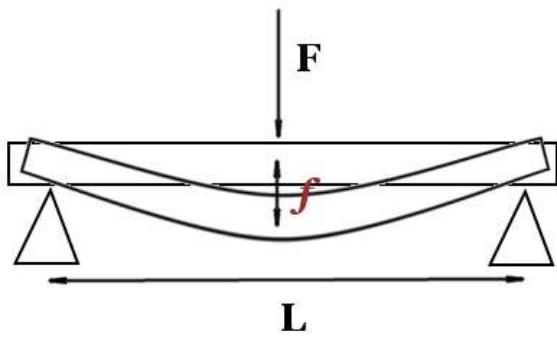


Figure 102: Simplified diagram of local loading.

$$f = \frac{FL^3}{48EI}$$

where  $I = \frac{\pi d^4}{64}$  thus  $f = \frac{4FL^3}{3\pi E d^4}$

The diameter of the femoral shaft defining the distance between supports (L) was measured.

The diameter of the screw was 3.5 mm. The nominal diameter for screw resistance was calculated  $d=2.94\text{mm}$ . L is the diameter of the femoral shaft (average of 26mm in these specimens).

$f$  is the displacement of the screw in the compression machine just before the 1st fracture that is known.

E is Young's modulus of the screw (steel: 199GPa).

The rigidity  $k$  has been obtained from the force/displacement curves and was compared to the calculated rigidity  $k_0$ .

$$k_0 = \frac{F}{f} = \frac{3\pi E d^4}{4L^3}$$

#### 4.2.4. Data analysis.

The mechanical behaviour seen in the curve was identified and assessed. Several parameters were calculated in the force-displacement curve.

As the global structure involved bone and screw, the initial stiffness  $k(N/mm)$  and the overall structure stiffness were calculated. Other parameters as  $F_{max}$ ,  $Drup_1$  (first rup),  $Frup_1$  (first rup),  $Drup$ ,  $Frup$  were calculated when it was possible (Fig.103). The end-point of linear behaviour was determined in the force-displacement curve. The energy needed for the mechanical loading was calculated with the starting point at 50N (in order to eliminate the adjustment starting part of the curve) and up to 5mm of displacement. This distance was chosen in order to be able to evaluate all the curves as the rupture occurred at different distances. Five millimetre distance is much more than the screw diameter used to lock the nail.

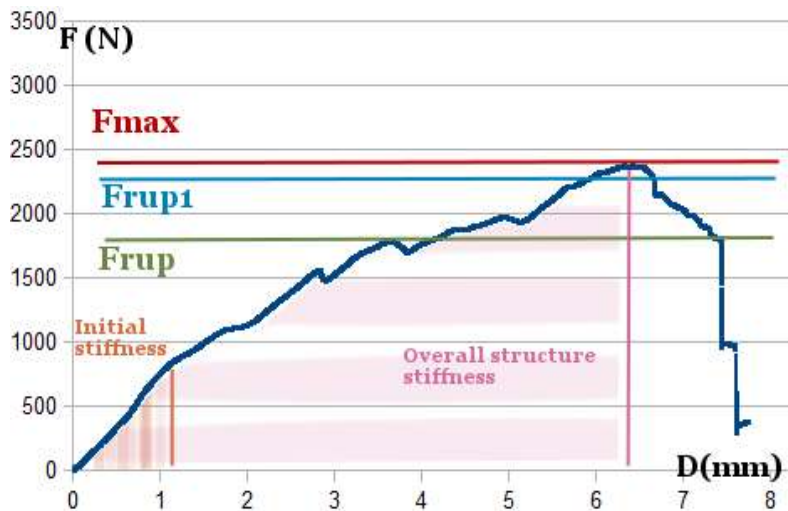


Figure 103: Diagram showing the way different parameters were assessed.

The curves were then evaluated in relationship with the video recorded. An attempt was made to find out when the bone fracture occurred if it was seen on the video.

The Pearson's coefficient and Student's test was used for statistical analysis.

A simplified experiment modelisation was done in order to get theoretical values

and compare them to obtained results.

## **4.3. Results.**

### **4.3.1. Qualitative and quantitative curve analysis.**

All the curves had a linear behaviour in the beginning. The curves obtained in this study are summarised in Figure 104. The shape of force-displacement curves had multiple fracture patterns, but a global shape of a curve could be defined. Double linear behaviour could be seen in some curves. The bone damaging in the 3<sup>rd</sup> group was slower, with no major rupture in the curve.

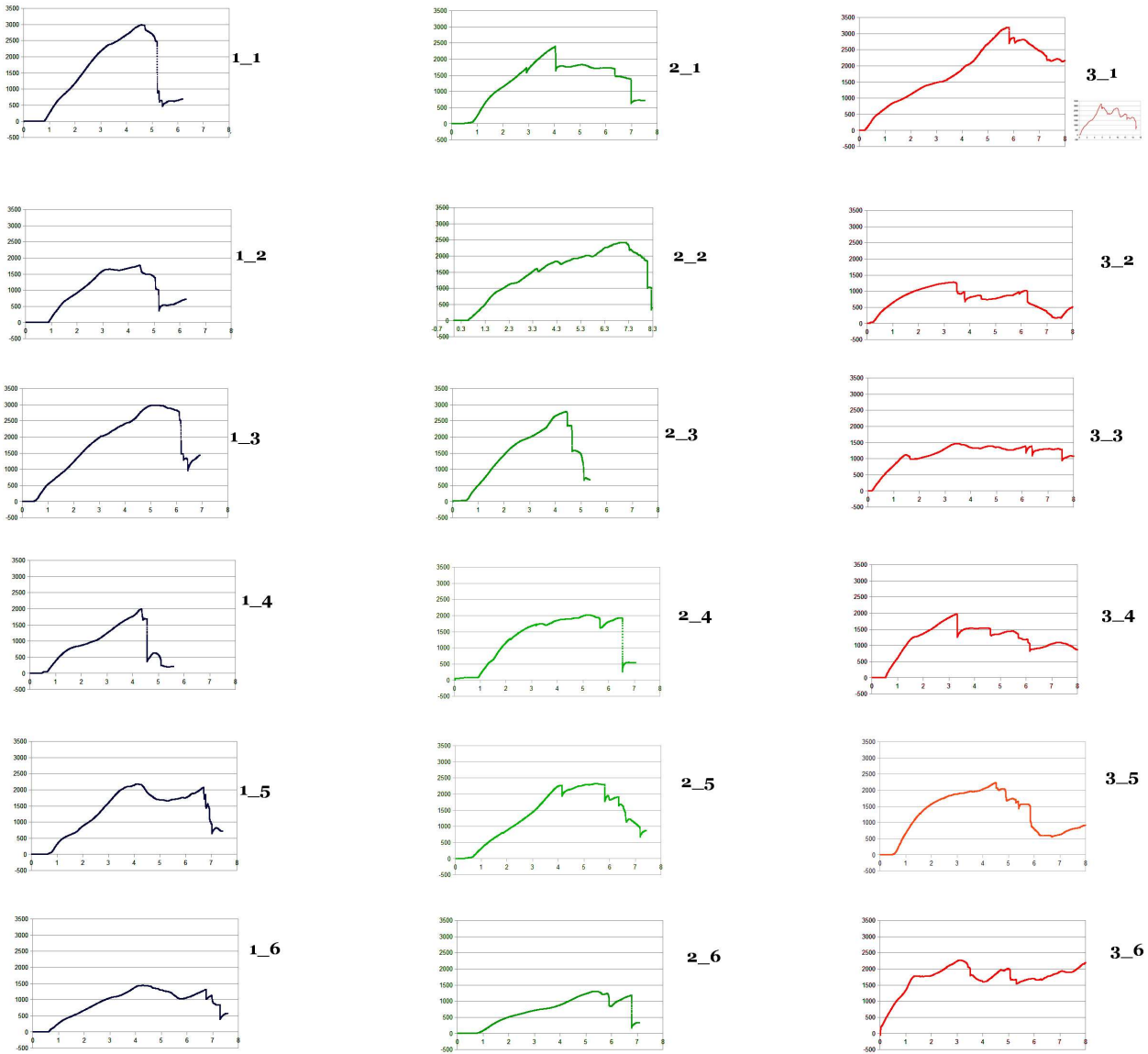


Figure 104: The shape of force-displacement curves have multiple fracture patterns. Scale adjusted.

The average stiffness was 647N/mm. The first rupture occurred at 4mm of displacement and the rupture force was 2087N on average. The results are summarised in the Table 13.

Table 13. Results of the compression experimentation of a locking screw.

Group 1 (strait)	Specimen Nr.	Initial stiffness k (N/mm)	global structure stiffness k (N/mm)	Fmax (N)	Drup1 (first rup) (mm)	Frup1 (first rup) (N)	DendL	FendL	Initial energy W (J)	Energy W 0 to 5mm (J)
no screw rupture	1	1135	785	2985	4.65	2985	3.79	2931	0.24	8.45
	2	1083	731	1768	4.44	1768	2.06	1537	0.15	5.45
	3	1023	654	2981	6.11	2753	4.20	2814	0.14	8.88
	4	735	509	1996	4.33	1996	3.81	1941	0.30	4.49
	5	865	680	2167	4.25	2167	2.84	1988	0.13	6.74
	6	558	401	1438	4.34	1438	3.49	1388	0.15	4.55
average		900	627	2222	4.69	2184	3.36	2100	0.19	6.43
StDev		223	145	638	0.71	588	0.78	642	0.07	1.92
Group 2 (15°in horizontal plain)	Specimen Nr.	Initial stiffness k (N/mm)	Global structure stiffness k (N/mm)	Fmax (N)	Drup1 (first rup) (mm)	Frup1 (first rup) (N)	DendL	FendL	Initial energy W (J)	Energy W 0 to 5mm (J)
	1	1085	720	1792	4.29	1792	3.25	2343	0.31	7.28
	2	706	376	2373	7.25	2373	6.58	2333	0.57	6.28
	3	895	737	2783	4.41	2783	3.86	2730	1.91	7.44
	4	605	518	2021	5.65	1888	2.66	1551	0.84	5.84
	5	620	637	2328	4.13	2267	3.48	2217	0.51	7.13
	6	430	278	1304	5.42	1301	4.46	1254	0.24	3.68
average		724	544	2100	5.19	2067	4.05	2071	0.73	6.27
StDev		233	188	515	1.19	518	1.38	554	0.61	1.42
Group 2 (15°in vertical plain)	Specimen Nr.	Initial stiffness k (N/mm)	Global structure stiffness k (N/mm)	Fmax (N)	Drup1 (first rup) (mm)	Frup1 (first rup) (N)	DendL	FendL	Initial energy W (J)	Energy W 0 to 5mm (J)
no screw rupture	1	692	564	3195	5.82	3195	2.43	1358	0.64	6.89
	2	843	377	1279	3.37	1279	1.49	917	0.16	4.11
	3	861	431	1467	1.48	1119	1.28	1068	0.70	5.28
	4	1127	695	1974	3.31	1974	1.07	1203	0.71	6.48
	5	1326	1052	2239	4.49	2239	1.10	1315	0.44	7.79
	6	1485	1247	2256	3.19	2256	1.33	1709	0.36	8.00
average		1056	728	2068	3.61	2010	1.45	1262	0.50	6.43
StDev		309	350	682	1.45	755	0.51	273	0.22	1.50

There was statistical difference regarding the end-point of the linear behaviour between the 3<sup>rd</sup> group (15° screw in a vertical plane) and other groups. To reach the end-point of linear behaviour much less displacement and force was required in this group.

#### 4.3.2. Mathematical analysis of the bone and the screw interface during the local loading.

The calculated and empirically obtained values of the rigidity were very different, they are summarized in Table 14.

Table 14. Calculated and obtained stiffness.

		$k_{\text{initial from curve}}$	$k_0$
Group 1 (strait)	1	1135	2237
	2	1083	2237
	3	1023	1593
	4	735	1681
	5	865	1989
	6	558	1295
Group 2 (15°in horizontal plain)	1	1085	1989
	2	706	2529
	3	895	2873
	4	605	2237
	5	620	1776
	6	430	1989
Group 3 (15°in vertical plain)	1	692	3775
	2	843	2873
	3	861	1681
	4	1127	1681
	5	1326	1593
	6	1485	4370

Those differences may have occurred because the width of the cortical bone was not taken into account in the calculations. The mechanical properties of the cortical bone cannot be completely dissociated from the mechanical behaviour of the screw in this experimentation setting. The stiffness of the bone and the screw have to be taken into account as they act together as a part of the whole structure. The contact area changed as the compression continued. It has been described earlier in the application of the Hertz theory.

The experimentation was not a simple three-point bending compression testing, the gap between the cortical bone and the nail was not taken into account (Fig.105).

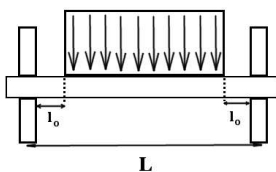


Figure 105: Schematic representation on the nail and screw compression.

Those parameters are important as the shear forces increase if the gap between the nail and the cortical bone increases (Fig.106).

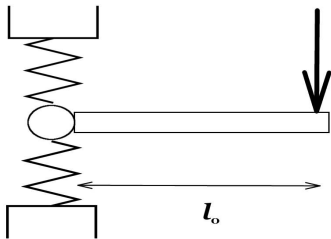


Figure 106: Lever arm diagram as the shear forces occur between the nail and the cortical bone.

The nail can be considered as a non deformable material and bone as a elastic material represented as a spring for analytical purposes in this diagram. The threading of the screw is not taken into account and the contact area between the bone and the screw is assimilated to the ball joint.

#### **4.4. Discussion and Conclusion.**

##### **4.4.1. Experimental method.**

After having evaluated the local mechanical behaviour of a metallic rod placed on the cortical bone, the next step was to evaluate the mechanical behaviour of a nail locking screw in a setting that was closer to clinical environment. A 3D printed drill guide, attached to the nail was appropriate in this situation and allowed drilling in chosen different directions.



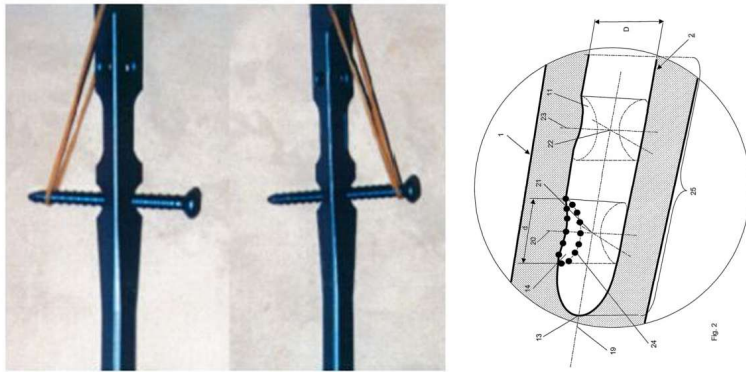


Figure 20. „Toggeling“ of the interlocking screws.

Figure 107: Angles of interlocking screws.[Kuhno8]

As it was not known what the mechanical behaviour could be expected, the angulations with 15° error in the second and third group was chosen to slightly exceed the 10° technically allowed in some operating techniques (Fig.107) [Kuhno8].The intramedullary nail was custom made in order to adapt to compression machine.

The chosen diameter of the nail was 10mm while the average diameter of the intramedullary canal was about 21mm. Taken into account that the femoral bone is slightly curved the diameter of the nail of 10mm allowed to avoid any major friction between the cortical bone and the nail during experimentation.

Quasi-static compressions were performed with a loading speed of 0.5mm/min which is compatible with a quasi-static loading definition for bone [Toen14].

#### 4.4.2. Discussion of the results.

##### **Mechanics.**

This experimentation allowed to evaluate the combined mechanical behaviour of the bone and the locking screw together under a local mechanical load. It is important to note

that most of the curves had a rather mixed pattern with several fractures occurring subsequently as the displacement continued (Fig.104). This may be related to mechanical properties of the bone and to several materials involved.

The end-point of the linear behaviour in the force-displacement curve was considered as an important point where the system gets destabilised. Nearly half of the force and half of displacement was needed to destabilise the system in the 3<sup>rd</sup> group where the screw was placed at 15° in vertical plane in comparison to other two groups. This is related to the fact that in this case the nail compresses the locking screw at one side of the bone cylinder inducing a flexion.

The locking screw is likely to break at the higher point of contact with the bone cylinder. As it has been shown, the force needed was nearly twice as low as in other groups to destabilise the structure. The Fmax does not need to be very high, which is consistent with the experimentation results (curves 3<sup>rd</sup> group).

The experimentation showed that the mechanical behaviour was rather mixed showing multiple fractures that may be related to the bone damage and the locking screw damage. In all but 2 cases the locking screw underwent a rupture which is consistent to the reports in the literature [Boen96][Whit95][Weni09].

A clear bone fracture could be seen on video in 10 cases. It is not clear whether in other 8 cases the bone fracture could not be detected on the video or the rupture seen in the curve corresponded to a screw rupture. It's not very clear when the screw rupture happened exactly because the curves of mechanical behaviour showed features of several ruptures that could be small incomplete bone fractures. One of those ruptures however was a screw rupture. It was impossible to clearly define when the screw rupture occurred that is why the mechanical behaviour of the screw and the bone could not be clearly dissociated.

### **Video evaluation.**

Regarding the video evaluation, a correlation could be found between the rupture seen in the curve and a bone fracture seen on the video in 10 cases. The fracture in the video and the rupture seen in the curve occurred at the same time and were clearly related. In 1 of those cases there was no screw rupture at all.

It is not clear whether in other 8 cases the bone fracture could not be detected on the video or the rupture seen in the curve corresponded to a screw rupture. Screw rupture occurred in all but 2 cases. It's not very clear when it happened exactly because the curves of mechanical behaviour showed features of several ruptures that could be small incomplete bone fractures. One of those ruptures however was a screw rupture. It was impossible to clearly define when the screw rupture occurred that is why the mechanical behaviour of the screw and the bone could not be clearly dissociated.

### **Limits of the Study.**

The limits of this study are that this was a biomechanical study in vitro and it didn't take into account the biological processes taking place during cyclic local loading. The biomechanical phenomena may be different in a real setting. Depending on the local bone damage around the distal locking screw the bone may undergo some resorption and loosening may occur. Cyclic local loading on the screw may also make the screw fail which is sometimes observed in a clinical settings.

### **Clinical aspects.**

This experimental model has shown that the intramedullary fixation failure most frequently occurs at the locking screw area which is consistent with the literature [Boen96]. In fact, in this study, in all but two cases the distal locking screw broke. The

hypothesis of this experimental model was based on an assumption that 15° error in the locking screw direction could induce a potentially damaging strain in the bone. It is interesting to note that the strain increased gradually in the third group (15° vertical screw orientation) with the linear behaviour end-point occurring after a shorter distance of displacement. This may have a clinical impact as the end of linear behaviour is related to the structure destabilisation which means that further development is with no return resulting in either bone fragment secondary displacement or bone damage.

## **5. General Conclusion and Perspectives**



## 5. General Conclusion and Perspectives

Intramedullary bone fixation devices are frequently used in fracture fixation and their use is increasing. Experimental protocols were defined and animal bone models were created in order to study the bone and locking screw interaction. The *in vitro* animal bone model using a segment of ewe femoral bone were appropriate for this purpose.

The first phase of this study has allowed to have a detailed analysis of phenomena occurring at the distal locking screw and to analyse the structure formed by the bone and the distal locking screw of intramedullary nail. No previous studies could be found in the literature specifically describing the intramedullary nail locking screw and the bone contact area. It was shown that the Hertz's contact theory applies to the very beginning of the force-displacement curve. This study has shown multiple force-displacement curve patterns which reveals the complexity of the fracture propagation and multiple phenomena that take place during the fracture propagation.

This study has shown no statistical significance in fracture propagation regarding the BV/TV ratio and geometry of the bone. In fact, the fractures propagated mostly always in a longitudinal direction which means that there must be other factors involved in containing the fracture, such as collagen fibres, other proteins and substances. Without surprise more bone fractures occurred in greater displacement groups.

The second phase of this work involved experimentation in order to understand whether the position of the screw can have influence to the bone resistance and eventually to the fracture propagation if it occurs in the contact area. For this purpose an angulation of 15° was chosen. This study showed statistical differences between group with 15° locking screw angulation in vertical planes and the control group regarding the end of linear behaviour. In fact, the linear behaviour ended after a much shorter distance of displacement and required less force. This means that the 15° range of error could be

acceptable in intramedullary nail distal locking in horizontal plane, but may destabilize the structure with less strain if put in at 15° in vertical plane. This has potential clinical impact as the destabilised structure can end up with a secondary bone fragments displacement and result in deformity, fracture of the bone or fixation failure requiring another surgical procedure. At the same time if the strain that does not exceed the linear part of the curve has clinical significance as the the strain without structure destabilisation stimulates bone formation and healing [Duan21].

Though the second part of this study was closer to clinical settings, the biological and physiological phenomena are still to be evaluated because the bone reaction as a constantly changing and reconstructing structure to the screw takes place. This also means that even if there are some micro-fractures at the locking screw area, bone remodelling could intervene and localise the bone damage.

As seen in the second part of this study, which is also consistent with clinical findings [Boen96][Whit95][Wenio9], there were much more screw ruptures than complete bone fractures. This shows that though the Young's modulus of the steel is much higher, its position in the overall nail-bone-screw structure exposes it to potential damage.

The quasi-static compressions differ from cyclical loading in clinical settings but this was the first analysis of the locking screw and bone contact area, which has allowed to determine the force and displacement values required to induce bone or screw rupture and to show the absence of relationship between fracture and the BV/TV and other studied parameters of the cortical bone. This may indicate that other factors play an more important role in fracture propagation than the BV/TV ratio. To identify and evaluate these factors could be a perspective of further research.

Further studies would be needed to evaluate greater error in distal locking screw direction. It would be interesting to study the effect in cyclical loading of a locking screw *in*

*vitro* but also *in vivo* on a living bone during short and longer period of time in order to understand the biological and biochemical response in a setting much closer to clinical situations. Studies would be needed to evaluate the clinical significance of the locking screw direction and its relationship with overall clinical outcome (locking screw failure, bone damage, secondary displacement, limb shortening or deformity). It would be important to define what locking screw angle is acceptable and whether more precise locking screw guiding tools are necessary in order to avoid complications related to interlocking intramedullary nail fixation and have a better clinical outcome.



# References



1. [Weiso9] Weiss RJ, Montgomery SM, Al Dabbagh Z, Jansson KA. National data of 6409 Swedish inpatients with femoral shaft fractures: stable incidence between 1998 and 2004. *Injury*. 2009 Mar;40(3):304-8.
2. [Yli12] Yli-Kyyny TT, Sund R, Juntunen M, Salo JJ, Kröger HP. Extra- and intramedullary implants for the treatment of pertrochanteric fractures – results from a Finnish National Database Study of 14,915 patients. *Injury*. 2012 Dec;43(12):2156-60.
3. [Sarm76] Sarmiento A, Kinman PB, Murphy RB, Phillips JG. Treatment of ulnar fractures by functional bracing. *J Bone Joint Surg Am*. 1976 Dec;58(8):1104-7.
4. [Kola10] Kolar P, Schmidt-Bleek K, Schell H, Gaber T, Toben D, Schmidmaier G, Perka C, Buttgerit F, Duda GN. The early fracture hematoma and its potential role in fracture healing. *Tissue Eng Part B Rev*. 2010 Aug;16(4):427-34.
5. [Guo09] Z. Guo, J. Fu, Y.Q. Zhang, Y.Y. Hu, Z.G. Wu, L. Shi, M. Sha, S.J. Li, Y.L. Hao, R. Yang, Early effect of Ti–24Nb–4Zr–7.9Sn intramedullary nails on fractured bone, *Materials Science and Engineering: C*, Volume 29, Issue 3, 30 April 2009, Pages 963-968.
6. [Inam05] T. Inamura, H. Hosoda, K. Wakashima, S. Miyazaki. Anisotropy and Temperature Dependence of Young's Modulus in Textured TiNbAl Biomedical Shape Memory Alloy. *Materials Transactions*, Vol. 46, No. 7 (2005) pp. 1597 to 1603.
7. [Kret97\_1] Krettek C, Mannss J, Könemann B, Miclau T, Schandelmaier P, Tscherne H. The deformation of small diameter solid tibial nails with unreamed intramedullary insertion. *J Biomech*. 1997 Apr;30(4):391-4.
8. [Kret97\_2] Krettek C, Könemann B, Miclau T, Schandelmaier P, Blauth M, Tscherne H. In vitro and in vivo radiomorphometric analyses of distal screw hole position of the solid tibial nail following insertion. *Clin Biomech (Bristol, Avon)*. 1997; Apr;12(3):198-200.

9. [Kret98] Krettek C, Mannss J, Miclau T, Schandelmaier P, Linnemann I, Tscherne H. Deformation of femoral nails with intramedullary insertion. *J Orthop Res.* 1998 Sep;16(5):572-5.
10. [Ster96] K. A. Steriopoulos, G. M. Kontakis, P. G. Katonis, I. A. Galanakis, E. K. Dretakis. Placement of the distal locking screws of the femoral intramedullary nail without radiation. *Arch Orthop Trauma Surg* (1996) 115:43-44,1996.
11. [Hash94] A. Hashemi-Nejad, N. Garlick and N. J. Goddard A simple jig to ease the insertion of distal screws in intramedullary locking nails. *Injury*, 1994, Vol. 25, 407-408.
12. [Arleo8] Y. Arlettaz, A. Akiki, F. Chevalley, P.F. Leyvraz. Targeting device for intramedullary nails: A new high-stable mechanical guide. *Injury, Int. J. Care Injured* (2008) 39, 170–175.
13. [What06] G.M. Whatling, L.D.M. Nokes *Injury, Int. J. Care Injured* (2006) 37, 109–119 Literature review of current techniques for the insertion of distal screws into intramedullary locking nails.
14. [Micho8] Michael J. Gardner , Musa Citak, Daniel Kendoff, Christian Krettek, Tobias Hufner *Injury, Int. J. Care Injured* (2008) 39, 176–180.
15. [Lang13] Langfitt MK, Halvorson JJ, Scott AT, Smith BP, Russell GB, Jinnah RH, Miller AN, Carroll EA. Distal locking using an electromagnetic field-guided computer-based real-time system for orthopaedic trauma patients. *J Orthop Trauma.* 2013 Jul;27(7):367-72.
16. [Noau10] No authors listed. US Food and Drug Administration. White paper: initiative to reduce unnecessary radiation exposure from medical imaging, 2010. <http://www.fda.gov/Radiation-EmittingProducts/RadiationSafety/RadiationDoseReduction/ucm199994.htm>, accessed in 2013.

17. [Metto8] Mettler FA Jr, Huda W, Yoshizumi TT, Mahesh M. Effective doses in radiology and diagnostic nuclear medicine: a catalog. *Radiology* 2008;248:254-63.
18. [Madao2] Madan S, Blakeway Ch. Radiation exposure to surgeon and patient in intramedullary nailing of the lower limb. *Injury, Int. J. Care Injured* 33 (2002) 723–727.
19. [Kesa12] Kesavachandran CN , Haamann F, Nienhaus A. Radiation exposure of eyes, thyroid gland and hands in orthopaedic staff: a systematic review. *European Journal of Medical Research* 2012, 17:28.
20. [Mast05] Giuseppe Mastrangelo, Ugo Fedeli, Emanuela Fadda, Angelo Giovanazzi, Luca Scoizzato, Bruno Saia Increased cancer risk among surgeons in an orthopaedic hospital. *Occupational Medicine*. 2005 ; Volume 55 Issue 6 ; Pp. 498-500.
21. [Chou12] Chou LB, Chandran S, Harris AH, Tung J, Butler LM. Increased breast cancer prevalence among female orthopedic surgeons. *J Womens Health (Larchmt)*. 2012. Jun;21(6):683-9.
22. [Wrix08] A D Wrixon. New ICRP recommendations. *J. Radiol. Prot.* 28 (2008) 161–168.
23. [Pica11] Picano E, Vano E. The Radiation Issue in Cardiology: the time for action is now. *Cardiovascular Ultrasound* 2011, 9:35.
24. [Cher16] Cheriachan D, Hughes AM, du Moulin WS, Williams C, Molnar R. Ionizing Radiation Doses Detected at the Eye Level of the Primary Surgeon During Orthopaedic Procedures. *J Orthop Trauma*. 2016 Jul;30(7):e230-5.
25. [Noau13] No authors listed. Nuclear Radiation and Health Effects. World Nuclear Association 28 June 2013. <http://www.world-nuclear.org/info/Safety-and-Security/Radiation-and-Health/Nuclear-Radiation-and-Health-Effects/>.
26. [Mill10] Miller DL, Vano E, Bartal G, Balter S, Dixon R, Padovani R, Schueler B, Cardella JF, de Baere Th. Occupational Radiation Protection in Interventional Radiology: A Joint Guideline of the Cardiovascular and Interventional Radiology Society of

Europe and the Society of Interventional Radiology. *Cardiovasc Intervent Radiol.* 2010 ; 33:230–239.

27. [Sing07] Singh PJ, Perera NS, Dega R. Measurement of the dose of radiation to the surgeon during surgery to the foot and ankle. *J Bone Joint Surg Br* August 2007 vol. 89-B no. 8 1060-1063.

28. [Mast05] Giuseppe Mastrangelo, Ugo Fedeli, Emanuela Fadda, Angelo Giovanazzi, Luca Scoizzato, Bruno Saia Increased cancer risk among surgeons in an orthopaedic hospital. *Occupational Medicine.* 2005 ; Volume 55 Issue 6 ; Pp. 498-500.

29. [Van098] Vano E, Gonzalez L, Guibelalde E, Fernandez JM, Ten JJ: Radiation exposure to medical staff in interventional and cardiac radiology. *Br J Radiol* 1998, 71:954-960.

30. [Mill83] Miller ME, Davis ML, MacClean CR, Davis JG, Smith BL, Humphries JR: Radiation exposure and associated risks to operating-room personnel during use of fluoroscopic guidance for selected orthopaedic surgical procedures. *J Bone Joint Surg Am* 1983, 65:1-4.

31. [Harso5] Harstall R, Heini PF, Mini RL, Orlor R: Radiation exposure to the surgeon during fluoroscopically assisted percutaneous vertebroplasty: a prospective study. *Spine (Phila Pa 1976)* 2005, 30:1893-1898.

32. [Muza05] Muzaffar TS, Imran Y, Iskandar MA, Zakaria A: Radiation exposure to the surgeon during femoral interlocking nailing under fluoroscopic imaging. *Med J Malaysia* 2005, 60(Suppl C):26-29.

33. [Sing05] Singer G. Occupational Radiation Exposure to the Surgeon. *J Am Acad Orthop Surg* ; 2005 vol.13 no.1 69-76.

34. [Coet92] Coetzee JC, van der Merwe EJ. Exposure of surgeons-in-training to radiation during intramedullary fixation of femoral shaft fractures. *S Afr Med J.* 1992 Mar 21;81(6):312-4.

35. [Hamm13] Hammer GP, Scheidemann-Wesp U, Samkange-Zeeb F, Wicke H, Neriishi K, Blettner M. Occupational exposure to low doses of ionizing radiation and cataract development: a systematic literature review and perspectives on future studies. *Radiat Environ Biophys.* 2013 Aug;52(3):303-19.
36. [Klei12] Kleiman NJ. Radiation cataract. *Ann ICRP.* 2012 Oct-Dec;41(3-4):80-97.
37. [Litt12] Little MP, Azizova TV, Bazyka D, Bouffler SD, Cardis E, Chekin S, Chumak VV, Cucinotta FA, de Vathaire F, Hall P, Harrison JD, Hildebrandt G, Ivanov V, Kashcheev VV, Klymenko SV, Kreuzer M, Laurent O, Ozasa K, Schneider T, Tapio S, Taylor AM, Tzoulaki I, Vandoolaeghe WL, Wakeford R, Zablotska LB, Zhang W, Lipshultz SE. Systematic review and meta-analysis of circulatory disease from exposure to low-level ionizing radiation and estimates of potential population mortality risks. *Environ Health Perspect.* 2012 Nov;120(11):1503-11.
38. [Ziel09] Zielinski JM, Ashmore PJ, Band PR, Jiang H, Shilnikova NS, Tait VK, Krewski D. Low dose ionizing radiation exposure and cardiovascular disease mortality: cohort study based on Canadian national dose registry of radiation workers. *Int J Occup Med Environ Health.* 2009;22(1):27-33.
39. [Egol04] Egol KA, Chang EY, Cvitkovic J, Kummer FJ, Koval KJ. Mismatch of current intramedullary nails with the anterior bow of the femur. *J Orthop Trauma.* 2004 Aug;18(7):410-5.
40. [Arne88] Arneson TJ, Melton LJ 3rd, Lewallen DG, O'Fallon WM. Epidemiology of diaphyseal and distal femoral fractures in Rochester, Minnesota, 1965-1984. *Clin Orthop Relat Res.* 1988 Sep;(234):188-94.
41. [Bart13] David Bartle, John Keating. Femoral and tibial fractures. *Surgery (Oxford)*; Volume 31, Issue 9, September 2013, Pages 460-465.
42. [Lars15] Larsen P, Elsoe R, Hansen SH, Graven-Nielsen T, Laessoe U,

Rasmussen S. Incidence and epidemiology of tibial shaft fractures. *Injury*. 2015 Apr;46(4):746-50.

43. [Matt18] Mattisson L, Bojan A, Enocson A. Epidemiology, treatment and mortality of trochanteric and subtrochanteric hip fractures: data from the Swedish fracture register. *BMC Musculoskelet Disord*. 2018 Oct 12;19(1):369.

44. [Bjør07] Bjørgul K, Reikerås O. Incidence of hip fracture in southeastern Norway: a study of 1,730 cervical and trochanteric fractures. *Int Orthop*. 2007 Oct;31(5):665-9.

45. [Kara96] Karagas MR, Lu-Yao GL, Barrett JA, Beach ML, Baron JA. Heterogeneity of hip fracture: age, race, sex, and geographic patterns of femoral neck and trochanteric fractures among the US elderly. *Am J Epidemiol*. 1996 Apr 1;143(7):677-82.

46. [Quea14] Queally JM, Harris E, Handoll HH, Parker MJ. Intramedullary nails for extracapsular hip fractures in adults. *Cochrane Database Syst Rev*. 2014 Sep 12; (9):CD004961.

47. [Bosk99] A.L. Boskey, M. Wright and R.D. Blank. Perspective Collagen and Bone Strength. *Journal of Bone and Mineral Research* Volume 14, Number 3, 1999.

48. [Smit73] Smith DM, Nance WE, Kang KW, Christian JC, Johnston CC Jr 1973 Genetic factors in determining bone mass. *J Clin Invest* 52:2800–2808.

49. [Sowe86] Sowers MR, Burns TL, Wallace RB 1986 Familial resemblance of bone mass in adult women. *Genet Epidemiol* 3:85–93.

50. [Dequ87] Dequeker J, Nijs J, Verstraeten A, Geusens P, Gevers G 1987 Genetic determinants of bone mineral content at the spine and radius: A twin study. *Bone*. 8:207–209.

51. [Poko87] Pokock NA, Eisman JA, Hopper JL, Yeates MG, Sambrook PN, Ebert S 1987 Genetic determinants of bone mass in adults. *J Clin Invest* 80:706–710.

52. [Bail92] Bailey AJ, Wotton SF, Sims TJ, Thompson PW 1992 Post-

translational modifications in the collagen of human osteoporotic femoral head. *Biochem Biophys Res Commun* 185:801–805.25.

53. [Oxlu96] Oxlund H, Mosekilde L, Ortoft G 1996 Reduced concentration of collagen reducible cross-links in human trabecular bone with respect to age and osteoporosis. *Bone* 19:479–484.26.

54. [Kowi97] Kowitz J, Knippel M, Schuhr T, Mach J 1997 Alteration in the extent of collagen I hydroxylation, isolated from femoral heads of women with a femoral neck fracture caused by osteoporosis. *Calcif Tissue Int* 60:501–505.

55. [Caei13] Caeiro JR<sup>1,2</sup>, González P<sup>3</sup>, Guede D<sup>1,4</sup>, Biomechanics and bone (& II): Trials in different hierarchical levels of bone and alternative tools for the determination of bone strength *Rev Osteoporos Metab Miner* 2013 5;2:99-108

56. [Curr88] Currey JD. The effects of drying and re-wetting on some mechanical properties of cortical bone. *J Biomech* 1988;21:439-41.

57. [Scha88] Schaffler MB, Burr DB. Stiffness of compact bone: Effects of porosity and density. *J Biomech* 1988;21:13-6.

58. [Reil74] Reilly DT, Burnstein AH, Frankel VH. The elastic modulus of bone. *J Biomech* 1974;7:271-2. 11.

59. [Burn76] Burnstein AH, Reilly DT, Martens M. Aging of bone tissue: Mechanical properties. *J Bone Joint Surg Am* 1976;58:82-6.

60. [Ceza90] Cezayirlioglu H, Bahniuk E, Davy DT, Heiple KG. Anisotropic yield behavior of bone under combined axial force and torque. *J Biomech* 1985;18:61-9. 13.

61. [Kell90] Keller TS, Mao Z, Spengler DM. Young's modulus, bending strength, and tissue physical properties of human compact bone. *J Orthop Res* 1990;8:592-603.

62. [Cupp04] Cuppone M, Seedhom BB, Berry E, Ostell AE. The longitudinal Young's modulus of cortical bone in the midshaft of human femur and its correlation with CT scanning data. *Calcif Tissue Int* 2004;74:302-9.

63. [Keav94] Keaveny TM, Wachtel EF, Ford CM, Hayes WC. Differences between the tensile and compressive strengths of bovine tibial trabecular bone depend on modulus. *J Biomech* 1994;27:1137-46.
64. [Nallo03] Nalla, R. K., Kinney, J. H., & Ritchie, R. O. (2003). Mechanistic fracture criteria for the failure of human cortical bone. *Nature Materials*, 2(3), 164–168.
65. [Rho98] Rho, J.-Y., Kuhn-Spearing, L., & Zioupos, P. (1998). Mechanical properties and the hierarchical structure of bone. *Medical Engineering & Physics*, 20(2), 92–102.
66. [Koes08] Koester KJ, Ager JW 3rd, Ritchie RO. The true toughness of human cortical bone measured with realistically short cracks. *Nat Mater*. 2008 Aug;7(8):672-7. Doi: 10.1038/nmat2221. Epub 2008 Jun 29.
67. [Fant05] Fantner GE, Hassenkam T, Kindt JH, Weaver JC, Birkedal H, Pechenik L, Cutroni JA, Cidade GA, Stucky GD, Morse DE, Hansma PK. Sacrificial bonds and hidden length dissipate energy as mineralized fibrils separate during bone fracture. *Nat Mater*. 2005 Aug;4(8):612-6. Epub 2005 Jul 17.
68. [Pars01] Parsamian, G.P., Norman, T.L. Diffuse damage accumulation in the fracture process zone of human cortical bone specimens and its influence on fracture toughness. *Journal of Materials Science: Materials in Medicine* 12, 779–783 (2001).
69. [Pete05] Peterlik, H., Roschger, P., Klaushofer, K., & Fratzl, P. (2005). From brittle to ductile fracture of bone. *Nature Materials*, 5(1), 52–55.
70. [Nallo05] Nalla, R. ., Kruzic, J. ., Kinney, J. ., & Ritchie, R. . (2005). Mechanistic aspects of fracture and R-curve behavior in human cortical bone. *Biomaterials*, 26(2), 217–231.
71. [Guo98] Guo, X. E., Liang, L. C., Goldstein, S. A.. Micromechanics of Osteonal Cortical Bone Fracture. *J Biomech Eng*. Feb 1998, 120(1): 112-117.
72. [Mart93] Martin B. Aging and strength of bone as a structural material.

Calcif Tissue Int. 1993;53 Suppl 1:S34-9; discussion S39-40. Review.

73. [Auga06] Augat P, Schorlemmer S. The role of cortical bone and its microstructure in bone strength. *Age Ageing*. 2006 Sep;35 Suppl 2:ii27-ii31. Review.

74. [Zimm15] Zimmermann EA, Köhne T, Bale HA, Panganiban B, Gludovatz B, Zustin J, Hahn M, Amling M, Ritchie RO, Busse B. Modifications to nano- and microstructural quality and the effects on mechanical integrity in Paget's disease of bone. *J Bone Miner Res*. 2015 Feb;30(2):264-73.

75. [Mirz16] Mirzaali MJ, Schwiedrzik JJ, Thaiwichai S, Best JP, Michler J, Zysset PK, Wolfram U. Mechanical properties of cortical bone and their relationships with age, gender, composition and microindentation properties in the elderly. *Bone*. 2016 Dec;93:196-211.

76. [Wach01\_1] Wachter NJ, Augat P, Krischak GD, Sarkar MR, Mentzel M, Kinzl L, Claes L. Prediction of strength of cortical bone in vitro by microcomputed tomography. *Clin Biomech (Bristol, Avon)*. 2001 Mar;16(3):252-6.

77. [Wach01\_2] Wachter NJ, Augat P, Krischak GD, Mentzel M, Kinzl L, Claes L. Prediction of cortical bone porosity in vitro by microcomputed tomography. *Calcif Tissue Int*. 2001 Jan;68(1):38-42.

78. [Ziou08] Zioupos P, Cook RB, Hutchinson JR. Some basic relationships between density values in cancellous and cortical bone. *J Biomech*. 2008;41(9):1961-8.

79. [Boux06] Bouxsein ML, Karasik D. Bone geometry and skeletal fragility. *Curr Osteoporos Rep*. 2006 Jun;4(2):49-56. Review.

80. [Morg15] Morgan S, Poundarik AA, Vashishth D. Do Non-collagenous Proteins Affect Skeletal Mechanical Properties? *Calcif Tissue Int*. 2015;97(3):281-291.

81. [Atha12] Atharva A, Poundarik, Tamim Diab, Grazyna E. Sroga, Ani Ural, Adele L. Boskey, Caren M. Gundberg, Deepak Vashishth. Dilatational band formation in bone. *Proceedings of the National Academy of Sciences* Nov 2012, 109 (47) 19178-19183.

82. [Köse00] Köse N, Günal I, Wang X, Athanasiou KA, Agrawal CM, Mabrey JD. Setscrew distal locking for intramedullary nails: a biomechanical study. *J Orthop Trauma*. 2000 Aug;14(6):414-9.
83. [Pear07] AI Pearce, RG Richards, S Milz, E Schneider and SG Pearce. Animal Models For Implant Biomaterial Research In Bone: A Review. *European Cells and Materials* Vol. 13. 2007 ; 1-10.
84. [Shaw 12] Shaw J; Hunter S; Gayton, J.; Boivin, G; Prayson, M. Repeated Freeze-thaw Cycles Do Not Alter the Biomechanical Properties of Fibular Allograft Bone. *Clinical Orthopaedics & Related Research* . Mar2012, Vol. 470 Issue 3, p937-943. 7p.
85. [Ding15] Ding M, Henriksen SS, Theilgaard N, Overgaard S. Assessment of activated porous granules on implant fixation and early bone formation in sheep. *J Orthop Translat*. 2015;5:38–47. Published 2015 Oct 29.
86. [Boug18] Boughton OR, Ma S, Zhao S, et al. Measuring bone stiffness using spherical indentation. *PLoS One*. 2018;13(7):e0200475. Published 2018 Jul 12.
87. [Bart10] Bartoníček J. Early history of operative treatment of fractures. *Arch Orthop Trauma Surg*. 2010 Nov;130(11):1385–96.
88. [Buhl19] Buhl CA. 80 Jahre intramedulläre Marknagelung: Neue Fakten und Informationen zu einem Meilenstein der Osteosynthese. *Unfallchirurg*. 2019 Feb;122(2):127–33.
89. [Born14] Born, C.T., Pidgeon, T., Taglang, G. 75 Years of Contemporary Intramedullary Nailing. *Journal of Orthopedic Trauma*, 2014. 10(8).
90. [Lesi12] Lesic A, Zagorac S, Bumbasirevic V, Bumbasirevic M. The development of internal fixation: Historical overview. *Acta chir iugo*. 2012;59(3):9–13.
91. [Hu19] Hu L, Xiong Y, Mi B, Panayi AC, Zhou W, Liu Y, et al. Comparison of intramedullary nailing and plate fixation in distal tibial fractures with metaphyseal damage: a meta-analysis of randomized controlled trials. *J Orthop Surg Res*. 2019

Dec;14(1):30.

92. [Gasi18] Gasiunas V, Prot M, Laporte S. CT Analysis of the Fracture Propagation and Bony Damage at the Interface Between the Distal Locking Screw and the Cortical Bone. In 2018. Available at: <https://app.oxfordabstracts.com/events/123/program-app/submission/23722>
93. [Ghae17] Ghaednia H, Wang X, Saha S, Xu Y, Sharma A, Jackson RL. A Review of Elastic–Plastic Contact Mechanics. *Applied Mechanics Reviews*. 2017 Nov 1;69(6):060804.
94. [Hert96] Hertz, H. *Miscellaneous Papers, with an intro. by Philipp Lenard*. Authorised English translation by D.E. Jones and G.A. Schott. Macmillan, London. (1896).
95. [John85] Johnson KL. *Contact mechanics*. Cambridge [Cambridgeshire] ; New York: Cambridge University Press; 1985. 452 p.
96. [Schm14] Schmid SR, Hamrock BJ, Jacobson BO. *Fundamentals of Machine Elements – SI Version*. CRC Press. (2014).
97. [Bhus01] Bhushan B, editor. *Modern tribology handbook*. Boca Raton, Fla.: CRC Press; 2001. 2 p. (Mechanics and materials science series).
98. [Aute12] Autefage A, Palierne S, Charron C, Swider P. Effective mechanical properties of diaphyseal cortical bone in the canine femur. *The Veterinary Journal*. 2012 Nov;194(2):202–9.
99. [Wolf16] Wolfram U, Schwiedrzik J. Post-yield and failure properties of cortical bone. *BoneKEy Reports [Internet]*. 2016 Aug 24 [cited 2020 Mar 29];5. Available from: <http://www.portico.org/Portico/article?article=phxjtvwzvc>.
100. [Wang13] Wang Q.J., Zhu D. Contact Yield. In: Wang Q.J., Chung YW. (eds) *Encyclopedia of Tribology*. Springer, Boston, MA. 2013.
101. [Gree05] Green I. Poisson Ratio Effects and Critical Values in Spherical and Cylindrical Hertzian Contacts. 2005.

102. [Libo14] Libonati F, Vergani L. Bone Toughness and Crack Propagation: An Experimental Study. *Procedia Engineering*. 2014;74:464–7.
103. [Fischo7] Fischer-Cripps AC. Introduction to contact mechanics. 2nd ed. New York: Springer; 2007. 221 p. (Mechanical engineering series).
104. [Bazao4] Bazant ZP. Scaling theory for quasibrittle structural failure. *Proceedings of the National Academy of Sciences*. 2004 Sep 14;101(37):13400–7.
105. [Pearo7] Pearce A, Richards R, Milz S, Schneider E, Pearce S. Animal models for implant biomaterial research in bone: A review. *eCM*. 2007 Mar 2;13:1–10.
106. [Eato19] John W. Eaton and David Bateman and Søren Hauberg and Rik Wehbring. {GNU Octave} version 5.1.0 manual: a high-level interactive language for numerical computations. 2019. Obtained from: <https://www.gnu.org/software/octave/doc/v5.1.0/>.
107. [Wang16] Wang Z, Golob MJ., Chesler NC. Viscoelastic Properties of Cardiovascular Tissues. In book: *Viscoelastic and Viscoplastic Materials 2016*.
108. [Brew76] Brewe DE and Hamrock BJ. Simplified Solution For Point Contact Deformation Between Two Elastic Solids . *Nasa Technical Memorandum X-3407*; 1976.
109. [Wach01] Wachter NJ, Augat P, Krischak GD, et al. Prediction of strength of cortical bone in vitro by microcomputed tomography. *Clin Biomech (Bristol, Avon)*. 2001;16(3):252-256.
110. [Zhao18] Zhao S, Arnold M, Ma S, Abel RL, Cobb JP, Hansen U, Boughton O. Standardizing compression testing for measuring the stiffness of human bone. *Bone Joint Res*. 2018 Sep 15;7(8):524-538.
111. [Fedo12] Fedorov, A., Beichel, R., Kalpathy-Cramer, J., Finet, J., Fillion-Robin, J. C., Pujol, S., Kikinis, R. (2012). 3D Slicer as an image computing platform for the Quantitative Imaging Network. *Magnetic Resonance Imaging*, 30(9), 1323-1341.

<https://doi.org/10.1016/j.mri.2012.05.001>.

112. [Choi90] K Choi, JL Kuhn, MJ Ciarelli and SA Goldstein (1990). The elastic moduli of human subchondral, trabecular, and cortical bone tissue and the size-dependency of cortical bone modulus. *J Biomech.* 23(11): 1103-1113.
113. [Choi92] K Choi and SA Goldstein (1992). A comparison of the fatigue behaviour of human trabecular and cortical bone tissue. *J Biomech.* 25(12): 1371-1381.
114. [Lotz91] JC Lotz, TN Gerhart and WC Hayes (1991). Mechanical properties of metaphyseal bone in the proximal femur. *J Biomech.* 24(5): 317-329.
115. [Bruy00] K Bruyère (2000). Caractérisation et modélisation mécanique de l'os spongieux et trabéculaire en relation avec ses propriétés structurales et architecturales. Thèse. INSA (Lyon).
116. [Reil75] DT Reilly and AH Burstein (1975). The elastic and ultimate properties of compact bone tissue. *J Biomech.* 8(6): 393-405.
117. [Hill20] M. Hill. Lecture - Musculoskeletal Development. [https://embryology.med.unsw.edu.au/embryology/index.php/Lecture\\_-\\_Musculoskeletal\\_Development](https://embryology.med.unsw.edu.au/embryology/index.php/Lecture_-_Musculoskeletal_Development). Last accessed Sep. 2020.
118. [Gilbo0] Gilbert SF. *Developmental Biology*. 6th edition. Sunderland (MA): Sinauer Associates; 2000. Osteogenesis: The Development of Bones.
119. [Mano59] Manolagas, S. C., & Jilka, R. L. (1995). Bone Marrow, Cytokines, and Bone Remodeling — Emerging Insights into the Pathophysiology of Osteoporosis. *New England Journal of Medicine*, 332(5), 305–311.
120. [Cart87] Carter, D. R., Fyhrie, D. P., & Whalen, R. T. (1987). Trabecular bone density and loading history: Regulation of connective tissue biology by mechanical energy. *Journal of Biomechanics*, 20(8), 785–794.

121. [Orya15] A. Oryan, S. Monazzah, A. Bigham-Sadeg. Bone Injury and Fracture Healing Biology. *Biomed Environ Sci*, 2015; 28(1): 57-71.
122. [Loi16] Loi, F., Córdova, L. A., Pajarinen, J., Lin, T. H., Yao, Z., & Goodman, S. B. (2016). Inflammation, fracture and bone repair. *Bone*, 86, 119–130.
123. [Lany85] Lance E. Lanyon and Clinton T. Rubin. Functional Adaptation in Skeletal Structures. Book. *Functional Vertebrate Morphology*. 1985 Publisher: Harvard University Press.
124. [Grif09] Griffin, L.V., Harris, R.M. & Zubak, J.J. Fatigue strength of common tibial intramedullary nail distal locking screws. *J Orthop Surg Res* 4, 11. 2009.
125. [Zell18] Zelle, Boris A et al. Safety and efficacy of a two-screw cephalomedullary nail for intertrochanteric femur fracture fixation: a retrospective case series in 264 patients. *Patient safety in surgery* vol. 12 31. 6 Nov. 2018.
126. [Glat17] Glatt V, Evans CH, Tetsworth K. A Concert between Biology and Biomechanics: The Influence of the Mechanical Environment on Bone Healing. *Front Physiol*. 2017 Jan 24;7:678.
127. [Cart98] Carter DR, Beaupré GS, Giori NJ, Helms JA. Mechanobiology of skeletal regeneration. *Clin Orthop Relat Res*. 1998 Oct;(355 Suppl):S41-55.
128. [Whit95] Whittle AP, Wester W, Russell TA. Fatigue failure in small diameter tibial nails. *Clin Orthop Relat Res*. 1995 Jun;(315):119-28.
129. [Wild20] Jason R Wild. *Complications of Fracture Fixation*. Cambridge University Press. [https://medapparatus.com/Complications/Complications\\_FractureFixation.html](https://medapparatus.com/Complications/Complications_FractureFixation.html). Last accessed Sep 2020.
130. [Bola92] Bolander ME. Regulation of fracture repair by growth factors. *Proc Soc Exp Biol Med*. 1992 Jun;200(2):165-70.
131. [Murdo04] Murdoch AH, Mathias KJ, Shepherd DE. Investigation into the

- material properties of beech wood and cortical bone. *Biomed Mater Eng.* 2004;14(1):1-4.
132. [Auga98] Augat, P., Link, T., Lang, T. F., Lin, J. C., Majumdar, S., Genant, H. K. (1998). Anisotropy of the elastic modulus of trabecular bone specimens from different anatomical locations. *Medical Engineering & Physics*, 20(2), 124–131.
133. [Yu11] Yu, B., Zhao, G.-F., Lim, J. I., & Lee, Y.-K. (2011). Compressive mechanical properties of bovine cortical bone under varied loading rates. *Proceedings of the Institution of Mechanical Engineers, Part H: Journal of Engineering in Medicine*, 225(10), 941–947.
134. [Reil75] Reilly DT, Burstein AH. The elastic and ultimate properties of compact bone tissue. *J Biomech.* 1975;8:393–96.
135. [Mirz16] Mirzaali MJ, Schwiedrzik JJ, Thaiwichai S, Best JP, Michler J, et al. Mechanical properties of cortical bone and their relationships with age, gender, composition and microindentation properties in the elderly. *Bone.* 2016;93:196–211.
136. [Evan76] Evans, F. G. (1976). Mechanical properties and histology of cortical bone from younger and older men. *The Anatomical Record*, 185(1), 1–11.
137. [Curr88] Currey, J. D. (1988). The effects of drying and re-wetting on some mechanical properties of cortical bone. *Journal of Biomechanics*, 21(5), 439–441.
138. [Bayr04] Bayraktar, H. H., Morgan, E. F., Niebur, G. L., Morris, G. E., Wong, E. K., & Keaveny, T. M. (2004). Comparison of the elastic and yield properties of human femoral trabecular and cortical bone tissue. *Journal of Biomechanics*, 37(1), 27–35.
139. [Weni09] Weninger P, Schueller M, Jamek M, Stanzl-Tschegg S, Redl H, Tschegg EK. Factors influencing interlocking screw failure in unreamed small diameter nails--a biomechanical study using a distal tibia fracture model. *Clin Biomech (Bristol, Avon)*. 2009 May;24(4):379-84.
140. [Aers98] J. Aerssens, S. Boonen, G. Lowet, J. Dequeker. Interspecies Differences in Bone Composition, Density, and Quality: Potential Implications for in Vivo

Bone Research. *Endocrinology*, Volume 139, Issue 2, 1 February 1998, Pages 663–670.

141. [Toen14] Van Toen C, Carter JW, Oxland TR, Cripton PA. Moment measurements in dynamic and quasi-static spine segment testing using eccentric compression are susceptible to artifacts based on loading configuration. *J Biomech Eng.* 2014 Dec;136(12):124505.
142. [Stra99] Straffelini, G., Fontanari, V., & Molinari, A. (1999). True and apparent Young's modulus in ferrous porous alloys. *Materials Science and Engineering: A*, 260(1-2), 197–202.
143. [Nafe00] Nafei A, Danielsen CC, Linde F, Hvid I. Properties of growing trabecular ovine bone. Part I: mechanical and physical properties. *J Bone Joint Surg Br.* 2000 Aug;82(6):910-20
144. [Wanc15] Wancket LM. Animal Models for Evaluation of Bone Implants and Devices: Comparative Bone Structure and Common Model Uses. *Vet Pathol.* 2015 Sep;52(5):842-50.
145. [Kuhn08] Kuhn S, Hansen M, Rommens PM. Extending the indications of intramedullary nailing with the Expert Tibial Nail. *Acta Chir Orthop Traumatol Cech.* 2008 Apr;75(2):77-87.
146. [Duan21] Duan ZW, Lu H. Effect of Mechanical Strain on Cells Involved in Fracture Healing. *Orthop Surg.* 2021;13(2):369-375.
147. [Boen96] Boenisch, U. W., de Boer, P. G., & Journeaux, S. F. (1996). Unreamed intramedullary tibial nailing—fatigue of locking bolts. *Injury*, 27(4), 265–270.
148. [Hedg17] Hedgeland M.J., Clark A M, Ciani M, Michalek A J, Kuxhaus L. A Proximally-Adjustable Variable Length Intramedullary Nail: Ex Vivo Quasi-Static and Cyclic Loading Evaluation. *Journal of Medical Devices* 11(4)Jul 2017.
149. [Akog18] H. Akoglu. User's guide to correlation coefficients, *Turkish Journal of Emergency Medicine*, Vol. 18, (3), 2018, p.91-93, ISSN 2452-2473.

150. [Sakao7] Sakaki MH, Crocci AT, Zumiotti AV. Comparative study of the locked intramedullary nail and Ender pins in the treatment of tibial diaphyseal fractures. *Clinics (Sao Paulo)*. 2007 Aug;62(4):455-64. 8.001.
151. [He22] He, M., Liu, J., Deng, X. et al. Controlling the angle between the distal locking screw and tibiotalar joint tangent helps to reduce the occurrence of misalignment of distal tibial fractures treated with intramedullary nail fixation. *BMC Musculoskelet Disord* 23, 671; 2022.



# **Annexes**



## **Annex I. X-rays' related problematics and risks.**

In order to put the intramedullary nail in good conditions and in order to have adequate fixation in a suitable position of the bone fragments it is very important to control the position of the implant and the fragments' position. X-rays are also done during the proximal and distal locking. The distal locking requires much more x-ray control than the proximal. During this x-ray control the people who are in the operating theatre are exposed to some dose of ionizing radiation (Fig.109).

In 2010 the United States administration has published an article which describes an initiative to reduce the exposure to the radiation related to medical imaging [Noau10]. As stated in this article the usage of the C-arm in operating theatre exposes the patient to an equivalent dose of between 250 and 500 lung x-rays. This depends on the performed procedure. In 2007 the medical imaging was the largest source of exposure to ionising radiation in the USA [Metto8].

It may be inevitable to use x-rays during the fracture reduction of long bone, during the placement of the reaming guide in the medullary canal and measurement of the length of the nail that is being placed or the length of the locking screws. It is though possible to avoid an excessive exposure to x-rays during the proximal locking as the guide handle attached to the proximal part of the nail allows an automatic locking. It is still needed to measure the length of the locking screw. It depends on the anatomy and the position of the implant which is slightly variable. It is not possible to use this type of guide handle for the distal locking as there is some deformation of the nail which has been exposed earlier.

The studies have shown that the radiation time during the surgical procedure of intramedullary nailing of long bone can be twice or three times longer if this procedure is carried out by a junior surgeon as opposed to a senior surgeon. The radiation time during

the tibial nailing done by a junior surgeon was 1.28 minutes and the same operation done by a consultant surgeon was 0.56 minutes [Madao2]. If the femoral nailing was done, the total radiation time during the procedure performed by junior surgeon was 1.61 minutes and it was 0.52 minutes if it was done by a senior surgeon (Fig.110). Despite those differences, the total radiation time was acceptable in both cases and it didn't exceed the established normal range of radiation time.

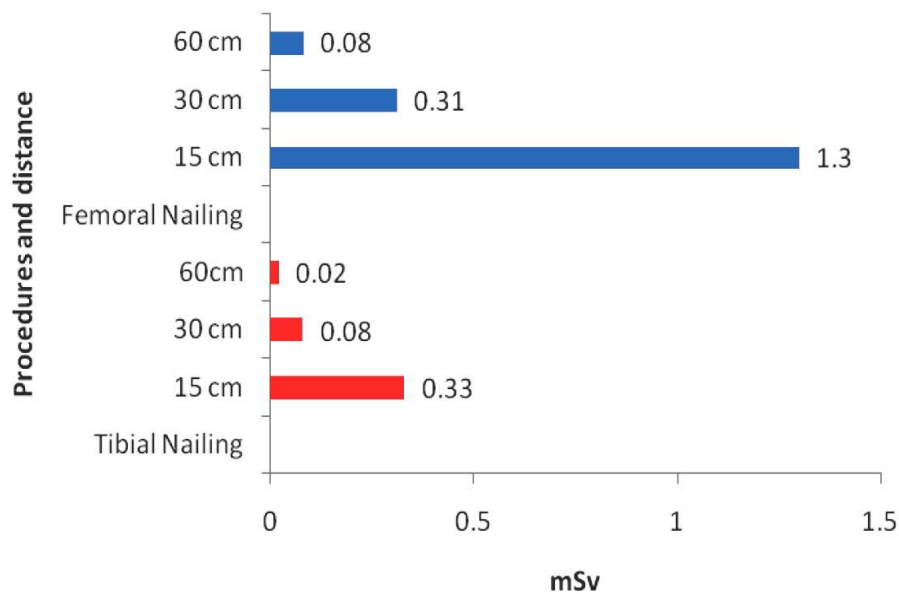


Figure 108: Annual X-ray dose while performing femoral and tibial nailing depending on distance [Kesa12].

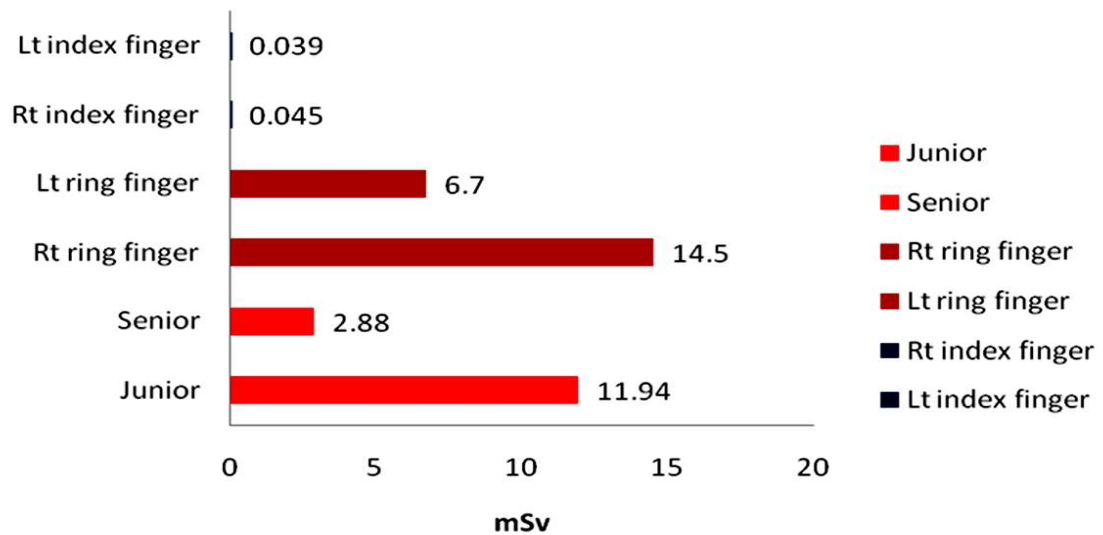


Figure 110: Annual cumulative X-rays dose depending on surgeon's experience [Kesa12].

Other studies confirm the data and show some evidence that the junior surgeons are more exposed to ionizing radiation [Kesa12].

It is admitted that the procedures requiring minimally invasive techniques expose the surgeons and patients to a higher dose of radiation. This is because there is less visual control therefore the control is done under x-rays (Fig.111). The direct visual control would reduce the dose of ionizing radiation, though the surgical indications of those two techniques are not the same and the minimally invasive surgery is preferable when it is possible [Kesa12].

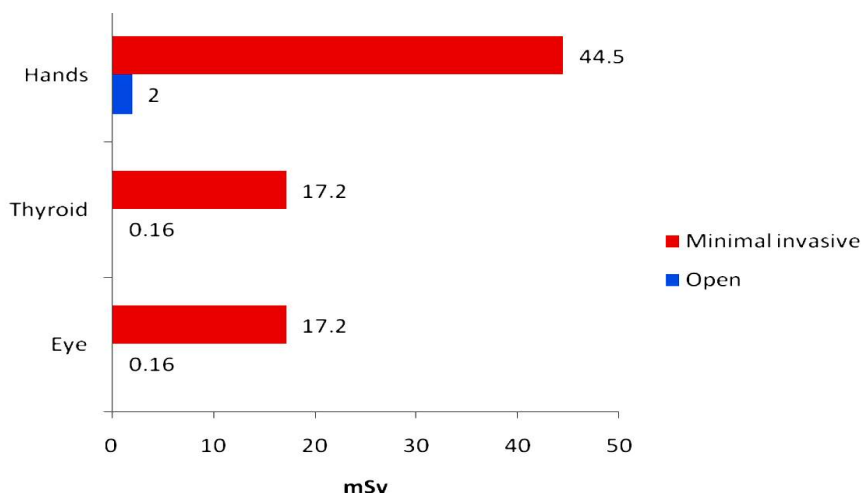
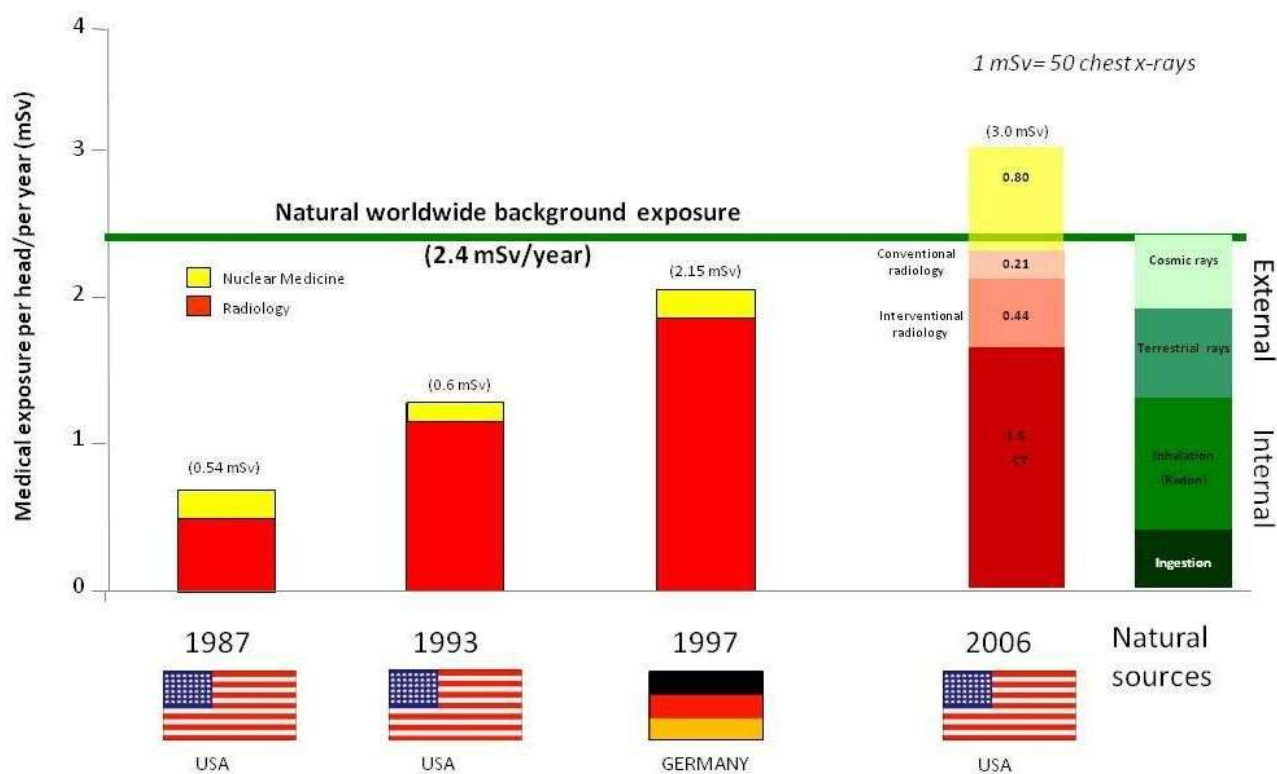


Figure 125: Cumulative doses received by orthopaedic surgeons performing minimally invasive or open surgery [Kesa12].

Several studies have been able to show the relationship between the practice of orthopaedic surgery and cancer [Mast05]. The cited paper [Mast05] describes the higher risk for the orthopaedic surgeons who are often exposed to x-rays to develop some form of cancer later in life.

The female surgeons have risk three times greater to develop a breast cancer and almost two times greater to develop other type of cancer than the general population [Mast05]. This statement has been confirmed by another study which has found that the risk to develop the breast cancer in female orthopaedic surgeons was 2.9 times greater than the risk to develop such cancer in general feminine population of the United States [Chou12]. This study didn't look specifically into direct relationship between the ionizing radiation and the risk to develop the breast cancer, it doesn't describe the risk factors to develop such cancer but the fact that differs the female orthopaedic surgeons from others can be the usage of x-rays and operating theatres.

The recommended doses that certain tissues and organs can be exposed to are different. The most recent recommendations of the ICRP (International Commission On Radiological Protection) say that the annual exceed those at work may not exceed 20mSv per year (the average dose calculated over five years), the x-ray does receive the within a year doesn't have to exceed 50mSv. The recommended x-ray doses per organ have been established: 20mSv/year for the eye lens [Cher16], 500mSv/year for the skin, 500mSv/year for hands and feet [Wrix08]. Those doses have been established for people exposed to x-rays at work (Fig.112).



Modified and updated (Mettler FA 2008) from Picano E. BMJ, March 6 2004

Figure 126: Medical exposure to ionising radiation.

It is admitted that there is a risk of 5% to develop a cancer over someone is exposed to to a unique dose of radiation of 1Sv. It is not very clear if there is a direct relationship between cancer and lower doses of ionizing radiation, doses that a lower than 100mSv/year [Noau13]. There are some countries where the inhabitants receive similar doses because of the natural radiation (250mSv/year in Ramsar, Iran) without detectable effect on their health.

Nevertheless some authors think that there is a risk of 1% to develop cancer if a person is exposed to irradiation of 100mSv [Pica11].

The established norms of radiation dose and the cumulative dose measurements may be different in different countries. Sometimes a unique those of radiation is used the as a reference in order to find the risks of cancer and other diseases related to radiation. The cumulative dose as a way to evaluate the risk is also important because the negative

effects of the ionizing radiation can be accumulated and has to be evaluated and taken into account when the risks related to radiation are defined. For this reason the total cumulative dose related to radiation work during the whole professional life is limited to 400mSv [Mill10] in Germany.

In addition to this, the World Health Organization suggests that an investigation has to be done if the cumulative doze exceeds 15mSv/month for hands and extremities and 5 mSv/month for the eye lens (risk to develop a cataract) [Mill10].

It is important to note that the doses of ionizing radiation received by the orthopaedic surgeon are relatively high during their intramedullary nailing of tibia or femur (Fig.113). There is quite a lot of variability between different studies. Some studies evaluate only sub specialities like orthopaedic surgery of lower limb. The orthopaedic surgeon who is involved specifically in the lower limb treatment has a risk to be more exposed to x-rays with the cumulative annual dose of 2.4 mSv [Sing07]. Sometimes the cumulative doze describing different studies vary about 10 times [Mast05].

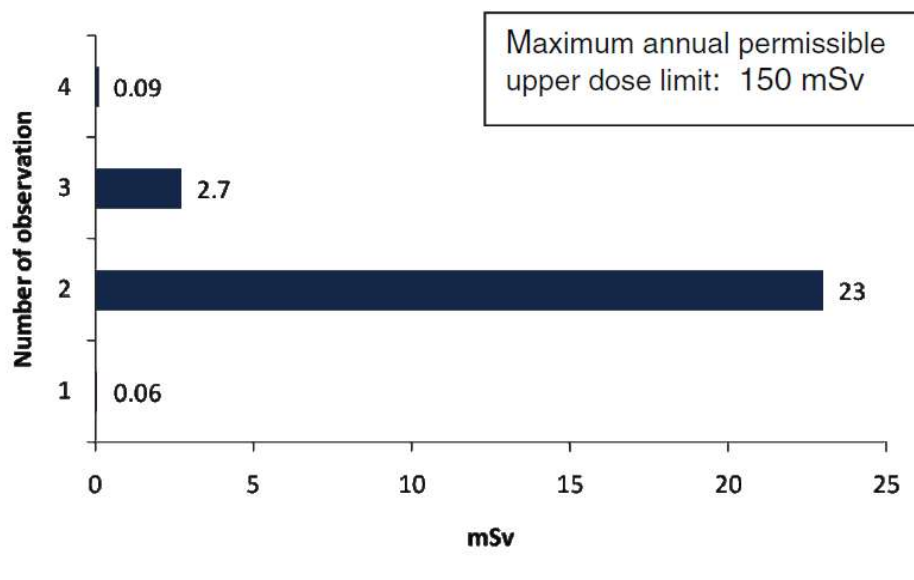


Figure 127: Annual cumulative dose received by surgeon on his assistant to his eyes or forehead [Kesa12][Van098][Mill83][Hars05][Muza05].

This remains lower than the allowed annual cumulative dose.

It is important to note that the patient who has to undergo the surgical procedure is more exposed to ionizing radiation than the surgeon during the short period of time of the surgery. The usage of the C-arm and x-rays exposes the patient to irradiation of 12 to 40mSv/min [Sing05]. However, the cumulative dose is important as the effect of radiation accumulate so the surgeon and the medical personnel receives a higher overall dose.

Several studies have been made evaluating the duration of irradiation needed during the intramedullary nailing. The data can be very variable. 1 of the studies has shown that they irradiation time during the femoral nailing procedure was 3.89 minutes [Muza05]. Another study has shown a much greater irradiation time during a similar operation than the preceding study. The average irradiation time was a 14min45s [Coet92]. Thirty percent of this time was needed for the distal locking of the intramedullary nail. It seems that those discrepancies are related to the experience of every surgeon.

It is important to note that certain patients, especially polytrauma patients sometimes need multiple intramedullary nailing procedures because different bones are fractured thus the irradiation doses are greater. This can expose such patients to access irradiation and risks related to it.

## **Conclusion**

The x-ray use in the operating theatre is very important in order to control the position of the fracture fragments and the position of the fixation implants. The usage of x-rays during the operation exposes the surgeon and the medical staff and the patient to certain risks, for example the cancer and other diseases. Illnesses, other than cancer related to the excessive ionizing radiation include cataract [Hamm13][Klei12] and cardiovascular diseases [Litt12][Ziel09]. The relationship between the ionizing radiation's

and cardiovascular diseases is relatively recent, but there are some hypotheses that they can occur as a result ionizing radiation. The mortality of cardiovascular diseases can be several times greater than the mortality related to cancer [Litt12][Ziel09].

Reducing the operating time and the reducing the usage of x-rays during the operation is the recurrent subject, that is why many researchers continue to work in order to improve the technical equipment, procedures and the instrumentation which would allow the people present during the surgical procedure to receive less ionizing radiation and be less exposed to risk associated with it.

# Annex II. Force-displacement curves and their types, scale adjusted.

specimen	curve	specimen	curve	specimen	curve
1_5_1	L	3_1	2L + Crack	6_1	2L + Y
1_5_2	L	3_2	2L	6_2	2L + Y + FR
1_5_3	2L	3_3	2L + Y	6_3	2L + Crack + FR
1_5_4	L	3_4	2L + Crack	6_4	2L + FR
1_5_5	L	3_5	2L + Crack	6_5	2L + Crack + FR
1_5_6	L	3_6	L + Y	6_6	2L + Crack
1_5_7	2L + Crack	3_7	2L + Y	6_7	2L + Crack + Plateau + FR
1_5_8	L + Y	3_8	2L + Y	6_8	2L + Crack
1_5_9	2L + Crack	3_9	2L + Crack	6_9	2L + Crack
1_5_10	2L + Crack	3_10	2L + Y	6_10	2L + Crack + FR
1_5_11	L + Y	3_11	2L + Crack	6_11	2L + Crack + Plateau + FR
1_5_12	L	3_12	2L + Crack	6_12	2L + Crack + Y
1_5_13	L	3_13	2L + Crack	6_13	2L + Crack
1_5_14	2L + Crack	3_14	2L + Crack + FR	6_14	2L + Crack + Y
1_5_15	L	3_15	2L	6_15	2L + Crack + Plateau + FR

## Annex III. Mechanical parameters and imaging data.

specimen	curve	Yield strength (N)	Eapp (Mpa)	average Eapp	Fmax (avec ou sans rupture) (N)	Average Fmax	Stiffness k0(N/mm)	Average Stiffness k0(N/mm)	Max fracture line length (mm)	Average fracture line length (mm)	average BV/TV
1_5_3	2L		1885.0	1658.2	-3088.69	-3486.3	3460	3882.3	11	10.3	0.927
3_2	2L		2058.4		-3972.42		3071		11		0.925
3_15	2L		1031.1		-3397.86		5116		9		0.924
1_5_7	2L + Crack		984.7	1257.7	-1423.39	-3099.0	5910	4429.3	3	20.5	0.919
1_5_9	2L + Crack		1833.6		-2723.84		3151		58.5		0.934
1_5_10	2L + Crack		1808.4		-2376.96		4164		15		0.926
1_5_14	2L + Crack		1697.2		-2811.51		2258		7		0.929
3_1	2L + Crack		1193.8		-2968.85		5615		9		0.936
3_4	2L + Crack		1460.2		-2605.61		4827		5		0.937
3_5	2L + Crack		1080.8		-2687.57		4738		3		0.941
3_9	2L + Crack		1185.1		-3438.31		4797		32.5		0.939
3_11	2L + Crack		1052.7		-2882.17		2332		45.5		0.940
3_12	2L + Crack		833.5		-2777.36		2165		32.5		0.923
3_13	2L + Crack		2122.0		-4085.82		4539		32.5		0.931
6_6	2L + Crack		703.8		-4088.41		4075		9		0.932
6_8	2L + Crack		1125.5		-4623.34		3764		3		0.936
6_9	2L + Crack		795.1		-3079.79		6548		45.5		0.941
6_13	2L + Crack		989.5		-3911.86		7556		7		0.944
3_14	2L + Crack + FR		1244.2	1160.2	-1911.31	-2963.8	4047	4708.6	32.5	42.3	0.956
6_3	2L + Crack + FR		1262.5		-3496.54		2686		32.5		0.933
6_5	2L + Crack + FR		953.5		-3777.07		7405		45.5		0.935
6_10	2L + Crack + FR		1180.6		-2670.21		4696		58.5		0.964
6_12	2L + Crack + Y	2048	2076.4	1523.6	-3430.17	-3644.6	4567	4010.3	45.5	39.0	0.927
6_14	2L + Crack + Y	3147	970.9		-3859.11		3453		32.5		0.953
6_4	2L + FR		1685.1	1685.1	-3986.38	-3986.38	8083	8083	32.5	32.5	0.934
3_3	2L + Y	3102	2403.1	2104.0	-4672.84	-3861.6	2868	3392.3	32.5	12.5	0.916
3_7	2L + Y	3644	1616.5		-4368.75		2070		9		0.918
3_8	2L + Y	2087	1798.6		-3079.06		6116		7		0.926
3_10	2L + Y	2087	3080.7		-3661.81		3144		7		0.930
6_1	2L + Y	2111	1621.2		-3525.67		2764		7		0.931
6_2	2L + Y + FR	1889	1795.8	1795.8	-2662.96	-2662.96	4081	4081	45.5	45.5	0.925
6_7	2L+ Crack + Plateau+ FR		2341.7	1931.3	-4960.98	-4333.7	4603	4581.5	58.5	47.3	0.964
6_11	2L+ Crack + Plateau+ FR		1150.6		-3738.71		3735		58.5		0.933
6_15	2L+ Crack + Plateau+ FR		2301.6		-4301.35		5406		25		0.964
1_5_1	L		1282.8	1328.2	-2908.17	-2644.5	2374	3493.9	5	2.8	0.935
1_5_2	L		1126.9		-2597.17		2138		3		0.927
1_5_4	L		1877.8		-2747.03		7273		1		0.943
1_5_5	L		1130.1		-2841.46		2921		3		0.931
1_5_6	L		1745.7		-3042.75		1894		3		0.938
1_5_12	L		924.9		-2609.19		2720		3		0.921
1_5_13	L		910.6		-1850.17		3350		1		0.921
1_5_15	L		1627.0		-2559.81		5280		3		0.914
1_5_8	L + Y	2221	1983.0	2094.7	-2335.86	-2792.3	2533	3731.6	20	10.0	0.916
1_5_11	L + Y	2949	1800.5		-3070.15		2356		7		0.914
3_6	L + Y	2849	2500.7		-2970.78		6305		3		0.932

# Annex IV. Fracture propagation cartography with segmental

BV/TV.

## Group1

1st group					
1	h (mm)	N	E	S	W
	1	0.950	0.950	0.887	0.951
	3	0.929	0.957	0.896	0.945
	5	0.811	0.941	0.905	0.947
	7	0.862	0.919	0.911	0.948
	9	0.909	0.958	0.906	0.964
	11	0.924	0.960	0.903	0.973
	13	0.912	0.964	0.912	0.979
	15	0.914	0.964	0.903	0.976
	20	0.913	0.966	0.909	0.986
	25	0.909	0.965	0.918	0.983
	33	0.909	0.969	0.919	0.979
	46	0.914	0.971	0.924	0.972
	59	0.905	0.972	0.925	0.976
	2	h (mm)	N	E	S
1		0.904	0.942	0.967	0.841
3		0.924	0.946	0.956	0.803
5		0.941	0.943	0.955	0.811
7		0.919	0.951	0.960	0.862
9		0.898	0.945	0.951	0.909
11		0.896	0.950	0.950	0.924
13		0.900	0.949	0.944	0.929
15		0.897	0.947	0.938	0.916
20		0.901	0.945	0.949	0.947
25		0.922	0.933	0.941	0.958
33		0.926	0.921	0.942	0.978
46		0.928	0.935	0.920	0.984
59		0.931	0.943	0.894	0.939
3		h (mm)	N	E	S
	1	0.816	0.912	0.940	0.964
	3	0.812	0.920	0.953	0.956
	5	0.811	0.941	0.945	0.956
	7	0.862	0.919	0.943	0.955
	9	0.909	0.902	0.940	0.960
	11	0.924	0.887	0.949	0.952
	13	0.939	0.900	0.953	0.944
	15	0.930	0.901	0.946	0.941
	20	0.951	0.908	0.943	0.938
	25	0.961	0.918	0.932	0.942
	33	0.970	0.923	0.929	0.934
	46	0.985	0.929	0.938	0.919
	59	0.940	0.934	0.940	0.910
	4	h (mm)	N	E	S
1		0.973	0.995	0.953	0.919
3		0.937	0.983	0.952	0.944
5		0.941	0.986	0.946	0.911
7		0.919	0.949	0.939	0.862
9		0.928	0.955	0.938	0.909
11		0.923	0.957	0.940	0.924
13		0.912	0.956	0.942	0.974
15		0.906	0.953	0.939	0.988
20		0.923	0.934	0.932	0.982
25		0.917	0.937	0.944	0.983
33		0.948	0.969	0.949	0.963
46		0.941	0.950	0.940	0.969
59		0.946	0.955	0.947	0.955
5		h (mm)	N	E	S
	1	0.966	0.964	0.897	0.962
	3	0.935	0.963	0.881	0.958
	5	0.941	0.958	0.899	0.911
	7	0.919	0.945	0.899	0.862
	9	0.937	0.951	0.897	0.909
	11	0.940	0.946	0.905	0.924
	13	0.952	0.953	0.890	0.956
	15	0.949	0.949	0.900	0.951
	20	0.945	0.954	0.901	0.951
	25	0.943	0.954	0.896	0.940
	33	0.949	0.961	0.899	0.936
	46	0.955	0.964	0.877	0.953
	59	0.971	0.964	0.878	0.948
	6	h (mm)	N	E	S
1		0.968	0.912	0.966	0.932
3		0.954	0.904	0.976	0.940
5		0.896	0.906	0.972	0.911
7		0.919	0.897	0.969	0.862
9		0.952	0.887	0.966	0.909
11		0.955	0.881	0.975	0.924
13		0.958	0.887	0.974	0.943
15		0.958	0.884	0.979	0.950
20		0.962	0.885	0.986	0.952
25		0.956	0.902	0.991	0.964
33		0.949	0.908	0.968	0.963
46		0.943	0.915	0.953	0.966
59		0.965	0.931	0.936	0.985
7		h (mm)	N	E	S
	1	0.899	0.908	0.935	0.947
	3	0.908	0.925	0.927	0.947
	5	0.941	0.921	0.914	0.911
	7	0.919	0.920	0.910	0.862
	9	0.899	0.928	0.896	0.909
	11	0.893	0.923	0.895	0.924
	13	0.903	0.920	0.888	0.960
	15	0.919	0.915	0.885	0.959
	20	0.949	0.926	0.865	0.958
	25	0.954	0.922	0.862	0.955
	33	0.966	0.950	0.880	0.945
	46	0.930	0.945	0.886	0.955
	59	0.919	0.981	0.897	0.923
	8	h (mm)	N	E	S
1		0.927	0.907	0.927	0.963
3		0.926	0.907	0.925	0.961
5		0.941	0.941	0.948	0.911
7		0.919	0.894	0.911	0.862
9		0.943	0.893	0.909	0.909
11		0.949	0.886	0.899	0.924
13		0.952	0.880	0.904	0.968
15		0.951	0.877	0.892	0.971
20		0.947	0.875	0.890	0.959
25		0.943	0.867	0.859	0.955
33		0.968	0.859	0.863	0.943
46		0.972	0.886	0.887	0.943
59		0.988	0.903	0.902	0.904
9		h (mm)	N	E	S
	1	0.956	0.951	0.908	0.938
	3	0.897	0.946	0.910	0.943
	5	0.811	0.941	0.944	0.945
	7	0.862	0.919	0.921	0.937
	9	0.909	0.952	0.914	0.933
	11	0.924	0.934	0.921	0.933
	13	0.956	0.944	0.920	0.931
	15	0.966	0.959	0.923	0.951
	20	0.970	0.951	0.926	0.928
	25	0.974	0.946	0.923	0.923
	33	0.974	0.947	0.952	0.929
	46	0.965	0.932	0.927	0.918
	59	0.965	0.938	0.937	0.916
	10	h (mm)	N	E	S
1		0.926	0.904	0.921	0.946
3		0.929	0.914	0.918	0.949
5		0.811	0.941	0.908	0.947
7		0.862	0.919	0.916	0.946
9		0.909	0.914	0.925	0.952
11		0.924	0.921	0.924	0.954
13		0.933	0.920	0.920	0.951
15		0.946	0.920	0.935	0.958
20		0.918	0.908	0.948	0.958
25		0.919	0.910	0.935	0.954
33		0.912	0.931	0.922	0.962
46		0.896	0.961	0.917	0.936
59		0.875	0.963	0.951	0.941
11		h (mm)	N	E	S
	1	0.899	0.896	0.918	0.947
	3	0.866	0.890	0.923	0.949
	5	0.811	0.941	0.922	0.943
	7	0.862	0.919	0.923	0.940
	9	0.909	0.889	0.919	0.946
	11	0.924	0.882	0.917	0.949
	13	0.914	0.891	0.920	0.935
	15	0.907	0.895	0.917	0.938
	20	0.910	0.881	0.921	0.945
	25	0.905	0.881	0.937	0.954
	33	0.915	0.885	0.935	0.953
	46	0.885	0.899	0.910	0.920
	59	0.930	0.917	0.899	0.909
	12	h (mm)	N	E	S
1		0.897	0.916	0.931	0.907
3		0.896	0.913	0.941	0.910
5		0.811	0.941	0.939	0.911
7		0.862	0.919	0.942	0.903
9		0.909	0.929	0.964	0.908
11		0.924	0.927	0.950	0.905
13		0.900	0.923	0.956	0.939
15		0.893	0.926	0.962	0.903
20		0.903	0.928	0.966	0.893
25		0.905	0.941	0.961	0.896
33		0.908	0.945	0.957	0.902
46		0.934	0.956	0.923	0.912
59		0.924	0.974	0.853	0.942
13		h (mm)	N	E	S
	1	0.922	0.890	0.899	0.957
	3	0.935	0.891	0.941	0.952
	5	0.941	0.889	0.936	0.811
	7	0.919	0.891	0.936	0.862
	9	0.896	0.943	0.943	0.909
	11	0.945	0.886	0.953	0.924
	13	0.940	0.891	0.941	0.940
	15	0.937	0.892	0.937	0.945
	20	0.956	0.895	0.948	0.942
	25	0.953	0.906	0.939	0.932
	33	0.938	0.917	0.940	0.925
	46	0.902	0.933	0.932	0.897
	59	0.880	0.941	0.935	0.865
	14	h (mm)	N	E	S
1		0.922	0.901	0.938	0.939
3		0.932	0.909	0.940	0.940
5		0.941	0.913	0.936	0.811
7		0.919	0.918	0.936	0.862
9		0.916	0.962	0.938	0.909
11		0.915	0.962	0.932	0.924
13		0.934	0.950	0.930	0.949
15		0.935	0.941	0.929	0.949
20		0.938	0.930	0.925	0.940
25		0.953	0.931	0.917	0.939
33		0.965	0.932	0.901	0.917
46		0.966	0.936	0.907	0.929
59		0.964	0.894	0.938	0.957
15		h (mm)	N	E	S
	1	0.897	0.928	0.918	0.919
	3	0.818	0.926	0.916	0.923
	5	0.811	0.941	0.920	0.940
	7	0.862	0.919	0.915	0.936
	9	0.909	0.931	0.924	0.939
	11	0.924	0.924	0.919	0.939
	13	0.879	0.932	0.910	0.944
	15	0.879	0.925	0.904	0.945
	20	0.880	0.935	0.904	0.953
	25	0.889	0.934	0.893	0.939
	33	0.905	0.926	0.891	0.95

# Group 2

2 <sup>nd</sup> group					
1	h (mm)	N	E	S	W
	1	<b>0.983</b>	0.894	0.975	<b>0.923</b>
	3	<b>0.980</b>	0.917	0.966	<b>0.897</b>
	5	0.980	0.927	0.961	<b>0.907</b>
	7	0.969	0.923	0.957	<b>0.901</b>
	9	0.960	0.943	0.951	<b>0.905</b>
	11	0.946	0.930	0.953	0.904
	13	0.949	0.927	0.953	0.908
	15	0.945	0.934	0.956	0.911
	20	0.934	0.901	0.948	0.916
	25	0.941	0.918	0.941	0.913
	33	0.945	0.918	0.934	0.925
	46	0.951	0.914	0.930	0.945
59	0.955	0.941	0.924	0.924	
2	h (mm)	N	E	S	W
	1	<b>0.911</b>	0.984	<b>0.893</b>	0.972
	3	<b>0.939</b>	0.914	<b>0.911</b>	0.935
	5	<b>0.944</b>	0.927	<b>0.903</b>	0.955
	7	<b>0.931</b>	0.921	<b>0.909</b>	0.943
	9	<b>0.933</b>	0.910	0.910	0.952
	11	0.928	0.902	0.913	0.946
	13	0.927	0.904	0.906	0.933
	15	0.926	0.901	0.917	0.945
	20	0.926	0.901	0.917	0.945
	25	0.937	0.906	0.926	0.927
	33	0.938	0.913	0.920	0.924
	46	0.945	0.909	0.931	0.931
59	0.943	0.888	0.955	0.912	
3	h (mm)	N	E	S	W
	1	<b>0.928</b>	0.835	<b>0.881</b>	0.912
	3	<b>0.950</b>	0.866	<b>0.924</b>	0.944
	5	<b>0.945</b>	0.876	0.944	0.949
	7	<b>0.938</b>	0.886	0.962	0.929
	9	<b>0.907</b>	0.887	0.970	0.923
	11	<b>0.910</b>	0.888	0.963	0.930
	13	0.895	0.887	0.974	0.923
	15	0.970	0.878	0.978	0.932
	20	0.874	0.875	0.964	0.940
	25	0.877	0.888	0.962	0.946
	33	0.873	0.905	0.939	0.959
	46	0.862	0.915	0.945	0.944
59	0.832	0.907	0.953	0.922	
4	h (mm)	N	E	S	W
	1	<b>0.909</b>	0.949	<b>0.914</b>	0.960
	3	<b>0.922</b>	0.937	<b>0.926</b>	0.945
	5	0.930	0.929	<b>0.926</b>	0.951
	7	0.963	0.924	<b>0.927</b>	0.957
	9	0.959	0.923	<b>0.926</b>	0.949
	11	0.962	0.928	<b>0.940</b>	0.952
	13	0.951	0.922	<b>0.928</b>	0.938
	15	0.939	0.924	<b>0.937</b>	0.928
	20	0.949	0.921	<b>0.932</b>	0.916
	25	0.952	0.921	<b>0.954</b>	0.921
	33	0.956	0.931	<b>0.956</b>	0.904
	46	0.952	0.928	0.963	0.907
59	0.964	0.917	0.958	0.924	
5	h (mm)	N	E	S	W
	1	<b>0.952</b>	0.927	<b>0.937</b>	0.939
	3	0.949	0.937	<b>0.941</b>	0.949
	5	0.944	0.933	<b>0.942</b>	0.949
	7	0.951	0.930	<b>0.947</b>	0.944
	9	0.947	0.940	<b>0.944</b>	0.940
	11	0.943	0.935	0.943	0.939
	13	0.943	0.940	0.956	0.927
	15	0.943	0.940	0.952	0.924
	20	0.944	0.918	0.952	0.938
	25	0.947	0.937	0.953	0.935
	33	0.947	0.937	0.959	0.938
	46	0.954	0.940	0.922	0.956
59	0.951	0.941	0.888	0.964	
6	h (mm)	N	E	S	W
	1	<b>0.898</b>	0.895	<b>0.939</b>	0.943
	3	<b>0.897</b>	0.913	0.931	0.944
	5	0.908	0.947	0.915	0.943
	7	0.906	0.954	0.914	0.936
	9	0.920	0.969	0.926	0.942
	11	0.913	0.956	0.915	0.935
	13	0.929	0.960	0.921	0.938
	15	0.934	0.963	0.926	0.932
	20	0.917	0.963	0.932	0.947
	25	0.922	0.965	0.936	0.938
	33	0.922	0.973	0.947	0.927
	46	0.902	0.973	0.944	0.907
59	0.887	0.982	0.927	0.886	
7	h (mm)	N	E	S	W
	1	<b>0.959</b>	0.918	<b>0.905</b>	0.887
	3	<b>0.950</b>	0.911	<b>0.935</b>	0.911
	5	0.938	0.911	0.939	0.905
	7	0.946	0.890	0.934	0.892
	9	0.962	0.911	0.942	0.908
	11	0.959	0.877	0.942	0.892
	13	0.942	0.887	0.938	0.895
	15	0.942	0.889	0.932	0.889
	20	0.936	0.882	0.932	0.898
	25	0.926	0.891	0.943	0.898
	33	0.930	0.887	0.951	0.899
	46	0.935	0.900	0.916	0.923
59	0.871	0.911	0.946	0.933	
8	h (mm)	N	E	S	W
	1	<b>0.945</b>	0.900	<b>0.966</b>	0.896
	3	0.928	0.926	<b>0.968</b>	0.898
	5	0.934	0.906	<b>0.969</b>	0.906
	7	0.928	0.924	<b>0.974</b>	0.880
	9	0.895	0.925	<b>0.973</b>	0.892
	11	0.930	0.899	0.921	0.893
	13	0.935	0.894	0.967	0.891
	15	0.929	0.895	0.964	0.901
	20	0.916	0.909	0.952	0.889
	25	0.920	0.911	0.941	0.915
	33	0.899	0.906	0.944	0.928
	46	0.917	0.914	0.957	0.929
59	0.939	0.918	0.942	0.946	
9	h (mm)	N	E	S	W
	1	<b>0.913</b>	0.981	<b>0.946</b>	0.948
	3	<b>0.915</b>	0.971	<b>0.947</b>	0.974
	5	<b>0.913</b>	0.969	<b>0.927</b>	0.957
	7	0.919	0.967	<b>0.913</b>	0.955
	9	0.908	0.957	0.915	0.962
	11	0.916	0.963	0.920	0.951
	13	0.911	0.960	0.917	0.949
	15	0.911	0.959	0.928	0.946
	20	0.920	0.951	0.913	0.947
	25	0.921	0.945	0.920	0.945
	33	0.923	0.950	0.933	0.945
	46	0.923	0.953	0.932	0.948
59	0.948	0.954	0.939	0.948	
10	h (mm)	N	E	S	W
	1	<b>0.922</b>	0.954	<b>0.849</b>	0.968
	3	<b>0.935</b>	0.962	<b>0.852</b>	0.994
	5	<b>0.934</b>	0.950	<b>0.842</b>	0.999
	7	0.915	0.945	<b>0.861</b>	0.999
	9	0.903	0.951	<b>0.854</b>	0.996
	11	0.915	0.952	<b>0.866</b>	0.987
	13	0.901	0.942	<b>0.866</b>	0.974
	15	0.896	0.943	<b>0.877</b>	0.965
	20	0.907	0.959	<b>0.881</b>	0.964
	25	0.900	0.964	<b>0.894</b>	0.962
	33	0.918	0.968	<b>0.888</b>	0.955
	46	0.923	0.968	0.913	0.949
59	0.951	0.985	0.924	0.912	
11	h (mm)	N	E	S	W
	1	<b>0.933</b>	0.967	<b>0.883</b>	0.973
	3	<b>0.943</b>	0.967	<b>0.884</b>	0.966
	5	<b>0.947</b>	0.957	<b>0.886</b>	0.966
	7	<b>0.945</b>	0.955	0.893	0.964
	9	0.934	0.943	0.921	0.960
	11	0.940	0.941	0.903	0.964
	13	0.939	0.950	0.926	0.969
	15	0.941	0.933	0.906	0.964
	20	0.948	0.940	0.913	0.960
	25	0.953	0.943	0.904	0.938
	33	0.964	0.954	0.924	0.946
	46	0.953	0.958	0.910	0.937
59	0.951	0.949	0.906	0.952	
12	h (mm)	N	E	S	W
	1	<b>0.966</b>	0.901	<b>0.962</b>	0.876
	3	<b>0.959</b>	0.907	<b>0.952</b>	0.875
	5	<b>0.947</b>	0.892	0.954	<b>0.879</b>
	7	0.944	0.896	0.955	<b>0.879</b>
	9	0.940	0.897	0.945	<b>0.887</b>
	11	0.954	0.896	0.941	<b>0.888</b>
	13	0.954	0.899	0.944	<b>0.886</b>
	15	0.964	0.899	0.948	<b>0.885</b>
	20	0.978	0.906	0.930	<b>0.910</b>
	25	0.944	0.896	0.915	<b>0.910</b>
	33	0.968	0.902	0.923	<b>0.911</b>
	46	0.983	0.939	0.917	<b>0.932</b>
59	0.930	0.919	0.928	0.915	
13	h (mm)	N	E	S	W
	1	<b>0.875</b>	0.917	<b>0.961</b>	0.968
	3	<b>0.880</b>	0.913	<b>0.921</b>	0.962
	5	<b>0.880</b>	0.913	0.921	0.962
	7	<b>0.921</b>	0.920	0.924	0.959
	9	<b>0.833</b>	0.919	0.914	0.954
	11	<b>0.935</b>	0.918	0.906	0.949
	13	<b>0.939</b>	0.913	0.899	0.971
	15	<b>0.942</b>	0.916	0.900	0.976
	20	<b>0.942</b>	0.920	0.898	0.966
	25	<b>0.953</b>	0.924	0.900	0.977
	33	<b>0.938</b>	0.928	0.896	0.969
	46	<b>0.940</b>	0.937	0.911	0.983
59	0.926	0.936	0.916	0.982	
14	h (mm)	N	E	S	W
	1	<b>0.962</b>	0.926	<b>0.948</b>	0.970
	3	<b>0.967</b>	0.944	<b>0.948</b>	0.968
	5	<b>0.964</b>	0.942	<b>0.947</b>	0.968
	7	<b>0.966</b>	0.940	<b>0.946</b>	0.967
	9	<b>0.994</b>	0.932	<b>0.937</b>	0.959
	11	<b>0.989</b>	0.934	<b>0.927</b>	0.997
	13	<b>0.988</b>	0.940	0.935	0.998
	15	<b>0.987</b>	0.934	0.936	0.991
	20	<b>0.999</b>	0.932	0.934	0.981
	25	<b>0.992</b>	0.931	0.924	0.943
	33	<b>0.969</b>	0.910	0.926	0.933
	46	0.958	0.935	0.926	0.927
59	0.941	0.993	0.912	0.943	
15	h (mm)	N	E	S	W
	1	<b>0.893</b>	0.950	<b>0.887</b>	0.887
	3	<b>0.907</b>	0.963	<b>0.908</b>	0.881
	5	<b>0.910</b>	0.962	<b>0.877</b>	0.909

# Group 3

1 <sup>st</sup> group					
h (mm)	N	E	S	W	
1	0.964	0.895	0.899	0.938	
3	0.952	0.949	0.891	0.945	
5	0.959	0.841	0.895	0.957	
7	0.954	0.938	0.897	0.958	
9	0.954	0.928	0.898	0.948	
11	0.952	0.919	0.896	0.945	
13	0.953	0.912	0.908	0.953	
15	0.956	0.911	0.909	0.945	
20	0.955	0.898	0.920	0.938	
25	0.944	0.898	0.922	0.932	
33	0.946	0.894	0.929	0.912	
46	0.953	0.909	0.937	0.903	
59	0.962	0.975	0.947	0.942	

2 <sup>nd</sup> group					
h (mm)	N	E	S	W	
1	0.865	0.955	0.893	0.909	
3	0.886	0.977	0.907	0.930	
5	0.868	0.957	0.897	0.946	
7	0.893	0.949	0.901	0.941	
9	0.898	0.949	0.898	0.941	
11	0.902	0.948	0.897	0.941	
13	0.903	0.952	0.898	0.957	
15	0.906	0.944	0.893	0.948	
20	0.912	0.950	0.905	0.956	
25	0.924	0.943	0.904	0.945	
33	0.929	0.944	0.902	0.941	
46	0.938	0.952	0.900	0.931	
59	0.938	0.946	0.906	0.922	

3 <sup>rd</sup> group					
h (mm)	N	E	S	W	
1	0.907	0.931	0.942	0.956	
3	0.908	0.912	0.969	0.959	
5	0.913	0.913	0.961	0.958	
7	0.918	0.912	0.960	0.956	
9	0.918	0.915	0.979	0.953	
11	0.924	0.912	0.972	0.945	
13	0.926	0.908	0.952	0.942	
15	0.926	0.920	0.947	0.944	
20	0.932	0.920	0.928	0.935	
25	0.933	0.917	0.940	0.931	
33	0.934	0.926	0.919	0.933	
46	0.916	0.940	0.914	0.924	
59	0.909	0.938	0.913	0.913	

4 <sup>th</sup> group					
h (mm)	N	E	S	W	
1	0.945	0.875	0.963	0.910	
3	0.940	0.888	0.975	0.900	
5	0.943	0.887	0.992	0.910	
7	0.938	0.881	0.987	0.911	
9	0.948	0.888	0.984	0.918	
11	0.954	0.893	0.978	0.917	
13	0.961	0.884	0.971	0.920	
15	0.954	0.901	0.973	0.935	
20	0.959	0.891	0.973	0.937	
25	0.949	0.912	0.982	0.939	
33	0.945	0.901	0.979	0.927	
46	0.941	0.924	0.949	0.926	
59	0.955	0.941	0.893	0.913	

5 <sup>th</sup> group					
h (mm)	N	E	S	W	
1	0.934	0.920	0.963	0.945	
3	0.931	0.909	0.985	0.943	
5	0.930	0.890	0.981	0.939	
7	0.919	0.904	0.991	0.933	
9	0.922	0.936	0.997	0.945	
11	0.914	0.930	0.949	0.928	
13	0.915	0.934	0.966	0.937	
15	0.909	0.929	0.960	0.937	
20	0.908	0.929	0.952	0.935	
25	0.915	0.931	0.958	0.925	
33	0.943	0.929	0.964	0.922	
46	0.948	0.944	0.977	0.905	
59	0.942	0.913	0.982	0.894	

6 <sup>th</sup> group					
h (mm)	N	E	S	W	
1	0.948	0.923	0.922	0.927	
3	0.953	0.918	0.930	0.928	
5	0.962	0.911	0.924	0.932	
7	0.969	0.902	0.925	0.932	
9	0.963	0.884	0.924	0.941	
11	0.962	0.896	0.922	0.940	
13	0.963	0.917	0.926	0.944	
15	0.959	0.900	0.933	0.945	
20	0.963	0.922	0.925	0.944	
25	0.964	0.897	0.925	0.944	
33	0.964	0.895	0.930	0.936	
46	0.955	0.881	0.942	0.932	
59	0.944	0.894	0.943	0.927	

7 <sup>th</sup> group					
h (mm)	N	E	S	W	
1	0.945	0.952	0.998	0.975	
3	0.945	0.957	0.996	0.977	
5	0.943	0.960	0.998	0.980	
7	0.937	0.958	0.999	0.980	
9	0.941	0.961	0.998	0.978	
11	0.951	0.973	0.998	0.986	
13	0.939	0.954	0.996	0.970	
15	0.939	0.966	0.997	0.968	
20	0.935	0.964	0.993	0.955	
25	0.934	0.975	0.991	0.943	
33	0.933	0.973	0.995	0.912	
46	0.929	0.987	0.977	0.928	
59	0.931	0.973	0.962	0.912	

8 <sup>th</sup> group					
h (mm)	N	E	S	W	
1	0.948	0.946	0.900	0.930	
3	0.950	0.954	0.915	0.921	
5	0.939	0.960	0.927	0.922	
7	0.931	0.954	0.940	0.925	
9	0.929	0.948	0.946	0.929	
11	0.927	0.944	0.946	0.933	
13	0.927	0.939	0.938	0.928	
15	0.923	0.932	0.935	0.926	
20	0.928	0.934	0.932	0.936	
25	0.937	0.927	0.938	0.933	
33	0.941	0.940	0.936	0.929	
46	0.960	0.930	0.943	0.943	
59	0.966	0.923	0.940	0.945	

9 <sup>th</sup> group					
h (mm)	N	E	S	W	
1	0.942	0.980	0.966	0.939	
3	0.938	0.984	0.956	0.942	
5	0.942	0.972	0.950	0.942	
7	0.939	0.951	0.957	0.937	
9	0.939	0.935	0.955	0.941	
11	0.938	0.925	0.959	0.935	
13	0.935	0.919	0.951	0.940	
15	0.938	0.920	0.951	0.936	
20	0.936	0.920	0.943	0.928	
25	0.939	0.921	0.943	0.923	
33	0.938	0.920	0.936	0.921	
46	0.979	0.945	0.934	0.912	
59	0.988	0.912	0.928	0.917	

10 <sup>th</sup> group					
h (mm)	N	E	S	W	
1	0.945	0.952	0.998	0.975	
3	0.945	0.957	0.996	0.977	
5	0.943	0.960	0.998	0.980	
7	0.937	0.958	0.999	0.980	
9	0.941	0.961	0.998	0.978	
11	0.951	0.973	0.998	0.986	
13	0.939	0.954	0.996	0.970	
15	0.939	0.966	0.997	0.968	
20	0.935	0.964	0.993	0.955	
25	0.934	0.975	0.991	0.943	
33	0.933	0.973	0.995	0.912	
46	0.929	0.987	0.977	0.928	
59	0.931	0.973	0.962	0.912	

11 <sup>th</sup> group					
h (mm)	N	E	S	W	
1	0.936	0.947	0.916	0.941	
3	0.935	0.945	0.896	0.949	
5	0.938	0.946	0.906	0.939	
7	0.937	0.944	0.907	0.941	
9	0.929	0.953	0.894	0.951	
11	0.930	0.958	0.897	0.954	
13	0.932	0.963	0.902	0.954	
15	0.933	0.958	0.902	0.957	
20	0.934	0.954	0.908	0.958	
25	0.923	0.942	0.911	0.958	
33	0.912	0.937	0.910	0.968	
46	0.899	0.947	0.897	0.955	
59	0.897	0.976	0.896	0.937	

12 <sup>th</sup> group					
h (mm)	N	E	S	W	
1	0.911	0.841	0.961	0.938	
3	0.920	0.885	0.961	0.930	
5	0.914	0.914	0.926	0.930	
7	0.928	0.929	0.917	0.929	
9	0.924	0.938	0.918	0.926	
11	0.934	0.947	0.919	0.932	
13	0.922	0.943	0.914	0.927	
15	0.931	0.945	0.923	0.930	
20	0.921	0.928	0.914	0.937	
25	0.965	0.942	0.914	0.948	
33	0.952	0.945	0.907	0.957	
46	0.914	0.934	0.903	0.961	
59	0.887	0.928	0.888	0.962	

13 <sup>th</sup> group					
h (mm)	N	E	S	W	
1	0.969	0.890	0.997	0.822	
3	0.966	0.896	0.938	0.841	
5	0.974	0.984	0.947	0.844	
7	0.973	0.985	0.941	0.853	
9	0.974	0.985	0.941	0.869	
11	0.975	0.980	0.946	0.871	
13	0.974	0.975	0.944	0.878	
15	0.984	0.971	0.943	0.896	
20	0.975	0.962	0.938	0.919	
25	0.942	0.951	0.946	0.935	
33	0.946	0.944	0.953	0.944	
46	0.950	0.940	0.959	0.955	
59	0.928	0.927	0.955	0.984	

14 <sup>th</sup> group					
h (mm)	N	E	S	W	
1	0.924	0.958	0.979	0.937	
3	0.939	0.975	0.988	0.948	
5	0.930	0.983	0.993	0.943	
7	0.930	0.991	0.997	0.946	
9	0.929	0.993	0.993	0.944	
11	0.930	0.985	0.982	0.944	
13	0.931	0.979	0.970	0.945	
15	0.927	0.971	0.962	0.942	
20	0.940	0.963	0.957	0.950	
25	0.921	0.952	0.930	0.944	
33	0.926	0.949	0.929	0.947	
46	0.921	0.954	0.927	0.948	
59	0.992	0.942	0.938	0.951	

15 <sup>th</sup> group					
h (mm)	N	E	S	W	
1	0.975	0.945	0.952	0.998	
3	0.977	0.945	0.957	0.996	
5	0.980	0.943	0.950	0.998	
7	0.980	0.937	0.958	0.999	
9	0.978	0.941	0.958	0.998	
11	0.986	0.951	0.973	0.998	
13	0.970	0.939	0.954	0.996	
15	0.968	0.939	0.966	0.997	
20	0.955	0.935	0.964	0.993	
25	0.943	0.934	0.975	0.991	
33	0.936	0.933	0.973	0.995	
46	0.928	0.929	0.987	0.977	
59	0.912	0.931	0.973	0.962	

## Annex V. Matlab/Octave Code

Function 1. Main Function: Hertz for Plane Stress

```
function [] = hertz_main_pstress(fname_in, fname_out, wsh_num)
    prompt = ("Type input file name: ");
    fname_in = input(prompt, "s"); %input file name of input excel file (Raw_data_1_5,
Raw_data_3, or Raw_data_6_5)
    prompt = ("Number of worksheets: ");
    wsh_tot = input(prompt); %input number of worksheets present in the input excel file
    prompt = ("Type output file name: ");
    fname_out = input(prompt, "s"); %input file name of output excel file where the extracted
data is placed

%% !! Important to set the maximum error for analysis !!
    lim_err2 = 0.0001; %declares maximum limit of error value for sum of err^2

    R = 0.002; %declaration of R for 2mm rod radius
    L = 0.006; %declaration of L for 3mm per side cortical bone thickness

%% This section is on data extraction from excel file

    for i = 5:wsh_tot;
        wsh_num = i;
        [dat_mat size_mat] = xlsread_func(fname_in, wsh_num); %each iteration extracts data
matrix from each worksheet (xlsread_func.m)
        for j = 1:size_mat; %for loop to extract all values from xlsread
            dii(j) = -dat_mat(j,1); %calls out all the values of 1st column of dat_mat and negates
            fii(j) = -dat_mat(j,2); %calls out all the values of 2nd column of dat_mat and negates
        endfor
    % display(dii); display(fii); %for debugging/troubleshooting only / hide when running
final iterations

%% This section is on curve fitting the experimental values to the mathematical model

    param = [0]; %initial declaration of param to reset every worksheet
    act_err2 = 0;
    iter = 0;
    di = dii;
    fi = fii;
    while act_err2 < lim_err2 %while loop to iterate the curve fitting starting from 0-1, 0-2,
0-3 and so on
        iter = iter+1;
        [A_eff, C_eff, E_eff, sum_err2, fitted_values, max_err2] = curvefit_func_pstress(di, fi,
R, L, iter); %curvefitting function (curvefit_func.m)
        param(iter,1:7) = [di(iter), fitted_values(iter), fi(iter), A_eff, C_eff, E_eff, max_err2];
    %param matrix containing all the parameter values including the sum of error^2
        act_err2 = max_err2;
        act_sum_err2 = sum_err2; %calls out sum or error^2 of current iteration
    % display(param); %display parameter matrix / hide when running final iterations
```

```

end

%% This section writes the parameter values inside a new .xlsx file, one worksheet per
specimen

[rstatus] = xlswrite_func(fname_out, param, wsh_num); %xlswrite function that writes
the parameters in the desired .xlsx file
if rstatus == 1;
    display(["xlswrite success for worksheet ", num2str(wsh_num),"!"]);
elseif rstatus == 0;
    display("xlswrite failed!");
endif

%% This section plots the graphs of each worksheet/specimen

d_iter = di(1:iter); %to scale x values for graph
f_iter = fi(1:iter); %to scale y values for graph

figure; %creates new figure
plot(d_iter,f_iter,"k",fitted_values,f_iter,"+"); title(["Plot of ", fname_in, ", Specimen
#", num2str(wsh_num), ", after ", num2str(iter), " iterations"]); xlabel("Displacement
(mm)"); ylabel("Force (N)"); %improve this later
legend("Experimental Data","Mathematical Model", "location", "northwest");
% hold off;
endfor

endfunction

Function 2. Subfunction 1: XLSRead Function
function [dat_mat, size_mat] = xlsread_func(fname_in, wsh_num)
n = wsh_num; %calls out total number of worksheets for iteration
data_in = fname_in; %calls out name of .xlsx file

dat_mat = xlsread(data_in, n); %reads the values in the .xlsx file
A = size(dat_mat);
size_mat = A(1);

endfunction

Function 3. Subfunction 2: Curve-fit Function
function [A_eff, C_eff, E_eff, sum_err2, fitted_values, max_err2] =
curvefit_func_pstress(di, fi, R, L, iter)
d_initial = di(1:iter);
f_initial = fi(1:iter);
ri = R; li = L;

f = @(p, f_initial) -p(1).*(log(4*ri)-0.5.*log((2*ri.*f_initial)/(li*pi())))-0.5*log(p(1))-0.5) +
p(2); %fit function

init_conditions = [0.5; 0.000001]; %[a; c] %initial conditions for curvefit function

```

```

%init conditions -> a = (1-v^2)/E, assuming v = 0.3 and E = 18.6e9; c = arbitrary value

[fitted_parameters, fitted_values, cvg, OUTF] = nonlin_curvefit(f, init_conditions,
f_initial, d_initial); %optimization function

A_eff = fitted_parameters(1); %parameter (a)
C_eff = fitted_parameters(2); %parameter (c)
E_eff = 1/A_eff; %Elastic modulus extracted from A_eff
err2 = (d_initial.-fitted_values).^2; %error^2 of each value fitted into to the original
curve
sum_err2 = sum(err2); %sum of error^2
max_err2 = max(err2); %maximum error pertains to limit of error

endfunction

```

#### Function 4. Subfunction 3: XLSWrite Function

```

function [rstatus] = xlswrite_func(fname_out, param, wsh_num)
fname = fname_out;
paramat = param;
wsh = wsh_num;
header = {"Displacement(mm)", "Fit_disp(mm)", "Force(N)", "param_a", "param_c",
"Modulus_E", "err^2"};

xlswrite(fname, header, wsh, "A1");
rstatus = xlswrite(fname, paramat, wsh, "A2");

endfunction

```

## Annex VI: Summary of Results of curve fitting.

### 1.5% Deflection

Specimen	Max_d	Max_d_model	Max_f	E
1	0.26186	0.251824	153.8811	10.09028
2	0.22763	0.217357	102.2826	10.51102
3				
4	0.10115	0.09098	3.33607	8.753755
5	0.21754	0.207293	214.3336	12.67125
6	0.16887	0.158848	248.2142	15.21497
7	0.1275	0.117334	21.17306	14.5741
8	0.0897	0.079622	3.47594	11.03048
9	0.23772	0.22741	152.7944	11.29597
10	0.09435	0.084339	11.35714	15.30267
11	0.16892	0.158755	215.7493	16.15007
12	0.22553	0.215142	162.7967	12.14988
13	0.13787	0.141531	18.07919	7.336761
14	0.17901	0.168841	211.0959	15.13985
15	0.23358	0.223385	184.4486	11.76082
Average	0.176516	0.167333	121.6441	12.28442
SD	0.058816	0.058177	92.1683	2.688047

### Summary: 3.0% Deflection

Specimen	Max_d	Max_d_mode l	Max_f	E
1	0.16722	0.157189	17.3984	6.258089
2	0.10115	0.090772	3.31689	8.204173
3	0.14002	0.129762	5.68534	7.884239
4	0.08058	0.070336	3.10785	5.90012
5	0.11475	0.117595	26.99673	10.82458
6	0.14433	0.141857	4.89425	7.415314
7	0.14223	0.149581	18.31933	7.892297
8	0.07384	0.081219	6.97374	7.345252
9	0.18723	0.177158	94.2149	12.3353
10	0.11917	0.108684	4.86565	8.066977
11	0.35779	0.347727	334.0841	8.489476
12	0.19754	0.187431	92.68318	11.38714
13	0.30169	0.291316	353.7792	9.064962
14	0.14835	0.137832	19.04488	9.464762
15	0.24367	0.233617	193.2753	11.32118
Average	0.167971	0.161472	78.57598	8.790258
SD	0.079934	0.077571	119.7796	1.921926

Summary: 6% Deflection

Specimen	Max_d	Max_d_model	Max_f	E
1	0.10614	0.095993	42.33439	32.68977
2				
3	0.06687	0.056517	1.51221	26.883
4				
5	0.07015	0.060041	3.82144	16.22002
6	0.09429	0.084188	5.7447	11.39132
7	0.0803	0.070155	7.55527	18.89676
8	0.0965	0.086113	8.19703	11.93577
9	0.08517	0.075163	5.81966	15.58054
10	0.20564	0.195467	20.94526	9.014228
11	0.11447	0.104281	25.93799	16.63721
12	0.07531	0.065132	3.44864	11.03894
13	0.06284	0.052207	3.21941	19.81279
14	0.1075	0.097473	26.27204	16.37986
15	0.08483	0.074569	6.48648	12.60342
Average	0.096155	0.085946	12.40727	16.85259
SD	0.036666	0.03671	12.46677	6.670516

## **Abstract**

The intramedullary nailing is one of the most commonly used techniques to fix broken long bones in the human body. The intramedullary nailing technique is increasingly used not only in diaphyseal bone fractures but also around the metaphyseal areas. It offers a relatively minimal surgical approach allowing to keep more of the soft tissues intact and thus accelerating recovery and overall functional outcome. The intramedullary nail must be locked proximally and distally to maintain good longitudinal and rotational stability. The proximal locking can be done using an automatic aiming device as there is almost no deformation of the nail in the proximal area. The automatic mechanical aiming device cannot be used distally because of the nail deformation and a shift of locking holes. The most commonly used technique for distal locking is a freehand technique.

The purpose of this work was to study the phenomena that take place around the distal locking screw and to analyse the interaction between the bone and the distal locking screw of intramedullary nail in order to better understand whether the position of the screw can have influence to the bone resistance and eventually to the fracture propagation if it occurs in the contact area. To achieve this goal the study was done in several stages. The first part involved an experimental work with the purpose to understand the local strain phenomena occurring at the interface between the bone and a metallic rod. It included medical imaging and compression experimentation. Three groups of 15 specimens were used. Local mechanical compression loadings at different quasi-static strain rates were imposed to the rod placed on the bone specimen. Medical imaging was used before and after the experimentation in order to evaluate different parameters including the geometrical shape of the bone and the bone matter density in distinguished areas under the metallic rod as well as to evaluate the extent of bone damage and the fracture propagation that occur during compression. This in vitro experimentation allowed

to evaluate the phenomena occurring due the local loading.

The results in this phase of the study have shown no statistical significance in fracture propagation regarding the BV/TV ratio and geometry of the bone. In fact, the fractures propagated mostly always in a longitudinal direction under the rod which means that there must be other factors involved in containing the fracture, such as collagen fibres, other proteins and substances. Without surprise more bone fractures occurred in greater displacement groups.

The second phase involved another experimental work which approached the real conditions that take place during the mechanical loading of the intramedullary nail locking screw. There were 3 groups of 6 specimens, each group defined by the distal locking screw aiming angle.

Introducing some alignment error and comparing it to the reference where the screw is perpendicularly inserted to the nail permitted to evaluate the influence of the position change to the strain and eventually the fracture propagation.

This part of the study showed statistical differences between group with 15° locking screw angulation in vertical plane and control group regarding the end of linear behaviour. In fact, the linear behaviour ended after a much shorter distance of displacement and required less force. This means that the 15° range of error could be acceptable in intramedullary nail distal locking in horizontal plane, but may destabilize the structure with less strain if it is put at 15° angle in vertical plane. This has potential clinical impact. As seen in the second part of this study, which is also consistent with clinical findings, there were much more screw ruptures than complete bone fractures. This shows that though the Young's modulus of the steel is much higher, its position in the overall nail-bone-screw structure exposes it to potential damage.

## Résumé

L'enclouage centromédullaire est une des techniques les plus utilisées de fixation des os longs chez l'homme. Cette technique est de plus en plus utilisée non seulement pour fixer les fractures diaphysaires mais aussi des fractures autour des régions métaphysaires. Elle permet d'utiliser la voie d'abord relativement minime et de respecter les tissus mous autour de la fracture ce qui accélère le rétablissement et le résultat fonctionnel. Le clou centromédullaire doit être verrouillé en proximal et en distal pour que la stabilité longitudinale et rotatoire soit maintenue. Le verrouillage proximal peut être fait de manière automatique en utilisant un guide attaché au clou, car il n'y a presque pas de déformation du clou dans la région proximale. Il ne peut pas être utilisé en distal, car à cause d'une déformation du clou les trous de verrouillage se décalent. La technique la plus utilisée pour le verrouillage distal est la technique à main levée.

L'objectif de ce travail a été d'étudier les phénomènes qui ont lieu au niveau de la vis de verrouillage distal et d'analyser l'interaction entre l'os et la vis afin de mieux comprendre si la position de la vis peut avoir de l'influence sur la résistance de l'os et éventuellement sur la propagation de fracture si celle-ci survient au niveau de contact. L'étude a été menée en deux parties. La première partie a impliqué le travail expérimental dans le but de comprendre les phénomènes de contrainte locale présente à l'interface entre l'os et un barreau métallique. Trois groupes de 15 échantillons ont été utilisés. Une compression mécanique locale quasi statique à des déplacements différents a été imposée au barreau métallique posé sur l'os. L'imagerie médicale a été faite avant et après l'expérimentation afin d'évaluer des paramètres : l'aspect géométrique de l'os, la quantité de substance osseuse, l'endommagement osseux et une propagation de fracture survenue éventuellement pendant la compression. Cette expérimentation a permis d'évaluer les phénomènes liés au chargement local. Elle n'a pas démontré de résultats statistiquement significatifs concernant le lien entre la propagation de fracture et le rapport BV/TV mais

aussi la géométrie de l'os. Le trait de fracture se propageait dans la plupart des cas de manière longitudinale ce qui voudrait dire qu'il existe d'autres facteurs impliqués dans la contention de fracture comme des fibres de collagène, d'autres protéines et des substances. Sans surprise, les fractures étaient peu nombreuses dans les groupes de déplacement plus important.

La deuxième partie a impliqué un travail expérimental qui se rapprochait des conditions réelles présentes au niveau de la vis de verrouillage distal du clou centromédullaire. Trois groupes de six échantillons ont été utilisés. Ces groupes ont été définis par l'angle de visée de la vis.

Une certaine erreur d'alignement a été introduite et comparée à la direction perpendiculaire de verrouillage distal du clou ce qui a permis d'évaluer l'influence de changement de la position sur la contrainte et éventuellement une propagation de fracture.

Cette partie a démontré une différence statistiquement significative entre le groupe où le verrouillage distal a été effectué à l'angle de  $15^\circ$  dans le plan vertical et le groupe de contrôle par rapport à la perte de la linéarité de comportement. La fin du comportement linéaire a été observée à une distance de déplacement moindre et a nécessité moins de force. Une erreur de  $15^\circ$  pourrait être acceptable dans le plan horizontal lors du verrouillage distal mais pourrait entraîner une déstabilisation de structure avec moins de contrainte en cas d'erreur de  $15^\circ$  dans le plan vertical. Cette partie d'étude a aussi démontré qu'il y avait beaucoup plus de fracture de vis que de fracture osseuse. Ces résultats montrent que même si le module de Young d'acier est beaucoup plus important, sa position dans la structure globale clou – os – vis l'expose à un potentiel endommagement.